Use of Diatomaceous Earth as a Siliceous Material in the Formation of Alkali Activated Fine-Aggregate Limestone Concrete

A Thesis

Submitted to the Faculty

of

Drexel University

by

Sean Anthony Miller

in partial fulfillment of the

requirements for the degree

of

Master of Science in Materials Science And Engineering

June 2009

ACKNOWLEDGEMENTS

I would first like to thank Dr. M. W. Barsoum for his invaluable guidance, support, and teaching throughout my years at Drexel University. I would especially like to thank Dr. Eva Jud Sierra for her mentorship and partnership in this research. I would also like to thank my colleagues, Aaron Sakulich and Alexander Moseson for their help and support. Although I could not name them all here, my thanks go to the faculty, staff, and students in the Materials Science and Engineering Department, without whose teaching and support none of this would have been possible. Last but not least, I would like to thank my family and friends for their continual love and support.

TABLE OF CONTENTS

LIST OF TABLES

LIST OF FIGURES

ABSTRACT

Use of Diatomaceous Earth as a Siliceous Material in the Formation of
Alkali Activated Fine-Aggregate Limestone Concrete

Sean A. Miller

Dr. M. W. Barsoum

The motivation behind this research has a historical, environmental, and developing world aspect. From a historical stand point the goal is to further the research established by Barsoum et al. claiming that parts of the Ancient Egyptian Pyramids were cast from a reconstituted limestone containing a binding phase of amorphous silica and/or calcium/magnesium silicates. From an environmental stand point the goal is to create an alternative cement to Portland cement, which has an enormous carbon footprint. For every 1 ton of Portland cement produced, roughly 0.8 tons of CO_2 are released into the environment. By creating an environmentally friendly concrete based on ubiquitous materials, the final goal is to some day be able to use such a concrete in developing countries where proper building materials are difficult to acquire. Experiments were developed to investigate and understand the role of diatomaceous earth (DE) as a source of silica in the formation of alkali activated fine aggregate concrete with lime as the alkali. In the 6 month trial four formulas were developed to investigate how hydraulic lime mortar using DE as the source of silica differs in strength and properties from naturally hydraulic lime mortar and non-hydraulic lime mortar. Formulas with low and high DE contents were created and compared with the naturally hydraulic and non-hydraulic lime mortar controls. The strength and binding phase properties of the four formulas were investigated over a 180 day testing period using compressive strength, XRD, TGA, SEM, and phenolphthalein tests. The results from the 6 month trial showed

that the high DE formula had the best compressive strength of the four formulas at 7 MPa, and the low DE formula had the second best strength at 5 MPa after 180 days. A major issue was discovered with the high DE formula however, as it was observed that its' humidity chamber and container cured concrete samples lost up to 50% of their strength when left to dry for 7 days in air. The low DE formula did not have this issue and thus it was hypothesized and supported by SEM images that the strength retention issue in the high DE formula resulted from the existence of undissolved diatoms throughout the sample. Cement paste experiments were set up to further investigate the binding phase properties of the formulas using XRD and TGA. The cement paste XRD showed that $Ca_{1.5}SiO_{3.5}\cdot xH_2O$ was the specific type of C-S-H that formed in the DE based cements and provided its strength. Celite 266 and Celite 400 DE were then used to investigate how changing the type of DE used affected the properties of the concrete. The results showed that the original Perma-Guard DE had the best strength properties. They also showed a counterintuitive correlation that the lower the surface area of the DE, the higher the compressive strength. The validity of this relationship was questioned and possible explanations provided. Finally, a Ca/Si ratio experiment was conducted to explore the relationship between Ca/Si ratio in the concrete, compressive strength, and the strength retention issue seen in the original high DE formula. Conclusions were made on the role of DE as a source of silica in alkali activated fine aggregate concrete, its viability as a building material in developing countries, and its cost and environmental competitiveness with Portland cement. Finally, future work and further optimization testing was discussed.

CHAPTER 1. INTRODUCTION

1.1 Introduction

The motivation behind this research has a historical, environmental, and developing world aspect. In the mid-1980's Davidovits postulated that the Ancient Egyptian Pyramids were made from cement blocks rather than carved natural limestone blocks. He suggested that the cement was made from an alkali solution made of lime, natron, or plant ash which would then be mixed with clay and kaolinitic limestone as an aggregate to form an alkali activated aluminosilicate.[1,2] These alkali activated aluminosilicate binding phases Davidovits called geopolymers.[3]

Geopolymers are interesting materials due to the fact that they have comparable strength to Ordinary Portland Cement (OPC) while emitting much less greenhouse gases. In addition to high compressive strengths, geopolymers have been shown to have low shrinkage, acid resistance, and low thermal conductivity. They can also be altered to have either fast or slow curing times depending on the application.[4]

With respect to the Ancient Egyptian Pyramids the use of alkali activated aluminosilicates as the binding phase in the proposed cast cement blocks however, was shown to be inaccurate by Barsoum et al.[5] Barsoum et al. found that the binding phase of the Great Pyramid of Khufu was composed of amorphous silica and/or calcium/magnesium silicates. No Na-Al silicate binder was found and so the use of clay and subsequently geopolymers as a binding phase was shown to be incorrect. The binding phase was shown to be from the alkali activation of amorphous silica.

The alkali used by the Egyptians is lime. Lime has long been used as a mortar in stone buildings by adding water to a typically 3:1 sand to lime volume ratio. The history of the use of lime mortar dates back to between 7000-12000 BC in Palestine and Turkey where evidence of lime mortar structures and floors have been found.[6,7] Since the Ancient Egyptian Pyramids Khufu and Khafre were constructed around 2500 BC it is not a far stretch to assume they were able to produce lime for lime mortar.[7] Lime is produced by calcination of limestone at around 900ºC in a lime kiln resulting in quick lime, CaO. Water is then added to quick lime to form lime putty, also known as slaked lime. Slaked lime is a paste consisting of particles of portlandite ($Ca(OH)_2$ and excess water). Lime putty is usually aged as the particle size of the $Ca(OH)_2$ decreases with time resulting in a mortar of higher quality.[8] The decrease in particle size of the portlandite particles is concurrent with an increase of the specific surface area. A higher surface area increases the capacity of water absorption and leads to increased plasticity, water retention, and workability. In addition, the increased surface area also contributes to shorter carbonation times and crystal interlocking, leading to increased strength development.[8,9] After aging, the lime putty is mixed with aggregate (usually sand) and typically used as a mortar between stones to build structures and houses.

In addition to calcium-based lime mortars it is also possible to produce dolomitic limes which have MgO in addition to CaO. Unfortunately dolomitic limes tend to have slow and late hydration which can lead to cracking and pitting of the lime mortar. They also are susceptible to SO_2 attack from air pollution that can form highly soluble and damaging magnesium sulfates. These two reasons are why calcium based lime mortars are preferred over dolomitic lime mortars.[8]

There are two types of calcium-based lime. If the lime can harden under water it is considered hydraulic; if it cannot it is non-hydraulic. Non-hydraulic lime is also known as fat lime or lime putty. It is usually associated with the following properties: high permeability, flexibility, and plasticity. It also has a tendency to shrink in early stages of hardening and has low mechanical strength at early stages.[10] Non-hydraulic lime hardens only by carbonation and is the type of lime used as an alkali throughout this research. Carbonation of non-hydraulic lime progresses from the surface inward as slaked lime, $Ca(OH)_2$.aq absorbs CO_2 from the atmosphere to form calcium carbonate $CaCO_3$. The process is limited by the rate of diffusion of CO_2 into the lime mortar so it could take months, years, or decades to fully carbonate and harden.[6] This lengthy time for carbonation is what makes lime mortar the preferred mortar between stones in ancient building restoration. The slow carbonation rate allows non-hydraulic lime mortars to retain their plasticity for extended periods of time. The plasticity allows lime mortar to withstand adjustments and small movements in the stone structures without cracking and failing at the joint when subjected to stress. It also allows the structure to breath and adjust to varying levels of humidity throughout the seasons.[6,11]

In the 20th Century Portland cement based mortars began to replace lime mortars in the conservation and repair of ancient stone buildings. It was thought that the quick setting and stronger cement based mortars would be superior to the lime mortars which take much longer to harden. This idea was incorrect as the Portland cement based mortars are often stronger than the historical stone material causing the historic stone or brick to fail first under stress.[12] Cement based mortars also tend to have low porosity which results in a build up and entrapment of water and soluble salts that are released by the

stones or cement at the substrate-mortar interface. This salt build up can lead to salt crystallization and freeze thaw issues in the mortar. Non-hydraulic lime mortars are much more porous than cement based mortars and thus they are able to release and eliminate the unwanted salt build up from the stone mortar interface.[6,12,13] Non-hydraulic lime mortars remain the mortar of choice for repair of ancient stone buildings because they do not release soluble salts that can cause serious damage in the mortar following crystallization. They are also more chemically, structurally, and mechanically compatible with ancient masonry than Portland cement. In addition, lime mortars have the ability to self-heal when fractures are developed due to calcite dissolution and reprecipitation.[8]

Typical compressive strength values for non-hydraulic lime mortars vary depending on the lime/aggregate ratio. A lime mortar with a cement/aggregate ratio of 1:2 typically has strength of 0.7-1.0 MPa after 1 day and around 1.6 MPa after 14 days.[14] A lime mortar with cement/aggregate ratio of 1:4 usually has lower strength values initially as there is less cement to hold the aggregate together.[15] Over time the strength of lime mortars will continue to rise as carbonation progresses. After a year of curing due to carbonation a typical non-hydraulic lime mortar with a 1:2 cement to aggregate ratio will have strengths around 3-5 MPa.[13] The type of aggregate and shape of aggregate used will also play a large role in the strength of lime mortars.[16] The rate of strength development depends not only on the cement/aggregate ratio but also on the size and shape of the sample as a smaller sample will be able to fully carbonate quicker than a large sample which has a more depth that the CO_2 must penetrate for carbonation to occur. The early strength, length of time that it takes lime mortars to harden, and compatibility with the

ancient mortar being repaired is why lime mortar is the cementious material of choice for historic building repairs and restorations.

As mentioned, hydraulic lime mortars are different from non-hydraulic lime as they can harden under water. The ability to harden under water results from the hydraulic binding phases that occur in addition to carbonation hardening. There are two ways to achieve a hydraulic lime mortar: by adding pozzolanic materials to lime, or by using a natural hydraulic lime. Natural hydraulic lime occurs when the original limestone contains impurities such as silica, SiO_2, or alumina, Al_2O_3. When this impure limestone is calcined at 900ºC the resulting lime will have silica or alumina which when combined with water will form the hydraulic phases calcium-silicate-hydrate and calcium-alumina-hydrate.[17] These hydraulic phases are what allow natural hydraulic lime to harden under water. Compared to non-hydraulic lime, hydraulic lime has lower permeability and flexibility, and better resistance to moisture, frost and salt attack. They also tend to have better mechanical strength due to the additional hydraulic binding phases. These properties make hydraulic lime mortars best used in strong masonry applications where damp environments may be an issue.[10,18]

Depending on the level of impurities in the natural hydraulic lime they may be considered feebly hydraulic. Feebly hydraulic lime hardens mostly by carbonation, just like non-hydraulic limes, but also has a small amount of hydraulic phases. These hydraulic phases help with initial strength gain during hardening.[10]

Since limestone with the proper impurities to produce natural hydraulic lime is rare compared to standard limestone, civilizations began to develop artificially hydraulic lime by adding pozzolanic materials to lime mortar. The Phoenicians used hydraulic lime

mortar in Jerusalem around 10,000 BC.[17] The Greeks produced hydraulic properties by adding Santorin's earth to lime mortar, and, of course, the Romans used volcanic ash to perfect their hydraulic mortar and cement.[17,19,20] The Santorin's earth used by the Greeks and volcanic ash used by the Romans are all examples of what are called pozzolanic materials. A pozzolanic material is any material which when combined with an alkali-earth substance such as $Ca(OH)_2$ and water exhibits cementitious properties by forming hydraulic binding phases such as calcium silicate hydrates. Typical pozzolanic materials include slag, fly ash, Roman volcanic ash, and various alkaline sludges such as red mud.[21] The Romans were able to perfect their hydraulic lime cements and concretes and apply them in structures like no other civilization at the time. Their knowledge of pozzolanic materials and cements was so extensive that they even had an understanding of additives and their effects on pot life and workability. Substances like egg whites, blood, beer, vegetable juices, and urine were used by the Romans to improve their hydraulic cements and concretes depending on the application and desired plasticity.[20]

As the Roman Empire expanded to control most of Europe they spread their expertise of hydraulic cements around the world. With thousands of years of research and knowledge of hydraulic lime mortars already completed the question becomes why are people still researching lime mortar and cements today? The answer is that like many things the technology and knowledge was lost during the middle ages.[19]

The addition of pozzolans to lime is one of the first types of what is now called alkali activated cements. The use of alkali activated cement (AAC) is not a new technology. The use of AACs dates back to at least the time of Nebuchadnezzar in the city of Ur, and as we believe to the time of the Ancient Egyptians.[22] In general AACs

involve the use of alkali activators such as CaO to stimulate the latent hydraulic properties of pozzolanic materials. If activated properly the hydraulic properties can lead to the formation of a hydraulic binder in the cement.[23] AACs have been shown as a viable replacement to OPC due to their high early and ultimate strength, rapid hardening, and low environmental impact.[24] The Ukraine and former Soviet Union not only invested heavily into research in AACs in the 1950's, they were also able to put them into production of buildings that still stand today.[25,26]

AACs are considered a sustainable, environmentally friendly material for a few reasons. For one the pozzolanic materials used in AACs are often waste products such as blast furnace slag or fly ash. The use of these materials to form a hydraulic binder reduces the processing steps associated with producing cement and also is a way of dealing with such waste products.[7] AACs have also been shown to be viable materials for the storage and management of hazardous and nuclear waste.[27] Compared to OPC AACs have improved resistance to corrosion, lower leachability of contaminants, and increased material stabilization over time. These characteristics are why AACs are thought of as a preferred option for the storage and containment of radioactive waste.[28]

The most important environmental characteristic that AACs have is their reduced carbon footprint compared to OPC. For every 1 ton of Ordinary Portland cement produced roughly 0.8 tons of CO_2 are released into the atmosphere.[9] Since billions of tons of OPC are produced each year, OPC is a major contributor to global warming.[30] To be specific the US cement industry accounts for nearly 7% of the nation's CO_2 emissions. In terms of CO_2 emissions from US industrial processes, the cement industry accounts for more than half of the carbon dioxide emissions.[21,31]

The emission of CO_2 associated with OPC comes from the calcinations of limestone to make lime. First fossil fuels must be used to heat limestone to around 1400ºC to produce lime. Secondly, the process itself chemically releases CO_2 from $CaCO_3$ to form lime, CaO.[32]

This research serves to investigate the formation of reconstituted limestone using the same materials available to the Egyptians to form alkali activated cement with limestone as a fine aggregate. Cement produced from the same materials available to the Ancient Egyptians could not only have a reduced environmental impact but also an impact in the third world. If the Ancient Egyptians were able to produce cement with little to no tools and basic materials, then how hard could it be to transfer the same technology to developing countries and communities? Cement based on the pyramids would be not only be simple but also durable as we know it has the ability to last over 4500 years.

Since it was proven by Barsoum et al. that clay and geopolymers did not form the binding phase of the cast Egyptian Pyramid blocks, the binding phase must have come from the alkali activation of amorphous silica.[5] This research proposes that the source of the amorphous silica is diatomaceous earth. Diatomaceous earth (DE) consists of the cell walls of dead diatoms which are microscopic single cell algae. Fossilized DE deposits can be found in both salt and fresh waters. There are thousands of different species of DE, but all are made of mostly amorphous SiO_2[33,34]. DE is currently used as a pesticide, filler, insulation, anti-caking animal feed additive, ingredient in dynamite, and as a filter for beer, wine, and oils. The US produced roughly 830,000 tons of DE in 2007, which

was 38% of the world's total DE production.[35] Although the US is the highest producer of DE, various types of DE have been found around the world including in Egypt.[36,37]

1.2 Hardening Processes

One of the main objectives of this research is to understand the hardening mechanisms that occur in non-hydraulic and natural or artificial hydraulic lime mortars. As mentioned non-hydraulic lime mortars cannot harden under water as they only harden through carbonation. Carbonation involves the absorption of CO_2 from the air to carbonate slaked lime to form calcium carbonate, also known as calcite ($Ca(OH)_2 + CO_2 \rightarrow CaCO_3 + H_2O$). The carbonation process is very slow for a few reasons. First of all the percentage of CO_2 in air is low, typically ranging from 3-5% depending on the season. In addition the rate of diffusion of CO_2 into the non-hydraulic lime mortar is very slow as well. The open porosity of the lime mortar and exposed surface area will influence the diffusion rate of the CO_2. If there are areas within the lime mortar which are closed off from the open porosity or areas which have a high percentage of relative humidity content the carbonation process will be inhibited and areas of pure $Ca(OH)_2$ will remain. The low CO_2 content in air and slow diffusion rate is why it can take months to years for complete carbonation to occur depending on the size and thickness of the lime mortar.[20]

For carbonation to occur the presence of water and portlandite is necessary. There are five stages involved in the carbonation process.[12]

1. Diffusion of gaseous CO_2 through the pores of the lime mortar
2. Dissolution of the CO_2 in the pore water to form carbonic acid H_2CO_3
3. Dissolution of $Ca(OH)_2$ in the pore water
4. Chemical equilibration of $Ca(OH)_2$ and H_2CO_3 in the pore water
5. Precipitation of calcite, $CaCO_3$

Figure 1 shows a Scanning Electroscope Microscopy (SEM) image of the formation of calcite crystals due to the carbonation of $Ca(OH)_2$ to form $CaCO_3$. The calcite originated as lime putty which was exposed to air for 14 days.

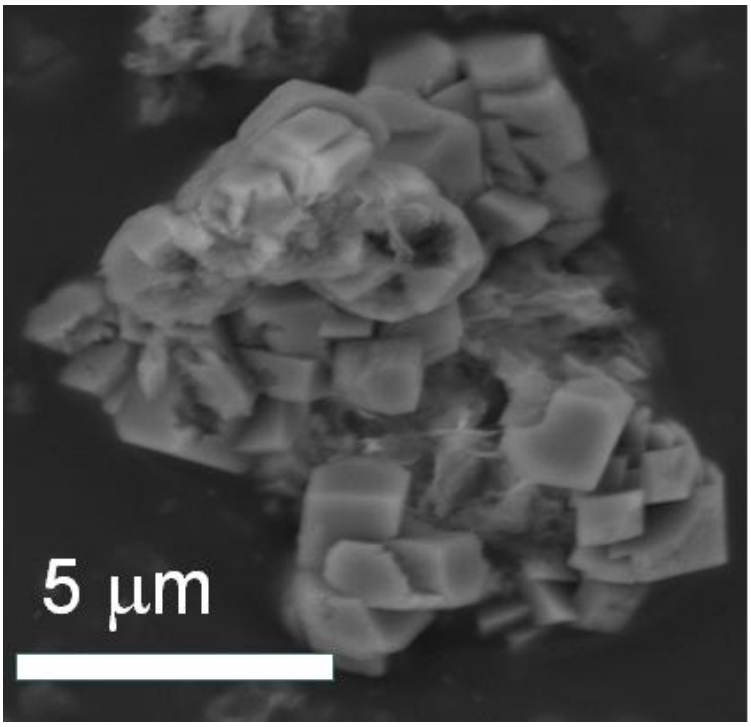

Figure 1: SEM Image of Calcite
SEM image of calcite crystals formed on a lime putty $Ca(OH)_2$ particle after 14 d of air curing.

The use of DE as a source of amorphous silica in lime based AACs is one example of an artificial hydraulic lime mortar. The key to using DE in an AAC is the

alkali activation of the amorphous silica. Thus the most important step is the dissolution of the DE to release Si^{4+} ions. The dissolution process can be divided into three steps: i) dissolution of diatom skeletons in an alkali solution, ii) formation of silicic acid that decreases the pH, and, iii) formation of reaction products, e.g. silica gel or calcium silicate hydrate.

Since DE is amorphous and has a very large specific surface area, it is expected to completely dissolve to form silicon hydroxide ($Si(OH)_4$) or complex silicate ions ($Si(OH)_5^-$ or $HSiO_3^-$) once above pH 10.7 at ambient temperatures.[38] To achieve a pH of 10.7, or higher, various alkalis can be used such as NaOH, $Ca(OH)_2$, or quicklime CaO. The maximum pH which can be obtained with quicklime is ≈ 12.5. Since this is above 10.7, a reasonable dissolution rate is expected. Temperature will also affect the dissolution of DE, as a higher temperature will allow for better dissolution. The dissolution of DE is associated with a pH drop as silicic acid is produced, lowering the pH of the alkali solution. This pH drop may only be showing a partial dissolution of DE however, as the accumulation of silicic acid can occur quickly, preventing the reaction and full dissolution from going forward.

In the cases where $Ca(OH)_2$ is used as alkali activators, the third step in the dissolution process is the formation of reaction products such as calcium silicate hydrates, C-S-H. The formation and type of such products is the key to forming strong and durable AACs. This research will investigate the early and long term hydration of alkali activated cements with DE as the source of silica since this is generally not well understood.[39]

C-S-H is the binding phase that holds our bridges, buildings, and world together as it accounts for up to 75 wt% of hardened Portland cement pastes. C-S-H comes from C→CaO; S→SiO_2; H→H_2O and thus C-S-H is $mCaO{\cdot}n\ SiO_2kH_2O$. In general there are more than 30 known types of C-S-H ranging from semi-crystalline to almost fully amorphous.[40]

At the semi-crystalline end of the C-S-H spectrum, as the C-S-H phases achieve higher levels of crystallinity over time they approach the chemistry of the rare minerals tobermorite and jennite. 1.4-nm Tobermorite and jennite are the models for crystalline C-S-H phases. Tobermorite ($Ca_5(Si_6O_{18}H_2){\cdot}4H_2O$, approximately $C_5S_6H_9$) is associated with a Ca/Si molar ratio less than 1.5. Jennite ($Ca_9Si_6O_{18}(OH)_6{\cdot}8H_2O$, approximately $C_9S_6H_{11}$) is associated with a Ca/Si molar ratio above 1.5. One of the important characteristics of 1.4-nm tobermorite and jennite is their ability to maintain the features of a composite layer structure, while varying in composition and extent of crystallization.[40,41]

C_3S and β-C_2S are important calcium silicates in OPC as C_3S provides the early strength development and β-C_2S provides the long term strength development. When C_3S and β-C_2S are combined at room temperature in aqueous solutions they have a tendency to form an imperfect version of tobermorite, with little more than two-dimensional order. This imperfect version of tobermorite is known as C-S-H I, which can handle a high concentration of defects and thus has a wide allowable Ca/Si range of 0.67-1.5. [40,41] If C_3S and β-C_2S are allowed react with excess water for longer times, they have a tendency to form an imperfect version of jennite, known as C-S-H II, for which the Ca/Si ratio is greater than 1.5. In Portland cement it is known that C-S-H is a combination of

tobermorite and jennite like structures, which after months and years become increasing dominated by the jennite structure.[40,41]

Continuing down the spectrum of C-S-H comes to an even less ordered structure than C-S-H I and C-S-H II, C-S-H gel. In OPC, C-S-H gel is a highly dispersed precipitate of colloidal semicrystalline calcium silicate hydrates. C-S-H gel is typically formed from the hydration of monoclinic C_3S and β-C_2S which are constituents in OPC clinker.[42] C-S-H gel has a disordered layer structure in which initially the layers are a combination of imperfect tobermorite and jennite like structures. Over time just as in C-S-H I and C-S-H II, C-S-H gel will be increasingly dominated by layers of jennite like structures. C-S-H gel typically has a Ca/Si ratio of 1.7-1.8.[40,43] The formation of C-S-H gel initiates from a few nuclei to grow into bundles or branching ribbons of lath like particles of nano-crystalline regions. C-S-H gel shows up on X-ray diffraction (XRD) as amorphous at early stages of growth as it has a semi-ordered structure initially. During these early stages the C-S-H gel consists mainly of dimeric silicate chains which are linked by monomers to form pentamers as the hydration process proceeds and the C-S-H begins to form semi-crystalline tobermorite and jennite like regions which show up as peaks in XRD. In OPC the microstructure of C-S-H is typically well defined after just 24 hours and is the reason that OPC has such high early strength.[44]

The Ca/Si ratio plays a large role in determining what type of C-S-H will form in the Portland cement. At early stages of hydration, the Ca/Si ratio is typically 1.7-2.0. As the cement matures and the hydration proceeds, the Ca/Si ratio can vary from 0.7-2.1. The average Ca/Si ratio in OPC is around 1.75 (Figure 2).[45] Ultra-high performance OPCs, which tend to be rich in silica, have Ca/Si values at around 0.7.[42,44-46]

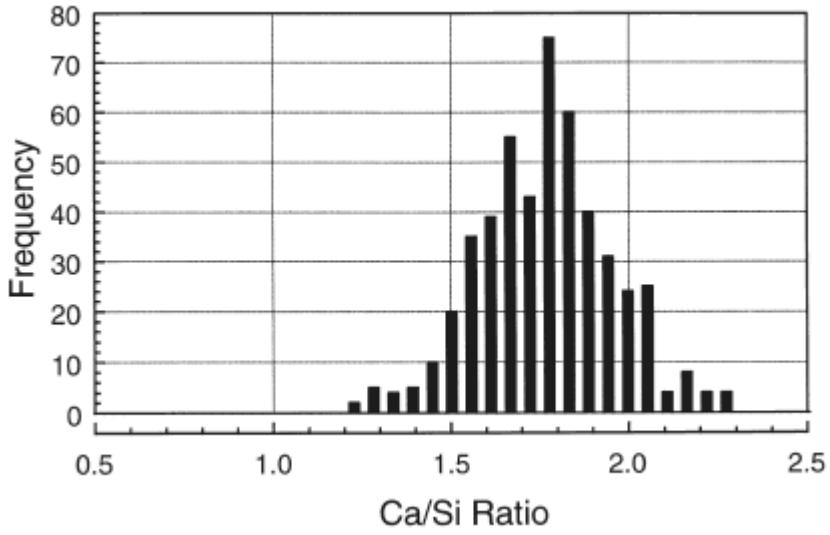

Figure 2: Portland Cement Average Ca/Si Ratio
Ca/Si ratio frequency histogram for C-S-H in Portland cement pastes aged 1 day to 3½ years.[45]

Just like in OPC, semi-crystalline C-S-H and C-S-H gel are also formed during the hydration of AACs with lime as the alkali activator. The formation of C-S-H gel in lime-pozzolan pastes is controlled by the pozzolanic reaction rate, diffusion of reactants through a layer of porous hydration products, and by the diffusion of reactants through a layer of dense hydration products.[44] Just as in OPC, the dissolution, distribution, and particle size of the lime and pozzolanic silica source play a major role in the C-S-H formation and ultimately the strength of the AAC. By using an amorphous silica source, like DE the expected hydraulic binding products are C-S-H. Figure 3 shows the formation of C-S-H on a diatom which has been in a 1M $Ca(OH)_2$ for 4 weeks. The leafy structure associated with C-S-H can be seen on the diatoms' surface. As Si ions dissolve from the diatoms' surface they combine with Ca ions in solution to form C-S-H.

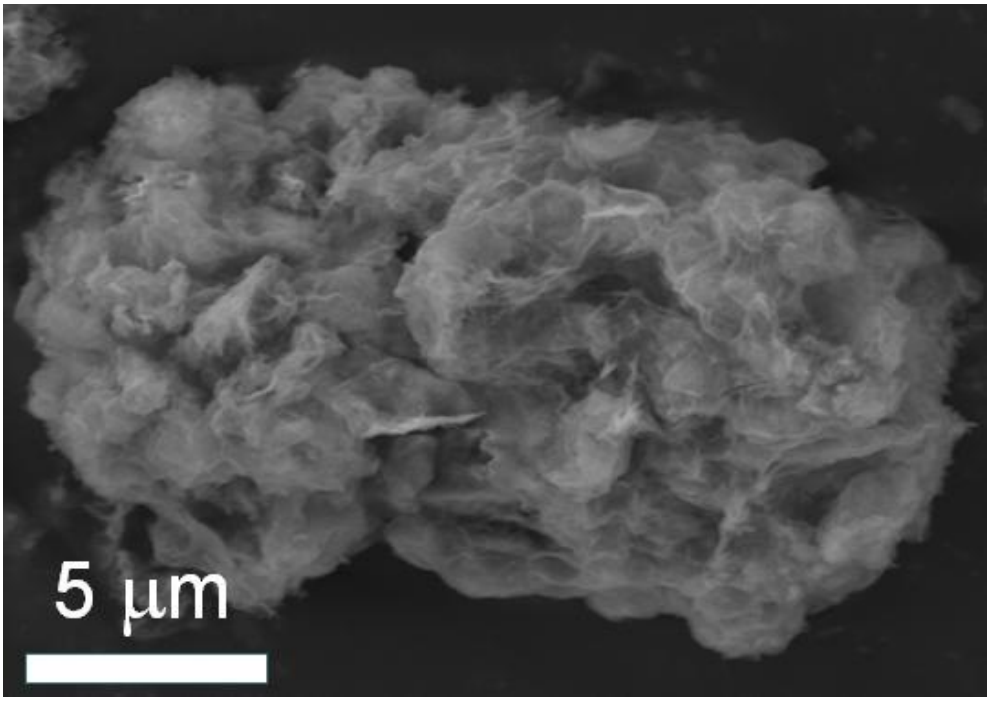

Figure 3: SEM Image of C-S-H on a Diatom
SEM image of a diatom which has been in a 1M $Ca(OH)_2$ solution for 4 weeks. The leafy like C-S-H structure can be seen forming on the surface of the diatom.

It is also possible to use a crystalline silica source instead of an amorphous one like DE. The expected binding product of crystalline silica is tobermorite as it is much harder for the silica ions to be leached out of the crystalline silica however. The ability of amorphous silica to easily leach out Si ions leads to a decrease in the Ca/Si ratio of the hydrated products. This is important as the Ca/Si plays a huge role in determining the type and character of the C-S-H of lime-pozzolan cements.[44]

The solubility of the individual ions also plays a major role in the formation of C-S-H phases formed in aqueous solution. At the surface of the silica material (DE in this research) a small amount of silica dissolves and reacts with calcium ions to form C-S-H. At low temperatures C-S-H I and C-S-H II semi-crystalline phases are formed, resulting in low expected cement strength as C-S-H I and C-S-H II are lower strength phases. To

form high strength tobermorite and jennite like phases, a hydrothermal process is needed to increase the temperature during C-S-H formation.[47] By increasing the curing temperature during cement production the pozzolanic reaction rate is accelerated, helping in the formation of C-S-H.[44] The influence of temperature on the formation of hydrated binding phases is another reason why extremely exothermic quicklime makes a good alkali activator.

Initially, hydraulic lime mortars set due to the formation of C-S-H. C-S-H may take up to 2 (eminently hydraulic) to 20 days (feebly hydraulic) to form and cause the initial hardening of hydraulic lime mortars.[6] Depending on the purity or type of natural or artificial hydraulic lime used there may also be initial hardening due to the formation of calcium alumina silicates (C-A-S). Dicalciumsilicate (C_2S) is the major hydraulic phase in most natural hydraulic limes, but they may also contain the phases C_2AS, C_3S, C_3A, and C_4AF. The latter minor phases are commonly formed at much higher processing temperatures than C_2S.[18]

One of the possible benefits of natural and artificial hydraulic lime mortars over OPC is their ability to have two hardening mechanisms. In addition to hydraulic phases which give natural and artificial hydraulic lime mortars their initial strength, they also have the ability to harden due to carbonation. The carbonation hardening processes can occur in hydraulic lime mortars in areas with excess $Ca(OH)_2$ that is not being used to form C-S-H. Since carbonation can take months or years to complete the carbonation of excess $Ca(OH)_2$ in hydraulic lime mortars gives them the ability to continually harden and gain strength over much longer periods of time than OPC. An optimal hydraulic lime mortar would have the proper amount of C-S-H to give the material early strength, with

excess $Ca(OH)_2$ to give the material long term strength due to carbonation. Thus the purpose of this research is to explore the two hardening mechanisms in hydraulic lime and determine how they interact, compete, and affect the properties of AACs with DE as the source of silica and quicklime as the alkali activator. Table 1 shows a brief overview of the two hardening mechanisms, carbonation and hydration.

Table 1: Hardening Processes of Hydraulic Lime Mortars[44,48]

Carbonation	Hydration
$Ca(OH)_2 + CO_2 \rightarrow CaCO_3 + H_2O$	**$Ca(OH)_2 + SiO_2 \rightarrow xCaO.ySiO_2.zH_2O$**
• Reaction progresses from outward to inward • Slow strength development (months to years) • Reaction limiting factor: diffusion of CO_2 to reaction site[48]	• Reaction happens within sample • Fast strength development (hours to days) • Reaction limiting factor: Dissolution of diatomaceous earth[44]

1.3 Materials

Three different types of DE were used in this research. The primary type of DE was Perma-Guard DE. Perma-Guard is a fresh water deposit of the diatom Melosira Preicelanica mined in Nevada.[49] The Perma-Guard DE is intended for use as a pesticide because of its' robustness and shape. The sharp jagged edges of the broken diatoms act as a pesticide by making it difficult or painful for the bugs to land on the plants covered in this DE.

Two types of Celite DE, Celite 266 and Celite 400, were also used in this research in Ch. 4. Celite 266 is a marine DE and Celite C-400 is a fresh water DE. Figure 4 and

Table 2 show what the three types of DE look like using SEM and their composition, respectively.

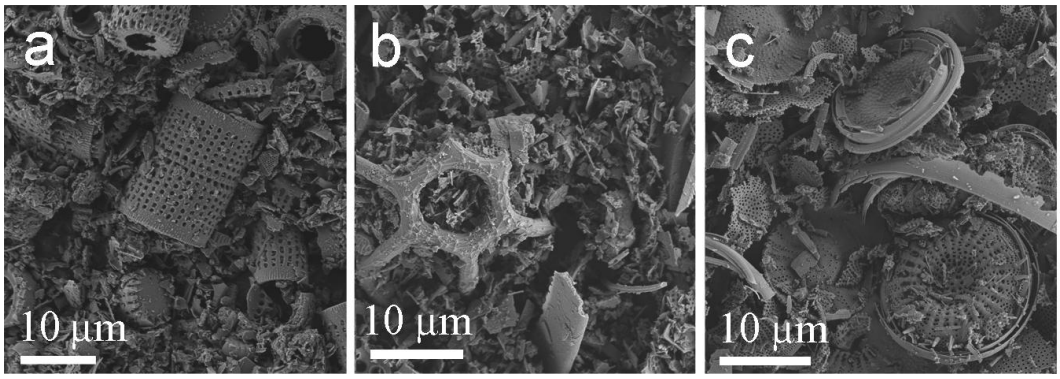

Figure 4: SEM Images of As Received DE a) Perma-Guard b) Celite 266 c) Celite 400

Table 2: As Received DE Composition in wt% and Surface Area

Permaguard Fresh Water DE	**Celite 266** Marine DE	**Celite 400** Fresh Water DE
89 wt% SiO_2 4 wt% Al_2O_3 1.7 wt% Fe_2O_3 1.4 wt% CaO 1.2 wt% Na_2O 0.6 wt% MgO 0.5 wt% K_2O Crystalline silica < 0.5 wt%	89 wt% SiO_2 3 wt% Al_2O_3 1.4 wt% Na_2O 1.4 wt% K_2O 1 wt% Fe_2O_3 0.7 wt% MgO 0.4 wt% CaO 0.2 wt% TiO_2	92.5 wt% SiO_2 3.2 wt% Al_2O_3 1.7 wt% Fe_2O_3 0.8 wt% CaO 0.6 wt% Na_2O 0.6 wt% K_2O 0.4 wt% MgO 0.2 wt% TiO2 0.1 wt% P_2O_5
BET Surface Area: 28.1 m^2/g	BET Surface Area: 30.0 m^2/g	BET Surface Area: 36.7 m^2/g

The quicklime CaO used in this research was MicroCal OFT15 from Mississippi Lime. The chemical and physical properties of the lime are listed in Table 3.

Table 3: MicroCal OFT15 Quicklime Chemical and Physical Properties [50]

TYPICAL CHEMICAL PROPERTIES	
CaO - Total	98.0%
CaO - Available	95.0%
Calcium (Ca)	70.0%
CO_2	0.4%
LOI	0.7%
Magnesium (MgO)	0.3%
Acid Insoluble Substances	0.2%
Alumina (Al_2O_3)	0.1%
Iron (Fe_2O_3)	0.04%
Silica (SiO_2)	0.3%
Crystalline Silica	<0.1%
Sulfur (S)	0.01%
Phosphorus (P2O5)	50 ppm
Manganese (MnO)	21 ppm

TYPICAL PHYSICAL PROPERTIES	
Specific Gravity	3.3
Median Particle Size	3 micron
pH	12.4
BET Surface Area	2 m^2/g
Top Cut, D98	15 micron
100 Mesh (150 µm) Residue	Trace
200 Mesh (75 µm) Residue	Trace
325 Mesh (45 µm) Residue	0.005%
Apparent Dry Bulk Density - Loose	50 lbs./ft3
Apparent Dry Bulk Density - Packed	70 lbs/ft^3
Reactivity 30 sec.	25°C
Reactivity 180 sec.	50°C
Total Temperature Rise	58°C
Total Reactivity Time	250 sec.

A natural hydraulic lime (NHL) was also used in this research. NHL-5 is a commercial product purchased from PA Lime Works that will serve as one of the controls in the experiment. NHL-5 is an eminently hydraulic lime used for applications such as building or repairing wall head copings.[51] It is created from a limestone in St. Astier, France that has approximately 11 wt% naturally occurring reactive silica. This naturally containing silica limestone is calcined at a maximum of 1000ºC to form the composition of lime and calcium silicates listed in Table 4.[52] This material will help to show how the properties of natural hydraulic limes differ from the activation of pozzolanic materials with lime.

Table 4: NHL-5 Chemical Composition[52]

NHL-5 Chemical Composition (wt%)	wt%
Free lime $Ca(OH)_2$	5.6
$CaCO_3$ UNBURNT	22
Calcium Silicate ($CaO.SiO_2$)	23
C2S ($2CaO.SiO_2$)	43
C3A ($3CaO.Al_2O_3$)	0.7
C2AS ($2CaO.\ Al_2O_3.\ SiO_2$)	1.3
C4AF ($4CaO.\ Al_2O_3.Fe_2O_3$)	0.7
$CaSO_4$	0.7

The aggregate used in the research is a granular limestone (Soil Doctor, Home Depot Garden section). Table 5 lists the chemical composition and screen size of this the limestone and its particle distribution. This limestone is considered a fine-aggregate because more than 60% of the limestone particles are < 300 μm in diameter.

Table 5: Soil Doctor Granular Limestone Chemical and Screen Analysis

Soil Doctor Granular Limestone Minimum Guaranteed Chemical Analysis	wt%
Calcium Carbonate Equivalent-CCE	91
Calcium Carbonate ($CaCO_3$)	78
Magnesium Carbonate ($MgCO_3$)	11

Soil Doctor Granular Limestone Minimum Guaranteed Screen Analysis	% Passing
8 Mesh	100%
10 Mesh	100%
20 Mesh	92%
40 Mesh	67%
50 Mesh	55%
60 Mesh	50%
100 Mesh	40%

Figure 5: Soil Doctor Limestone Particle Distribution

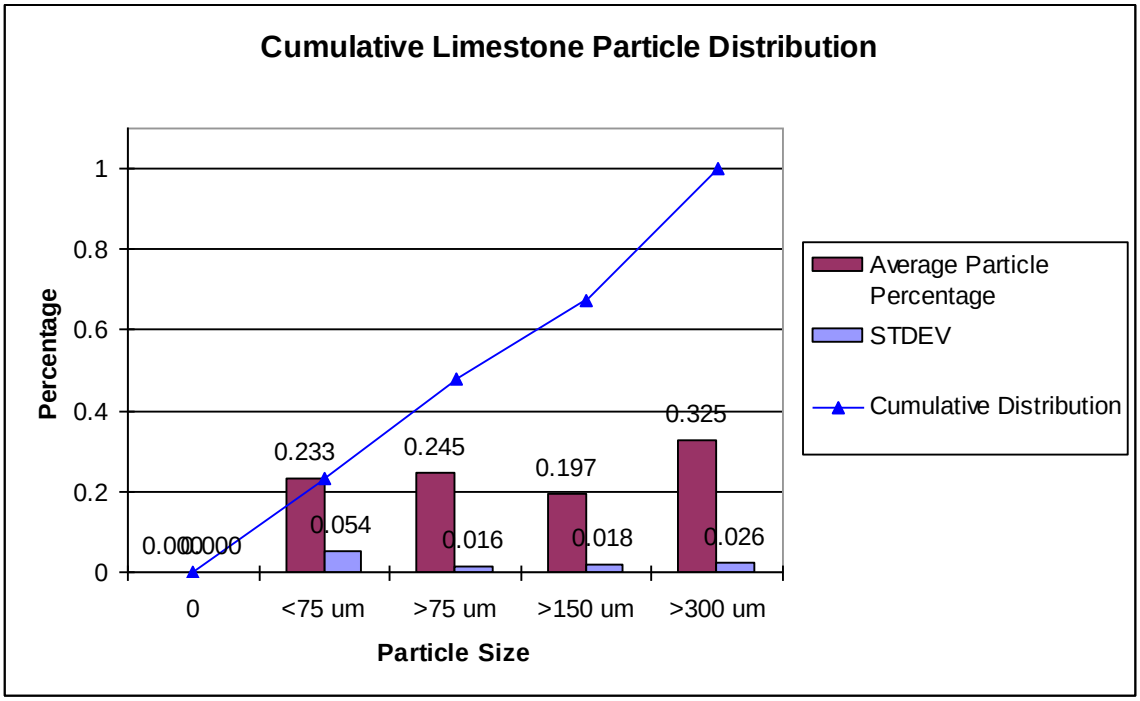

1.4 Objective

The goal of this research was to take some of the simple materials available to the Ancient Egyptians and use them to create an alkali activated concrete with DE as the siliceous material, lime as the alkali, and limestone as the fine aggregate. Such a material is not only more environmentally friendly than OPC, but also could someday be used in developing countries.

The objective of the experiments in this research was to understand the long term strength and properties of lime mortars, natural hydraulic lime, and DE based alkali activated concretes. Such things as the impact of the amount of DE, type of DE, and

curing environment were looked at over long periods of time to better understand the properties of these materials. One of the major goals of the experiments was to understand the relationship between the competing and coexisting carbonation and hydraulic binding phases so as to determine which one dominates and why. Experiments were also developed to optimize the DE based concrete formulas and determine their viability as a possible replacement material to OPC.

1.5 Experimental Technique

1.5.1 Cement Production

All concrete mixtures and samples were produced according to ASTM C0192. The dry ingredients were first mixed together for 5 minutes. The water was then added and the concrete was mixed for 10 minutes using an Arrow 850 (Arrow Inc, Hillside, NJ) table top mixer in simple plastic buckets. Upon completion of mixing the samples were slump tested and then placed in 2”x4” plastic testing cylinders. For each testing date and curing condition four samples were made. Three of the samples were for compression testing, with the fourth sample being used for characterization of the concrete. An extra 10 % of cylinders were also made with each experiment to account for any poorly made samples or additional testing not originally planned. The pour procedure for placing the concrete in the 2”x4” cylinders was as follows:

- Fill a cylinder half-full by pouring or with a trowel. Then consolidate by:

- If the slump is more than 25% (i.e. is reasonably fluid), the cylinder was placed on a sieve shaker and firmly covered with a piece of wood. A light pressure was applied and the shaker was run for 15-30 s.
- If the slump is less than 25% (i.e. it's rather play-doh like), a 3/8" steel rod was used to tamp the surface 25 times. Repeat to fill the cylinder, and consolidate again. Finally, the cylinder was topped off with enough concrete to slightly overfill the mold, and then "strike off" (make straight) the top with a trowel or another rigid, straight surface.

NOTE: Only the portions of the concrete which were uniform and representative of the whole batch were used. In some instances it was necessary to remix the batch during pouring to keep it consistent.

After being poured, each sample was covered with plastic wrap, which was held on by a rubber band. The samples were allowed to cure for 4 d prior to being removed from their cylinder and plastic cover. Once removed the samples were placed in specific curing environments. The curing environments used throughout the research were as follows: in ambient laboratory conditions (air samples), in a 100% relative humidity chamber (humidity samples), and left in their original cylinder and covered with plastic wrap (container samples). The ambient air curing environment exposed the samples to unlimited CO_2, but also lead to drying. This curing condition helped to explore the effects of carbonation on the strength of the samples. The 100% relative humidity chamber exposed the sample to unlimited water absorption and helped to show how this unlimited amount of water influenced the formation of hydraulic binding phases.

It is possible that some carbonation may occur as well with the samples placed in the humidity chamber as it is filled with 100% relative humidity air. The final curing condition, container cured, limited both the amount of drying and carbonation that occurred. Assuming that the samples were contained well enough to keep them air tight, then the container cured samples helped to show what strengths can be expected from the hydraulic phases only, as little carbonation is believed to have occurred in the container cured samples. They also showed the effect of drying as they retained their original moisture and water content and did not dry out like the air-cured samples.

1.5.2 Compression Testing

Testing was done on the cements after 14, 28, 90, and 180 d. In some of the experiments, tests were done after removing the samples from their cylinders at the 4 d mark to get initial information. At each testing date samples were compression tested according to ASTM C1231 and ASTM C0039. A minimum of 3 samples were tested at anytime to provide a statistical average and standard deviation. The compression tester was an Instron Load Cell 5800R (Norwood, MA). The samples were compression tested using steel caps with neoprene inserts to cap the top and bottom of the cylinders.

The fourth cylinder that was not compression tested but was cut and used for the following characterization methods: X-ray diffraction (XRD), scanning electron microscopy (SEM), thermogravimetric analysis (TGA), and phenolphthalein characterization. Figure 6 below shows how the characterization sample was cut and used for the various characterization tests.

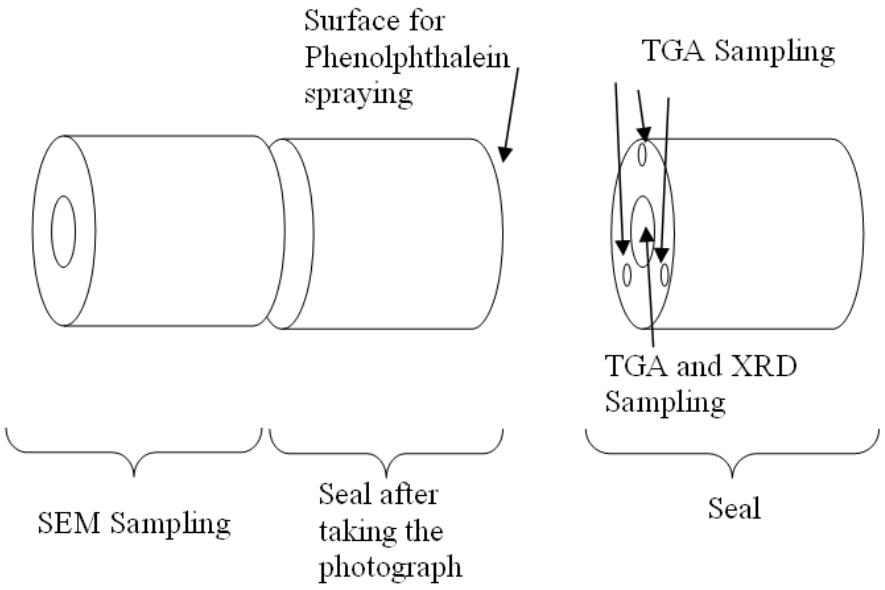

Figure 6: Sample Preparation for Characterization Tests
Showing how the 4th cylinder is cut for SEM, XRD, TGA, and Phenolphthalein characterization.

1.5.3 Phenolphthalein

The purpose of the phenolphthalein was to help indicate the level of carbonation that had occurred in the concrete samples. The concrete sample was cut in half using a hand saw and then the fresh cut surface was sprayed with 2% phenolphthalein indicator in ethanol (J.T. Baker, Phillipsburg, NJ). Areas of the concrete with a pH < 9.5 do not change in color, those areas which have a pH above 9.5 turn pink when sprayed with phenolphthalein.[53] When the phenolphthalein turns a pink color it indicates regions of the concrete which have not carbonated. This color change is due to the presence of OH- ions in the uncarbonated $Ca(OH)_2$ which has a high pH. In the areas in which carbonation has occurred and $CaCO_3$ has formed, the phenolphthalein does not change color as the

carbonated areas have a pH lower than 9.5. Although not an exact calculator of the level of carbonation, phenolphthalein tests help to visually show the extent of carbonation and the speed at which it occurs.[12]

After spraying with phenolphthalein the thickness of the carbonation ring and the diameter of the non-carbonated area were easily measured with a ruler. The surface was then photographed with a digital camera. Figure 7 below shows a NHL-5 natural hydraulic cement sample that was cured in ambient air for 14 d. The carbonated outer surface and uncarbonated pink regions can clearly be seen.

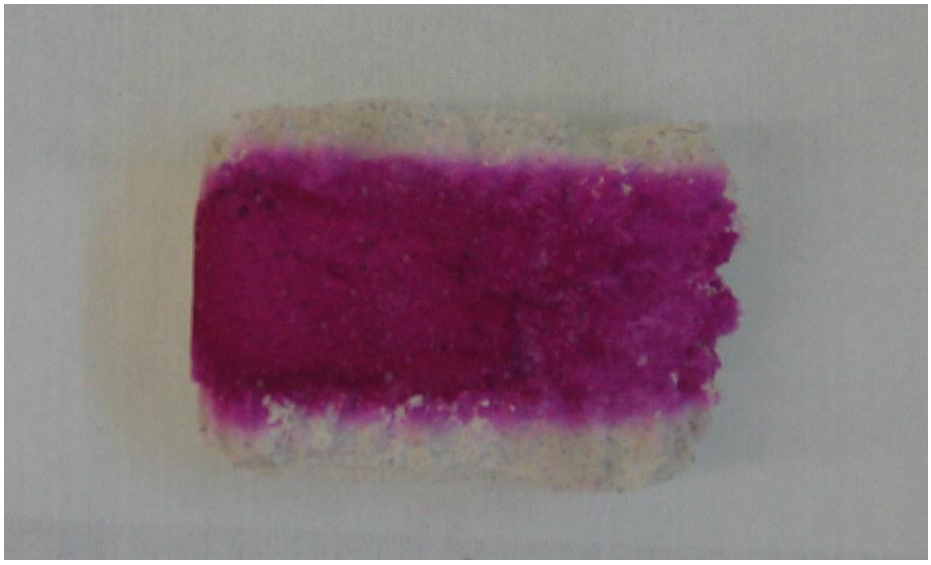

Figure 7: Natural Hydraulic Lime Mortar Phenolphthalein Test
A natural hydraulic lime mortar air cured for 14 d and then sprayed with phenolphthalein to show the carbonation ring. The pink area is un-carbonated; the cement colored area has absorbed CO_2 to form calcite, $CaCO_3$.

1.5.4 X-Ray Diffraction

At every testing date, samples were taken from the center section and outer surface of the 4th cylinder for XRD (Fig. 6). XRD can be used to identify the crystalline

phases in cement and how they change over time. It can also be used to identify the semi-crystalline C-S-H phases that form. The XRD samples were mixed with 16 wt% crystalline silicon standard (Alfa Aesar, Ward Hill, MA) at a ratio of 5:1 cement to standard. To make the XRD sample 0.25 g of concrete sample and 0.05 g of Si were mixed and ground to a fine powder using a mortar and pestle. The mixed powder was then placed on glass slides with ethyl alcohol. The samples were allowed to dry for at least 20 minutes prior to testing on the XRD. The XRD used was a Siemens D 500 X-Ray Diffractometer (Siemens, Karlsruhe, Germany). XRD was run from 10-70 degrees with a step size of 0.2 and a dwell time of 1 s, using a Cu Kα source, $\lambda = 0.154$ nm. The XRD diffractograms were subsequently analyzed with the software package MDI Jade 7 (MDI, Livermore, California).

1.5.5 Thermogravimetric Analysis, TGA

For TGA, samples were again taken from the center of the cylinder and from the outer surface of cylinder No. 4. 10-40 mg of the outer and center sections of the sample were heated at a rate of 20ºC/min from 50-800 °C in an air environment in the TGA (Perkin Elmer TGA 7, Waltham, MA). TGA shows the amount of unbound water, C-S-H, carbonation, and the amount of portlandite that remains in the sample. Unbound water is lost between 50-200 ºC, $Ca(OH)_2$, loses its bound water between 350-550ºC, and decarbonation of CO_2 from $CaCO_3$ occurs between 600-900ºC.[12] By measuring the weight loss between 350-550ºC the amount of un-carbonated $Ca(OH)_2$ that remains in the concrete can be calculated and compared to that present after the 180 d. This value of the

un-reacted portlandite can be calculated by taking the first derivative of the TGA data using a centered difference numerical differentiation equation.[12]

The TGA can also help determine if CSH is forming. Stepowska et al. writes that water is lost between 100-120ºC and CSH gel is lost between 200-400 ºC.[44] Lawrence, however, writes that CSH I and II form between 95-120ºC.[6] Both ranges overlap with the loss of unbound water in our cement samples and so separate freeze dried cement paste experiments were designed to determine the existence and extent of CSH formation. The cement paste experiments do not have limestone aggregate and so the possible issue of aggregate masking certain aspects of the thermal analysis curve is avoided.[55] Since there is some discrepancy in the literature in terms of what temperatures correspond to C-S-H weight loss in the TGA certain assumptions will be made going forward. It is assumed that in cement paste TGA, all weight loss from 50-400ºC is due to C-S-H, all weight loss from bound water in $Ca(OH)_2$ occurs between 400-600ºC, and weight loss from 600-800ºC is from decarbonation. These assumptions can not be made for TGA of samples that have not been freeze dried as the weight loss from 50-200ºC is from both unbound water and C-S-H. Therefore it is impossible to distinguish exactly how much C-S-H is lost in this region of the TGA data which has not been freeze dried. Figure 8 shows the results of a TGA conducted on a natural hydraulic lime and the various weight loss regions that are expected.[54,55]

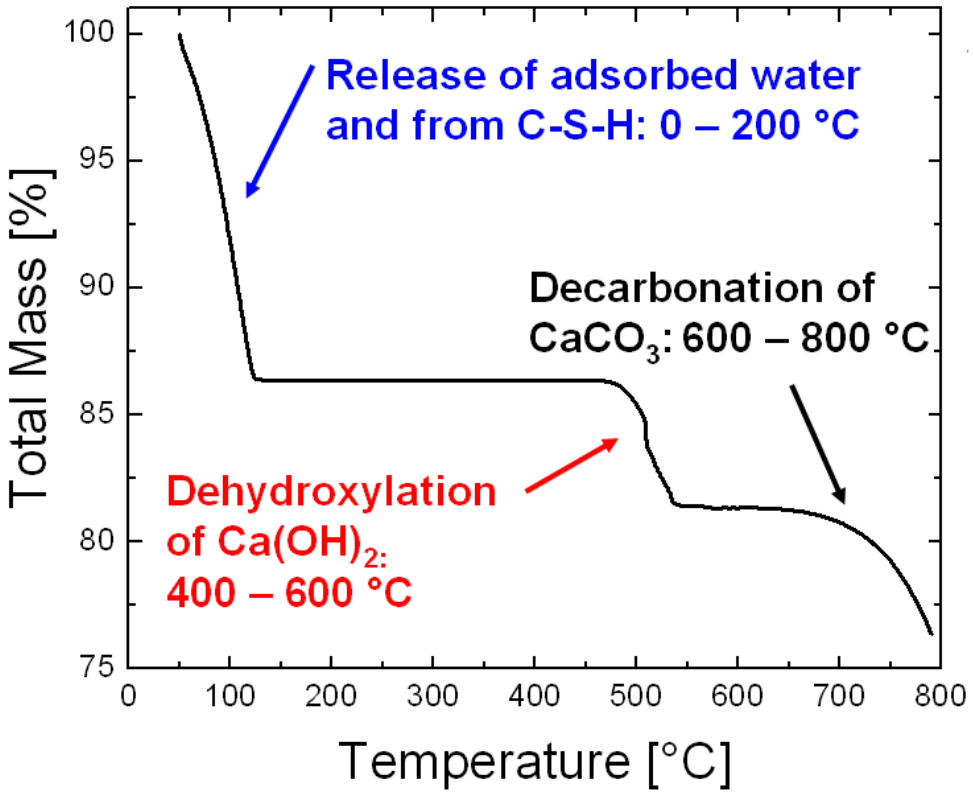

Figure 8: Sample Natural Hydraulic Lime TGA
TGA of a natural hydraulic lime mortar showing the loss of unbound water and C-S-H from 50-200 °C, dehydroxylation of $Ca(OH)_2$ from 400-600 °C, and the partial decarbonation of $CaCO_3$ from 600-800 °C.

1.5.6 SEM

For SEM analysis, a sample with length and width of approximately 0.5 inches was removed from the concrete sample. For each trial date there were 3 SEM samples, one from each curing environment. The samples were mounted in Bakelite using a Struers LaboPress-3 (Cleveland, Ohio). They were mounted by raising the thermoset Bakelite polymer to 180ºC for 7 minutes in the hot mount. Once mounted the samples were ground and polished using a Struers RotoPol-22. First the samples were ground for 5 minutes using 1200 grit grinding paper, a 10 N force, and 150 rpm. Once ground, the

samples were polished using Allied 3 μm and then a 1 μm polycrystalline water-based diamond suspension solution at the same force and RPM for 3-4 minutes. Once polished the samples were placed in an oven at 60ºC for 24 hours to remove unbound water absorbed during the grinding and polishing process. After 24 hours the samples were coated with platinum using a Cressington Sputter Coat 208 HR (Watford, England). The SEM used was a Zeiss Supra 50VP SEM (Thornwood, NY). During use, backscattering imaging was turned off and SEM images were taken using the secondary election mode. EDS mapping was conducted on the samples when appropriate using an EDS FEI XL30**.**

1.5.7 Sample Storage

Once the tests were complete the cut sections of the 4th sample were vacuum sealed using a FoodSaver® V2250 Vacuum Sealer to prevent carbonation. The sample was vacuum sealed just in case it needed to be looked again within a few days.

CHAPTER 2. 6 MONTH TRIAL

2.1 Introduction

The first set of experiments were created to help understand the long term strength development and characterization of hydraulic lime mortars with DE as the source of silica and limestone as the aggregate. Four different samples were created in July and August of 2008 to be tested after 14, 28, 90, and 180 D as described in section 1.5. The four samples consisted of 2 controls and 2 alkali activated fine-aggregate concretes using DE and lime.

The first control was a non-hydraulic lime with no added DE. The non-hydraulic lime cement served as a control to help understand what compressive strengths and properties can be achieved by lime mortars alone. Since non-hydraulic lime hardens only through the carbonation process this control shows what strengths result from the carbonation of lime to form calcite, $CaCO_3$ with no other hardening phases.

The second control was a naturally occurring hydraulic lime, NHL-5, from St. Astier France and distributed by US Lime Works in Milford Square, PA.[51] This material, NHL-5, has 23 wt,% calcium silicate (CS), and 43 wt% C2S (Table 4). By comparing the natural hydraulic lime with the non-hydraulic lime the effect of hydraulic binding phases on the strength and properties of the cements can be understood.

To compare to the controls, two hydraulic lime mortars with DE as the source of silica were created. The formulas are henceforth referred to as low and high DE formulas as one of them had a high amount of DE and the other had a low amount. The low DE formula had a Ca/Si ratio of 1.75, right around the typical Ca/Si ratio for OPC. The high

DE formula had a Ca/Si ratio of 0.28. The low and high DE samples are intended to shed light on a few different relationships. Since they are both artificial hydraulic lime mortars they can be compared to the natural hydraulic lime sample to see what difference results from adding silica (DE) to the lime as opposed to having it naturally occurring already. The low and high DE samples can also be compared to the non-hydraulic lime mortar sample to see how the existence of hydraulic phases, in addition to carbonation, affects the strengths and properties of the cement. Finally, by having two different formulas with varying amounts of DE the affect of Ca/Si ratio on the formation of hydraulic binding phases, C-S-H, strength, and properties can be analyzed. Table 6 below shows the formulas used for each of the four samples in the 6 month trial.

Table 6: 6 Month Trial Formulas

Formula	Water (ml)	Water weight %	Ca/Si ratio	DE (g)	CaO (g)	NHL-5 (g)	Limestone Aggregate (g)	Cement/ Agg Ratio	Slump (%)	Samples Made
Low DE	602	30.6	1.75	101	146	-	2234	1-2.67	18	6.88
High DE	1012	27.7	0.281	482	120	-	2040	1-1	10	9.6
Lime Mortar	818	29.5	-	-	336	-	1621	1-2.67	10	4.68
NHL-5	535	16.1	1.77	-	-	395	2384	1-2.67	20	7.25

A few comments should be made about Table 6. Initial testing was conducted on the low DE formula to determine the correct amount of water necessary to have a fine-aggregate concrete with good workability. The same procedure was conducting on the remaining three formulas to vary the amount of water added until a concrete with similar good workability was found. By using this method of trial and error with the water the formulas had slightly different consistencies.

One way to gauge the accuracy of the workability between the four formulas was to use a slump test based on ASTM C0192. The bottom of a paper cup was cut out for use in the slump test and the cup was placed on the table with cut bottom facing up. In this set up the cup becomes an open ended cone with the wide base on the table. The fine aggregate concrete was then poured into the cup in two layers by pouring and then rodding after each layer. The top of the cement was leveled off and then the paper cup was lifted allowing the concrete to slump down. The height of the slump was measured and compared with the initial cup height to produce the percent slump values listed in Table 6. The slump values for the four samples shows that the workability was kept fairly consistent but not perfect as the slump varied from 10-20%.

The other discrepancy that should be noted from the formulas in Table 6 has to do with the cement to aggregate ratios. The cement-to-aggregate ratios were determined from a volume stand point not from a mass ratio. This was done in case the formulas were ever used in a country or location which didn't have access to a scale. The description of a formula with a cement-aggregate volume ratio could say add 2 buckets of aggregate to every 1 bucket of cement and be accurate without having to weigh out the specific mass of each material. Table 6 shows that the high DE formula has a lower cement-aggregate ratio than the low DE, NHL-5, and lime mortar samples. This means that the high DE formula has less aggregate than the other formulas.

This discrepancy in cement-aggregate ratios occurred because the high DE formula was created from a side set of experiments aimed to understand the effects it had on the strength and properties of the concrete. A Design of Experiment (DOE) software was used for this set of experiments. Unfortunately the side DOE experiment did not

work due to the inability to properly control the water and aggregate content in the formulas generated by the DOE. Almost all of the formulas generated by the DOE were unworkable due to this water/aggregate issue. One of the only formulas from the DOE that did work was the high DE and therefore it was added to the 6 month trial set of experiments in the summer of 2008. The effect of having a lower vs. higher cement-aggregate ratio in the high DE formula will be discussed in detail later in this chapter and in Ch. 5.

Once the correct amount of water was determined for each formula, 48 2”x4” cylinder samples of each formula were produced according to ASTM C0192 (see section 1.5). The samples were removed from their cylinders after 4 d and placed in the following curing environments: in ambient laboratory conditions (air samples), in a 100% relative humidity chamber (humidity samples), and left in their original cylinder and covered with plastic wrap (contained until testing date and then demolded). It should be noted that the lime mortar formula did not have an exact container curing environment. Since non-hydraulic lime mortars harden only through carbonation it would be impossible for the lime mortar formula to harden in the container curing environment which is meant to prevent exposure to air and carbonation. The container curing environment for the lime mortar formula consisted of the samples being kept in their cylinders but not covered with plastic wrap. This set up attempted to simulate the curing that occurs in lime mortar used as a mortar between stones as only the top of the cylinder is exposed to air and carbonation.

Each formula was tested at 14, 28, 90, and 180 d. At each testing date and for every specific formula, 4 samples were taken from the 3 curing environments for a total

of 12 samples per formula per testing day. The first 3 samples from each curing environment were compression tested according to ASTM C1231 and C0039. The 4th sample from each curing environment was used for XRD, TGA, SEM, and phenolphthalein testing as described in section 1.5. After characterization the 4th sample was vacuum sealed and saved in case further testing was needed within a few days.

2.2 Results and Discussion

2.2.1 Compressive Strength Testing Results

Figure 9 shows the compression testing results from the high DE formula after testing at 14, 28, 90, and 180 d.

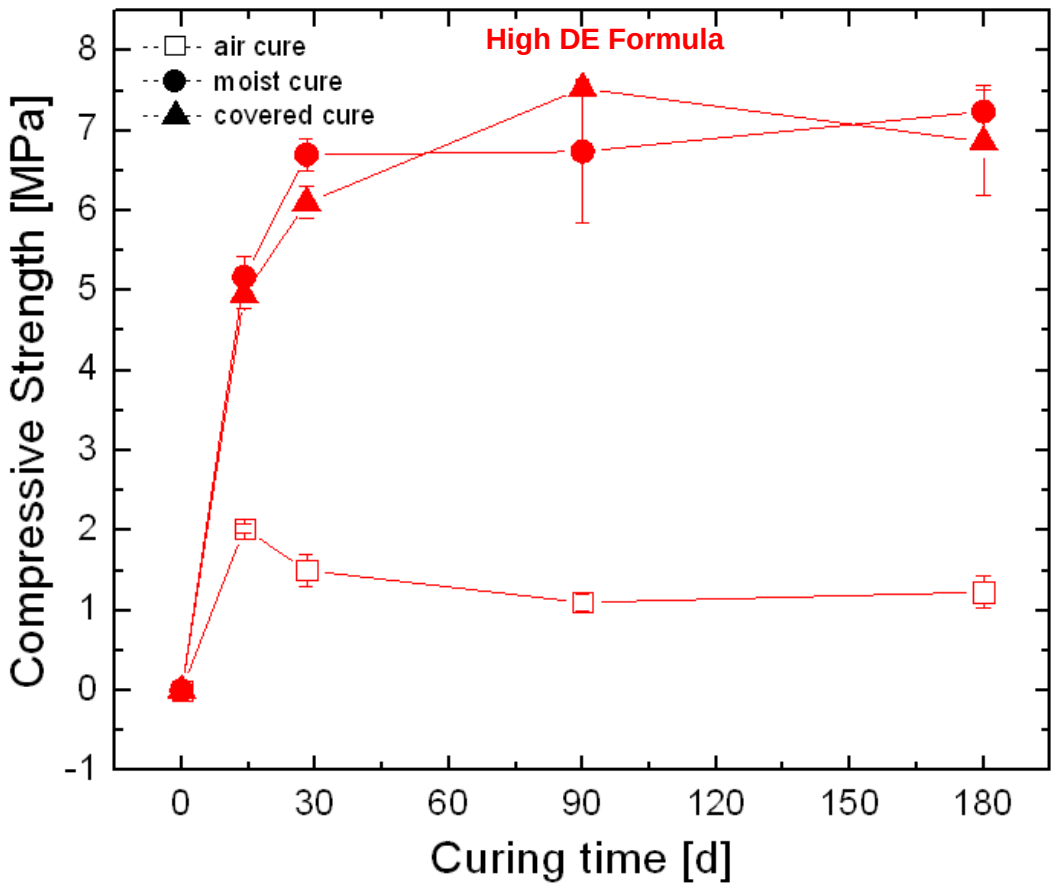

Figure 9: High DE Formula Compressive Strength as a Function of Time.

The reason that the high DE formula results were shown first is because they show a general trend in the data that occurs in the rest of the formulae. Figure 9 shows that the highest strength values occur in those samples which were cured in the containers or high relative humidity chamber. The lowest strengths occurred in the samples which were left in ambient air to cure. This data supports the conclusion that water is important for strength development in alkali-activated concretes with DE as the source of silica. As the air cured samples dry out they lose their unbound water. This unbound water is needed for the formation of C-S-H and for carbonation. Once the sample dries it loses the ability to form hydration phases and it makes the formation of calcite due to carbonation

more difficult as there is less pore water for CO_2 to dissolve in and combine with $Ca(OH)_2$.[12] Water is also needed for the dissolution of DE to dissolve Si ions so that they can form C-S-H. As the air cured samples dry out, the DE can no longer dissolve and therefore it is likely that more undissolved diatoms will be seen during SEM imagining in the air cured samples.

The strength of the air cured samples peaks after 14 d at which point it has the highest water content and has not fully dried out yet. After 14 d the sample is almost completely dry and the strength levels out around 1.2 MPa in the high DE formula. The reason for the decrease in strength as the sample dries past 14 d will be discussed in more detail in section 2.2.2 and in Ch. 5.

The humidity and container cured high DE samples in Figure 9 do not have the same issues as the air cured samples. They presumably retain their water over the 180 d and in the case of the humidity chamber samples, have unlimited water over that time period. This ability to retain water and not dry out allows the humidity and container cured samples to form hydraulic C-S-H binding phases over time. This leads the humidity and container cured high DE samples to have high strengths around 7 MPa after 180 d.

Figure 10 and Table 7 below show the compressive strength data from all four formulas over the 180 d testing period.

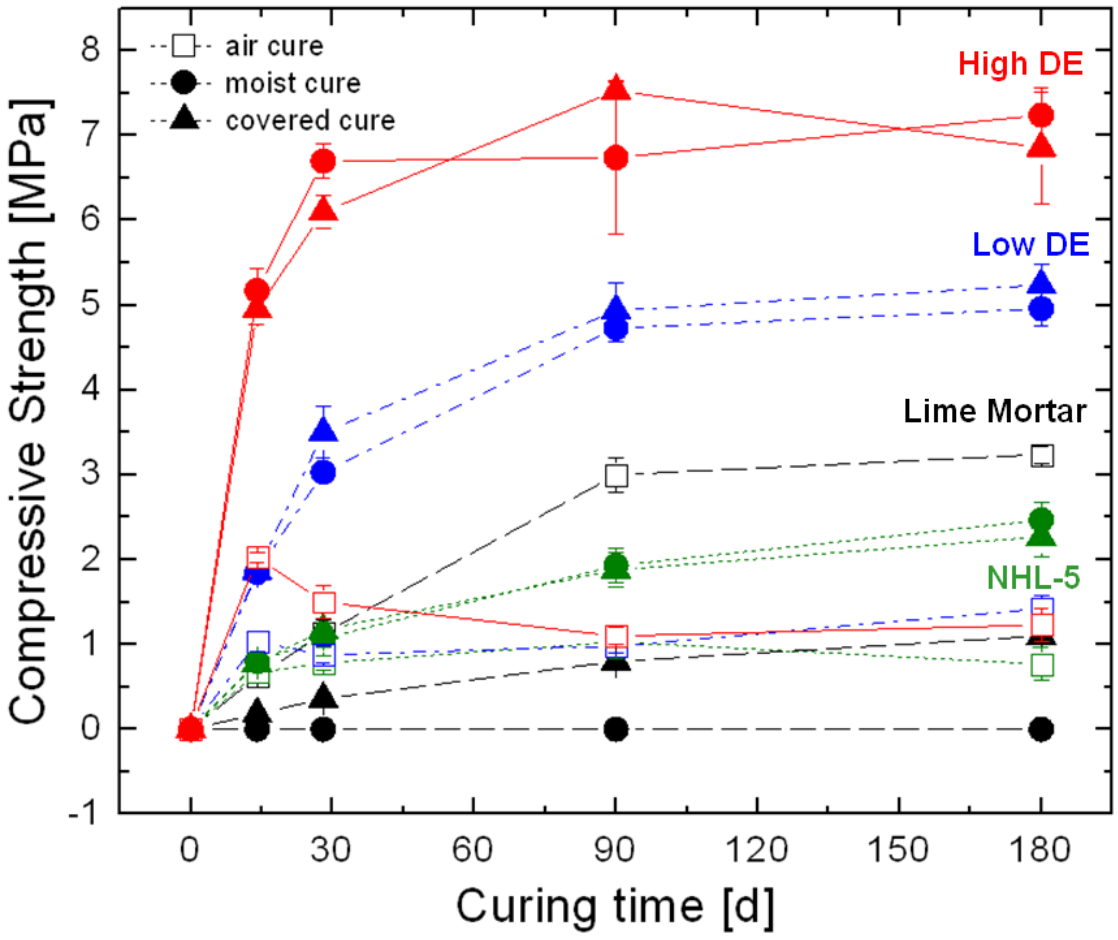

Figure 10: Time Dependence of Compressive Strength
Compressive Strength of high DE (red), low DE (blue), lime mortar (black), and Natural Hydraulic Lime NHL-5 (green) formulas after 180 d.

Table 7: 6 Month Trial Compressive Strength
The strength of each of the 4 formulas after curing in air, in the humidity chamber, and in the container curing environment.

Humidity Chamber Curing			**Strength (MPa)**		
Formula	**14 day**	**28 day**	**90 day**	**180 day**	**Error +/-**
Low DE	1.85	3.03	4.73	4.96	0.3
High DE	5.17	6.63	6.74	7.24	0.45
NHL-5	0.8	1.07	1.93	2.47	0.11
Lime Mortar	0	0	0	0	0

Container Curing

Formula	14 day	28 day	90 day	180 day	Error +/-
Low DE	1.87	3.5	4.94	5.24	0.3
High DE	4.95	6.1	7.53	6.86	0.33
NHL-5	0.78	1.17	1.88	2.27	0.2
Lime Mortar	0.16	0.36	0.8	1.1	0.1

Ambient Air Curing

Formula	14 day	28 day	90 day	180 day	Error +/-
Low DE	1.03	0.88	0.98	1.42	0.13
High DE	2.03	1.39	1.1	1.23	0.2
NHL-5	0.67	0.78	1.03	0.77	0.14
Lime Mortar	0.62	1.13	3	3.24	0.16

Figure 10 shows that the low DE formula had the same correlation between curing environment and strength as did the high DE formula in Figure 9. In the low DE formula, the humidity and container cured samples had the highest strength at approximately 5 MPa after 180 d. The air cured low DE sample peaked in strength at 14 d and then decreased in strength as the samples dried out and lost all unbound water. Once dry, the air cured low DE samples had strength around 1.4 MPa, slightly higher than the high DE formula at 180 d. This is the only curing environment in which the low DE formula had similar strengths to the high DE formula as the high DE formula humidity and container cured samples had the highest strengths of all the four materials tested over the 180 d trial. Figure 10 shows that the second highest strength came from the low DE humidity and container cured samples.

The natural hydraulic lime NHL-5 formula showed the same correlation between curing environment and strength as did the DE formulae. The highest strengths occurred

in the container-cured and high humidity curing environments, while the air cured had the lowest strength. This is again a result of water retention and the need for water for the formation of the hydraulic phases and carbonation. As the air cured sample dries it loses the ability to form hydraulic phases and there is less pore water for CO_2 to dissolve in and combine with $Ca(OH)_2$ to form calcite. Another observation that can be made about the NHL-5 strength data is the fact that after 180 d it has less than half the strength of the artificial hydraulic lime low and high DE formulas. This shows that creating hydraulic lime mortars through the addition of DE as a source of silica can give better strengths when compared to a natural hydraulic lime.

The third highest strength in Figure 10 came from the lime mortar air cured samples. This contradicts the relationship between curing environment and strength seen in the NHL-5, low and high DE formulas. The lime mortar formula had its highest strength when air cured and its lowest strength when cured in the high humidity chamber. This is an interesting result for a few reasons. The fact the air cured lime mortar had the 3rd highest strength of the 4 formulas after 180 d, and the fact that the air cured lime mortar sample hardens only through carbonation shows that carbonation can produce high strength concrete over time. The strength of the air cured lime mortar sample is able to reach 3.2 MPa after 180 d, without hydraulic binding phases. It is more than likely that the strength of the air cured lime mortar sample would have continued to increase past 180 d had the experiment been carried on further. This hypothesis is supported by the characterization testing discussed later in this chapter showing a large amount of portlandite that remains uncarbonated in the air cured lime mortar after 180 d and which therefore is free to carbonate and strengthen the concrete in the future.

The low strengths of the open container cured lime mortar and the lack of any strength in the humidity cured lime mortar is another interesting result to be discussed from Figure 10. It is understandable that the open container cured sample had low strengths due to the fact that only the top of sample was exposed to air and carbonation. It therefore had much less surface area for the CO_2 to penetrate and form strength compared to the air cured samples which are exposed on all sides of the cylinder except the base. This idea was supported by observations of the open container cured samples over the 180 d that the base of the samples remained soft due to the lack of carbonation. This soft base explains the extremely low strength of the open container cured lime mortar samples and also explains why lime mortars are the preferred choice for mortars in ancient stone buildings. Since it takes a long time for carbonation to reach the center of the lime mortar between stones those central areas remain soft and can accommodate shifts or stresses in the stone building prior to hardening over time.

During the initial stages of the 6 month trial it was unclear as to why the humidity cured lime mortar samples were not hardening at all. The samples are exposed to air in the humidity chamber and so they should form some calcite. The reason they do not harden in the humidity chamber can be explained as follows. The excess water that covers the lime mortar samples in the humidity chamber prevents carbonation from happening. Therefore all that the lime mortar samples were doing in the humidity chamber was aging. One conclusion that can be drawn from this data is that with any lime mortar or hydraulic lime mortar, carbonation cannot occur when there is excess water to impede the formation of calcite. This is a well known phenomenon in the field of lime mortars which occurs because lime mortars placed under water to age or in humidity

chambers will form a thin layer of carbonated lime on the surface of the material. This thin layer of carbonation impedes further carbonation as it acts as a diffusion barrier to CO_2. As a result, carbonation of lime mortars mainly occurs during drying. As the lime mortar dries, water leaves the samples through porous microstructure at the same time allowing CO_2 to diffuse through these pores and form calcite deep in the sample. Once the lime mortar is dry, the rate of carbonation slows as the concentration of water and CO_2 is low. Thus it can take months to years for lime mortars to fully carbonate and harden.[8,9]

The fact that the air cured lime mortar samples were almost 3 times stronger than the air cured low and high DE samples after 180 d brings up a question about these formulae. If these samples were hardening solely through carbonation then the air cured lime mortar samples have shown that the DE samples should have higher strength than they do. The low strength of the air cured samples in these two formulae must therefore have something to do with the DE and hydraulic binding phases which make the low and high DE formulas different from the lime mortar formula. The issue of drying and strength retention in the air cured low and high DE formulas is something that needed to be investigated.

2.2.2 Strength Retention Tests

During the 6 month trial a side set of experiments was set up to analyze the issue of strength retention in the low and high DE formulas as they were exposed to ambient air and dry out. After the 90 d testing, 3 samples were removed from the humidity

chamber and 3 from the container curing environments for a total of 12 samples from the low and high DE formulas. These demolded samples were allowed to dry in ambient air conditions for 7 d and then compression tested. Figure 11 shows the compressive strength of the high DE formula after the 7 d of air drying (97 d mark). Figure 12 shows the compressive strength of the low DE formula after 7 d of drying (97 d mark).

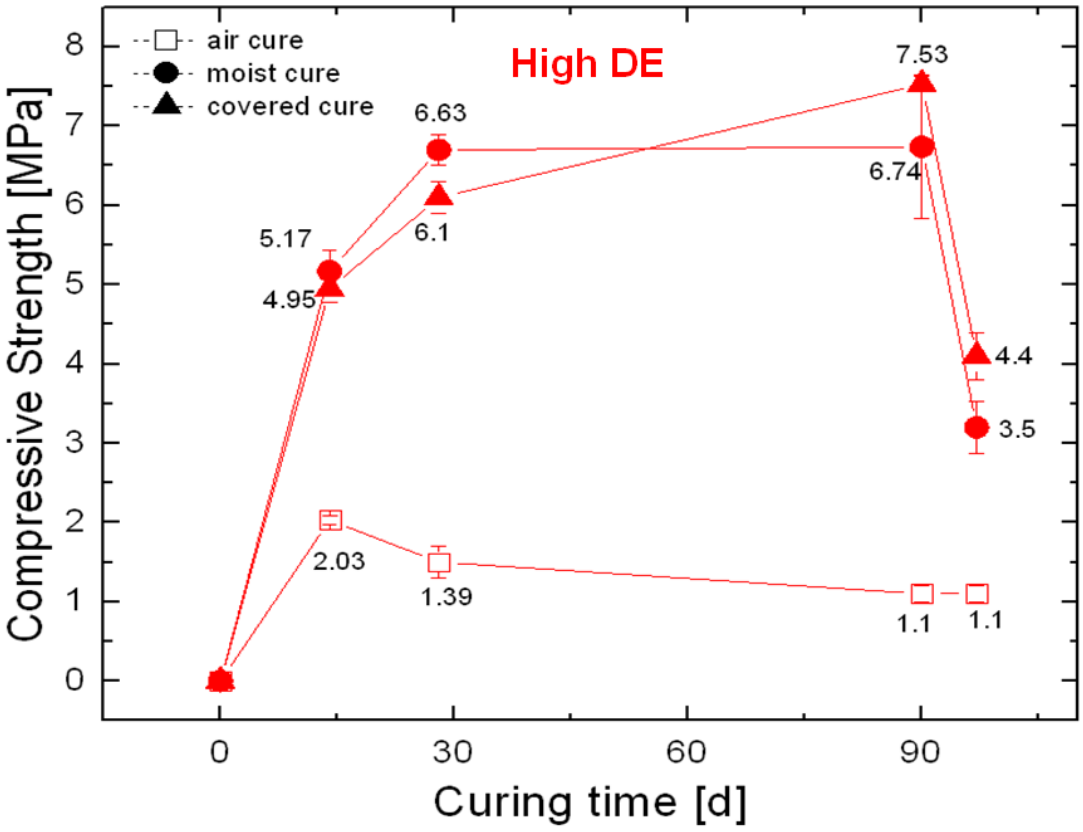

Figure 11: High DE Strength Retention as a Function of Time and Environment
Compressive strength of the high DE formula showing large strength losses as the humidity chamber and container cured samples were allowed to air dry for 7 d prior to testing at the 97 d mark.

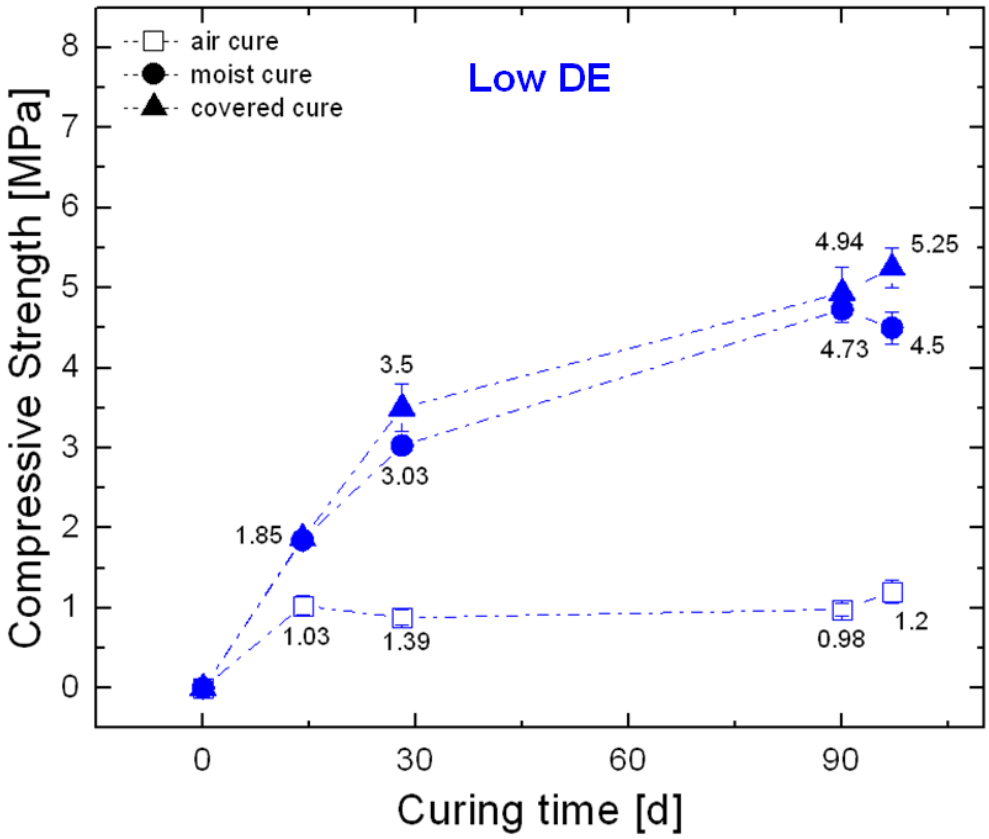

Figure 12: Low DE Strengths Retention as a Function of Time and Environment
Compressive strength of the low DE formula showing minimal to no strength loss as the humidity chamber and container cured samples were allowed to air dry for 7 d prior to testing at the 97 d mark.

Figure 11 and Figure 12 show that there is a major difference between the low and high DE formulas when it comes to strength retention. After air drying for 7 d the humidity and container cured 90 d high DE samples in Figure 11 lost almost half of their strength. This is a major concern for possible use of the high DE formula in third world or other applications. If it is a concrete that only has good properties when wet, then there are little to no applications where it can be used besides maybe the rain forest or under water.

The low DE humidity and container cured samples in Figure 12. however, do not show the same strength loss as the high DE formula. After being air dried the humidity chamber or moist cured samples as they are labeled in the graph, lose around 0.2 MPa which is within the standard deviation for the data. The container-cured samples actually show a slight strength increase after being air dried for 7 d, also within the standard deviation of the data. So the question becomes why does the strength of the high DE formula drop drastically once dry, but the same does not occur for the low DE formula?

The answer lies in the amount of DE used in each formula. It is hypothesized that the high DE formula has so much excess DE that once dry if these diatoms have not dissolved and formed hydraulic C-S-H then they become micron size defects scattered throughout the concrete. The result of this excess dry DE cuts the strength of the fine-aggregate concrete in half. Since the low DE formula has a higher Ca/Si ratio and a lower amount of DE it is suspected that less un-dissolved diatoms exist throughout the concrete to cause the same strength retention problems. With fewer diatoms in the formula, there is less of a chance of undissolved diatoms becoming micron size imperfections once dry. This may explain why the high DE formula drops in strength and why the low DE formula has good strength retention once dry.

To confirm whether this strength loss occurs at times other than the 97 d mark the same strength retention tests were carried out after 180 day. Table 8 shows the strength retention data from the 97 d tests and from the 187 d tests.

Table 8: Low DE and High DE Strength Retention Data

Strength retention in the a) low DE and b) high DE formulas after the 97 and 187 d compression tests. The good strength retention of the low DE formula and poor strength retention of the high DE formula is clearly shown.

a) Low DE Strength Data

	90 day Strength (MPa)	After 7 Days of Air Dry (MPa)	Change in Strength	% Change
Air	0.98	1.2	0.22	22.03
Humidity	4.73	4.5	-0.23	-4.93
Container	4.94	5.25	0.31	6.20
	180 day Strength (MPa)	**After 7 Days of Air Dry (MPa)**	**Change in Strength**	**% Change**
Air	1.42	1.4	-0.02	-1.41
Humidity	4.96	5.2	0.24	4.84
Container	5.24	5.15	-0.09	-1.72

b) High DE Strength Data

	90 day Strength (MPa)	After 7 Days of Air Dry (MPa)	Change in Strength	% Change
Air	1.10	1.1	0.00	0.00
Humidity	6.74	3.2	-3.54	-52.50
Container	7.53	4.1	-3.43	-45.58
	180 day Strength (MPa)	**After 7 Days of Air Dry (MPa)**	**Change in Strength**	**% Change**
Air	1.23	1.2	-0.03	-2.44
Humidity	7.24	4.1	-3.14	-43.37
Container	6.86	4.19	-2.67	-38.92

Table 8 shows that after 7 d of drying the 180 d humidity and container cured high DE samples had the same strength retention issues. After the 187 d tests the high DE humidity samples lost 43% of their strength and the container cured samples lost 39% of their strength. Just as before however, the low DE formula showed good strength retention at the 187 d test after 7 d of air drying. The strength loss or gain of the low DE formula at 187 d is within standard deviation of the data.

To confirm the hypothesis that excess diatoms cause the strength drop in the high DE formula the next step was to use SEM imaging and EDS mapping to try to find evidence for these undissolved diatoms in the fine-aggregate concrete.

2.2.3 SEM Imaging and EDS Mapping

SEM images were taken at every testing date after mounting and polishing the concrete samples. The SEM images taken throughout the 180 d tests confirm the idea that the reason the high DE formula has such poor strength retention is due to the existence of excess undissolved diatoms throughout the concrete which become basically defects once dry. Figure 13 below shows SEM images of the high and low DE samples which have been cured in the humidity chamber for 14 d.

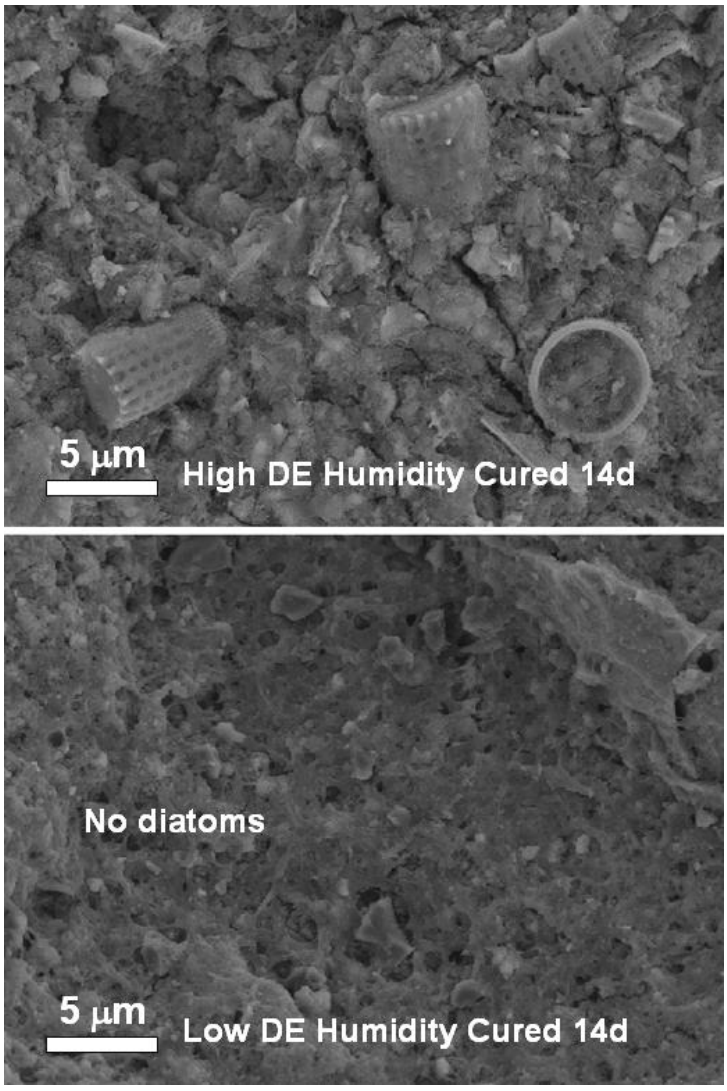

Figure 13: SEM Images of High and Low DE Humidity Cured Samples After 14 d
The top high DE image shows undissolved diatoms are clearly visible, and vise-versa for the low DE sample (bottom micrograph).

Figure 13 shows that in the high DE air-cured sample it is easy to spot undissolved and partially dissolved diatoms on the surface of the cut and polished samples. The bottom image in Figure 13 shows that it is more difficult to spot diatoms on the surface of the cut and polished low DE sample. The leafy like structure seen in the low DE image is C-S-H hydraulic binding phase between limestone aggregate. These

images confirm that there are much more undissolved diatoms in the high DE formula and support the explanation for the strength loss upon drying seen in the high DE formula. The container cured samples in Figure 14 show very similar images after 14 d. It is easy to spot undissolved diatoms in the top high DE container cured samples, and difficult to spot them in the low DE container cured samples.

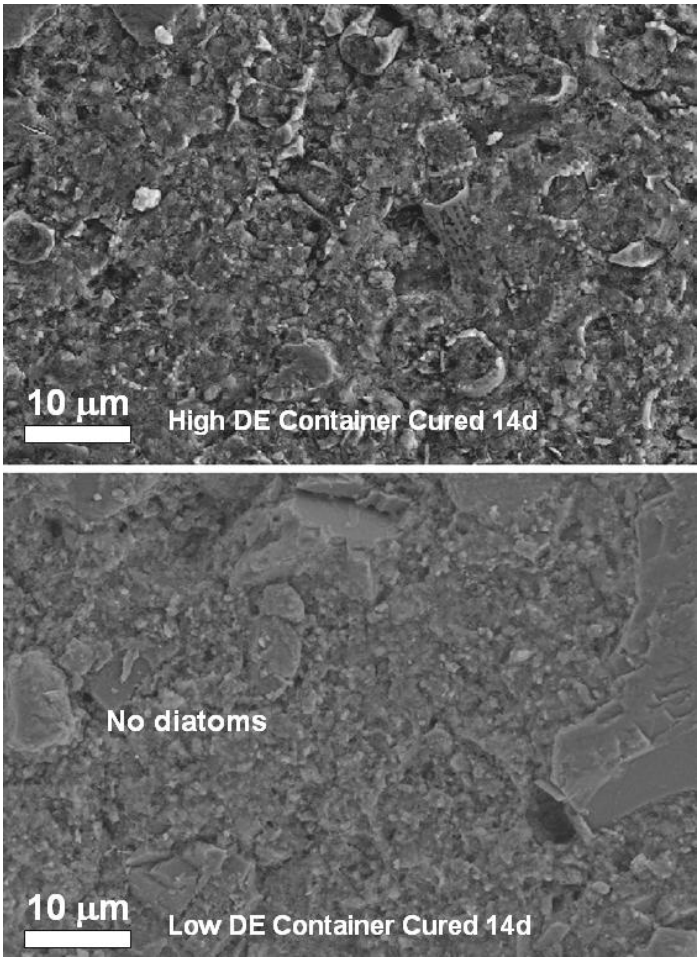

Figure 14: SEM Images of High and Low DE Container Cured Samples After 14 d
The top high DE image again shows that it is easy to spot undissolved diatoms on the surface of the sample. The bottom image again shows that it is difficult to spot undissolved diatoms under SEM on the low DE sample.

.

The one place where it was easier to spot undissolved diatoms after 14 d with the low DE formula was in the air-cured samples. Figure 15 shows SEM images of high and low DE samples after 14 d of air drying.

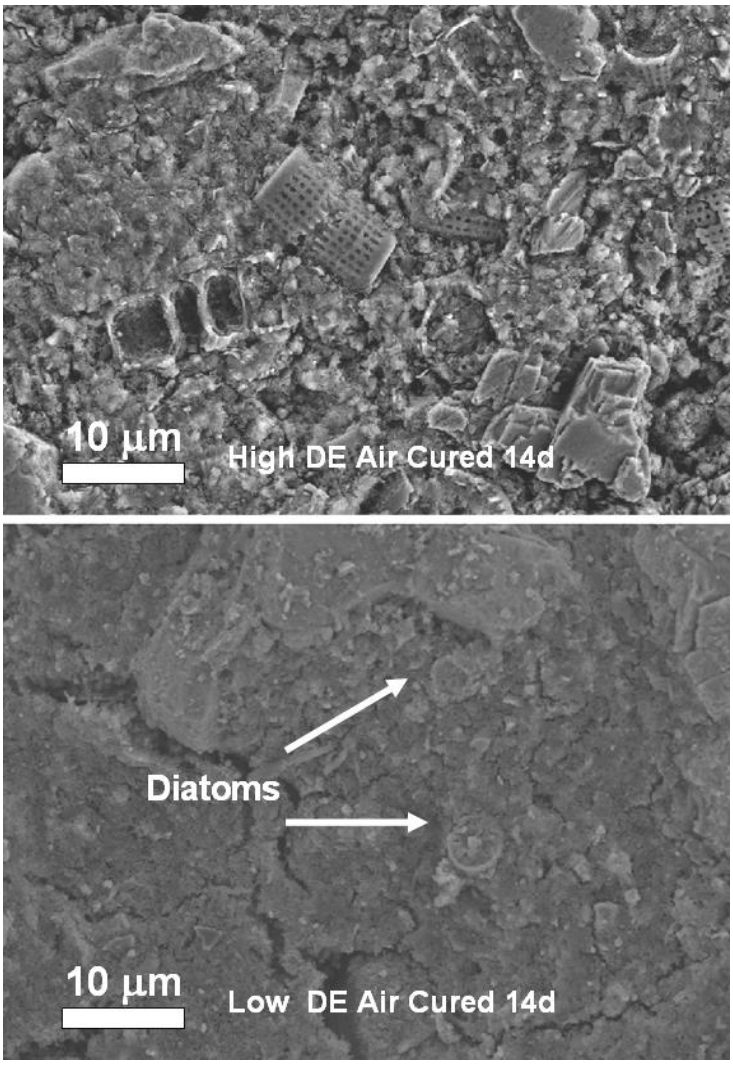

Figure 15: SEM Images of High DE and Low DE Air Cured Samples After 14 d
The top high DE image again shows that it is easy to spot undissolved diatoms on the surface of the sample. The bottom image shows that diatoms can be spotted more easily in the air cured low DE samples than in the humidity or container cured.

Figure 15 shows that it is much easier to find undissolved diatoms on the surface of the low DE air cured samples compared to the low DE humidity or container-cured samples. The images support the idea that as the samples dry out in air there no longer is water for DE dissolution and C-S-H formation. Thus undissolved diatoms are visible on the surface of both the low and high DE samples and their previously reported strengths are low. The cracking seen in the bottom low DE image of Figure 15, is most likely due to drying after mounting and polishing the samples.

The same correlation between high DE vs. low DE and the ability to see undissolved diatoms remained the same throughout the 180 d of testing. Figure 16 below shows the high and low DE humidity, container, and air-cured SEM images after 180 d.

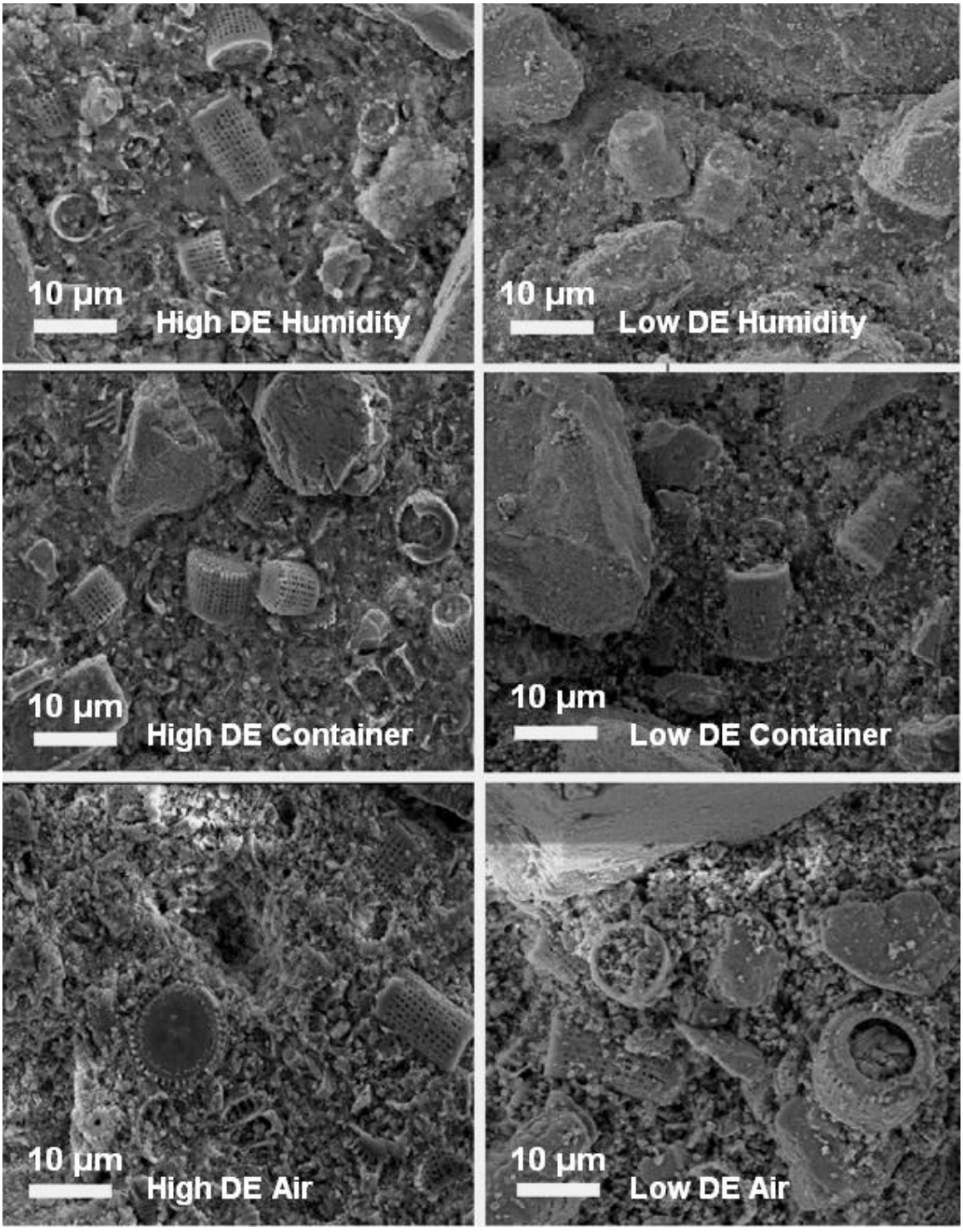

Figure 16: SEM Images of High DE and Low DE Air Cured Samples After 180 d
Diatoms can be seen in images of the humidity and container cured high and low DE samples. The low DE diatoms appear to be more dissolved however.

Figure 16 shows that just like with the 14 d SEM images, both the air cured low and high DE samples have undissolved diatoms. After the 14 d mark the low and high DE air-cured samples were almost completely dry and so their diatoms no longer were able to dissolve and form C-S-H. As a result many undissolved diatoms of the air cured samples remain after 180 d of curing.

Although it is possible to see diatoms on the surface of the low DE samples after 180 d as shown in Figure 16, it was still more difficult than finding diatoms on the high DE sample surfaces. One difference that can be seen between the diatoms on the surface of the low DE and the high DE samples is their level of dissolution and surface morphology. The top two images in Figure 16 show that the low DE diatoms appear to be more dissolved than the high DE humidity cured diatoms. If looked at closely it can be seen that the diatoms in the low DE image do not have holes on the sides of the diatom barrels. These holes are clearly seen in the high DE diatoms. The reason that the holes are not clearly seen in the low DE image is because they have been filled by the formation of C-S-H. Figure 17 below shows a higher magnification image of the low DE humidity cured diatom after 180 d from Figure 16.

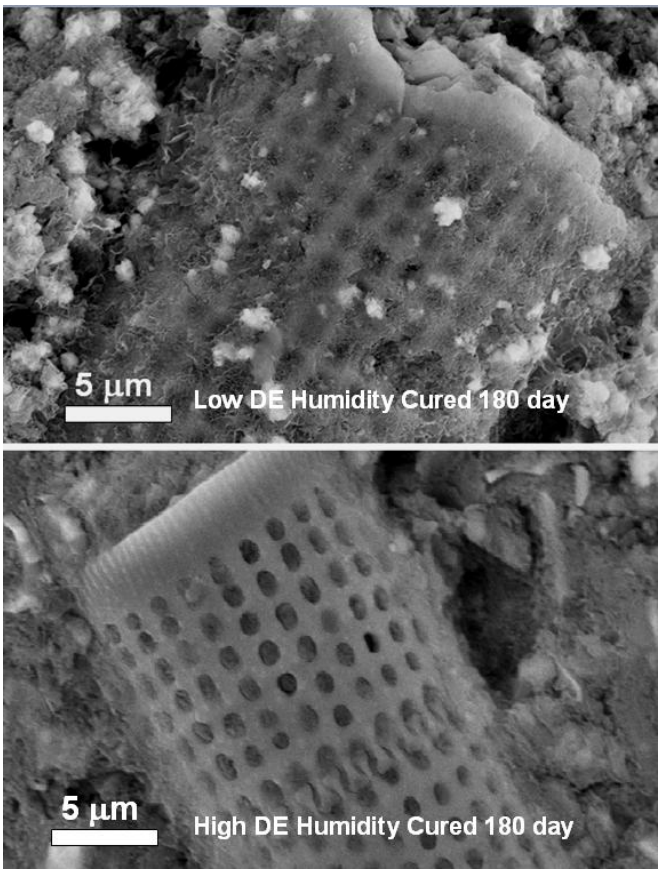

Figure 17: SEM Image of a Low and High DE Humidity Cured Diatom After 180 d
The leafy structure associated with C-S-H can be seen between the holes of the low DE diatom wall. The high DE diatom shows very little leafy structure.

The top image in Figure 17 shows that the low DE diatom surface has begun to react and form a hydraulic binding phase after 180 d of being in the humidity chamber. The high DE diatom however, appears to be in nearly perfect condition as it is evident that it has dissolved very little after 180 d. By going at higher magnification with the SEM some interesting C-S-H hydraulic binding phase structures can be seen in the low and high DE samples. Figure 18 below shows 2 high magnification SEM images of a low DE container cured diatom after 28 d.

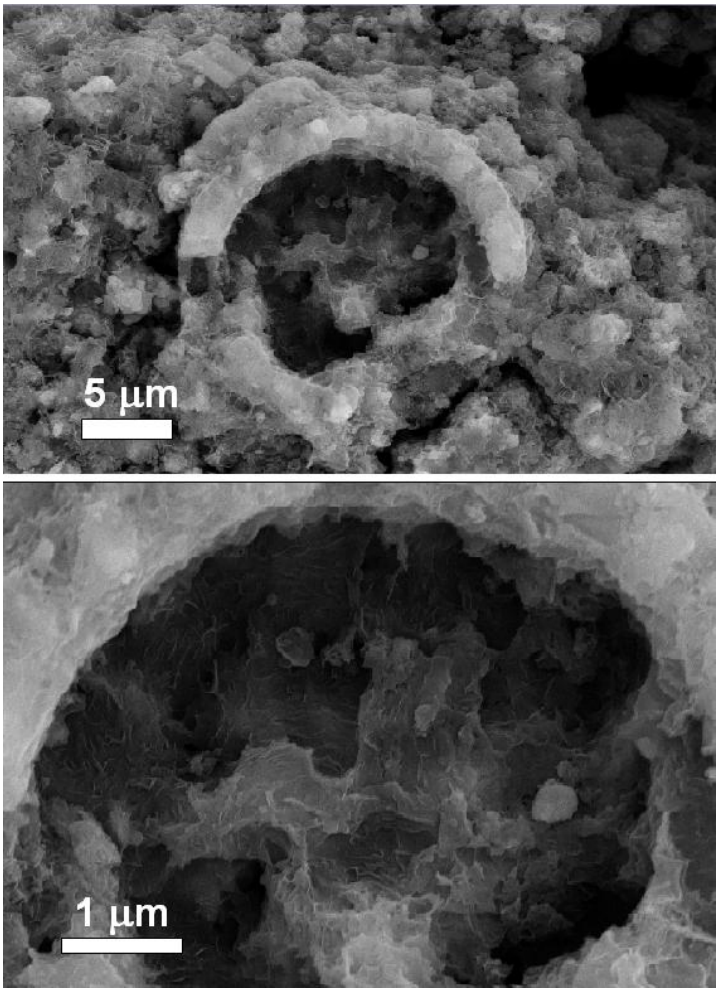

Figure 18: SEM Image of a Low DE Container Cured Diatom After 28 d
The leafy structure associated with C-S-H can be seen on the surface and in the center of the diatom barrel.

Figure 18 shows the leafy C-S-H structure on the surface and inner regions of a diatom from the low DE container cured sample at 28 d. The existence of C-S-H within the diatom is important for strength development and retention. Once the diatom is fully dissolved it is no longer a hollow cylinder which when dried and undissolved negatively impacts the concrete's strength. As discussed, it is easy to find undissolved diatoms on the surface of the high DE samples. It is also easy however, to find regions of fully dissolved diatoms. Figure 19 shows a high DE humidity-cured diatom after 28 days.

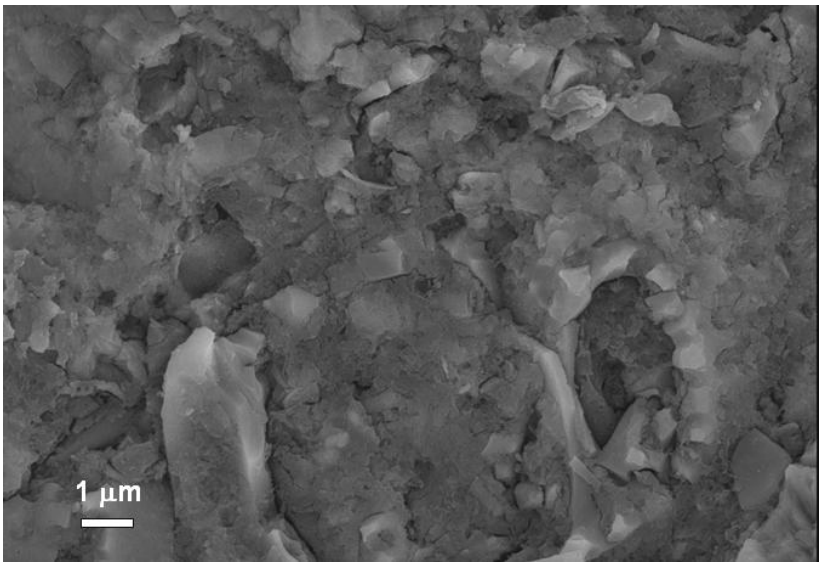

Figure 19: SEM Image of a High DE Humidity Cured Diatom After 28 d
The diatom can be seen partially dissolved and encompassed in C-S-H.

The high DE formula diatom in Figure 19 is partially dissolved and as a result is encompassed in a leafy C-S-H structure. It is the existence of a network of dissolved diatoms which we believe gives the high DE formula its strength. In an ideal system each diatom would be dissolved during the cement mixing phase and the dissolved Si ions from the diatom would be free to combine with Ca ions in solution to form a network of C-S-H. Such a network is formed in the low and high DE formulas. Figure 20 shows a high magnification SEM image of the C-S-H network in the low DE sample which has been cured in ambient air for 28 d.

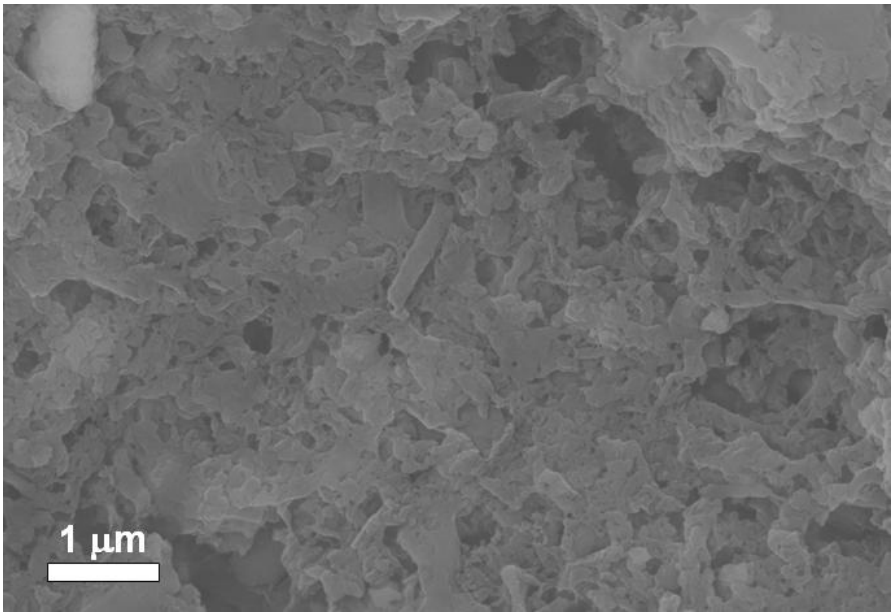

Figure 20: SEM High Magnification Image of C-S-H
The leafy C-S-H can be seen bridging and binding together in this SEM of a low DE air cured sample after 28 d.

Figure 20 shows a great image of the C-S-H formed in the low DE samples. The branches and bridges of C-S-H can be seen binding to each other. With the SEM images described and previously discussed compressive strength data, the question becomes if there are so many undissolved diatoms on the surface of the high DE formula which have not formed any binding phase yet why does the high DE formula has higher strength than the low DE formula?

The answer may be that the undissolved diatoms seen throughout the high DE samples are only a fraction of the diatoms in the formula. The rest of the diatoms have reacted and formed C-S-H hydraulic phases that give the high DE formula its high strength compared to the rest of the formulas in the 6 month trial. The low DE formula has fewer diatoms and so almost all of them have been dissolved to form C-S-H with little to no excess DE to cause the same strength retention issues that the high DE formula

has. The lower compressive strengths of the low DE formula most likely results from the fact that it has less diatoms and thus ultimately less hydraulic binding phase. The high DE formula is working in the opposite manner with more DE than is required to form the optimum amount of hydraulic binding phase. To further test this idea a set of experiments was set up to alter the Ca/Si by adjusting the amount of DE added to concrete (see Ch. 5).

Another possible answer to the question was thought to be the distribution of C-S-H. It was thought that maybe the low DE has just pockets of C-S-H, whereas the high DE has C-S-H throughout the samples. Figure 21 shows EDS conducted on a 28 d humidity chamber-cured high DE sample to investigate this hypothesis.

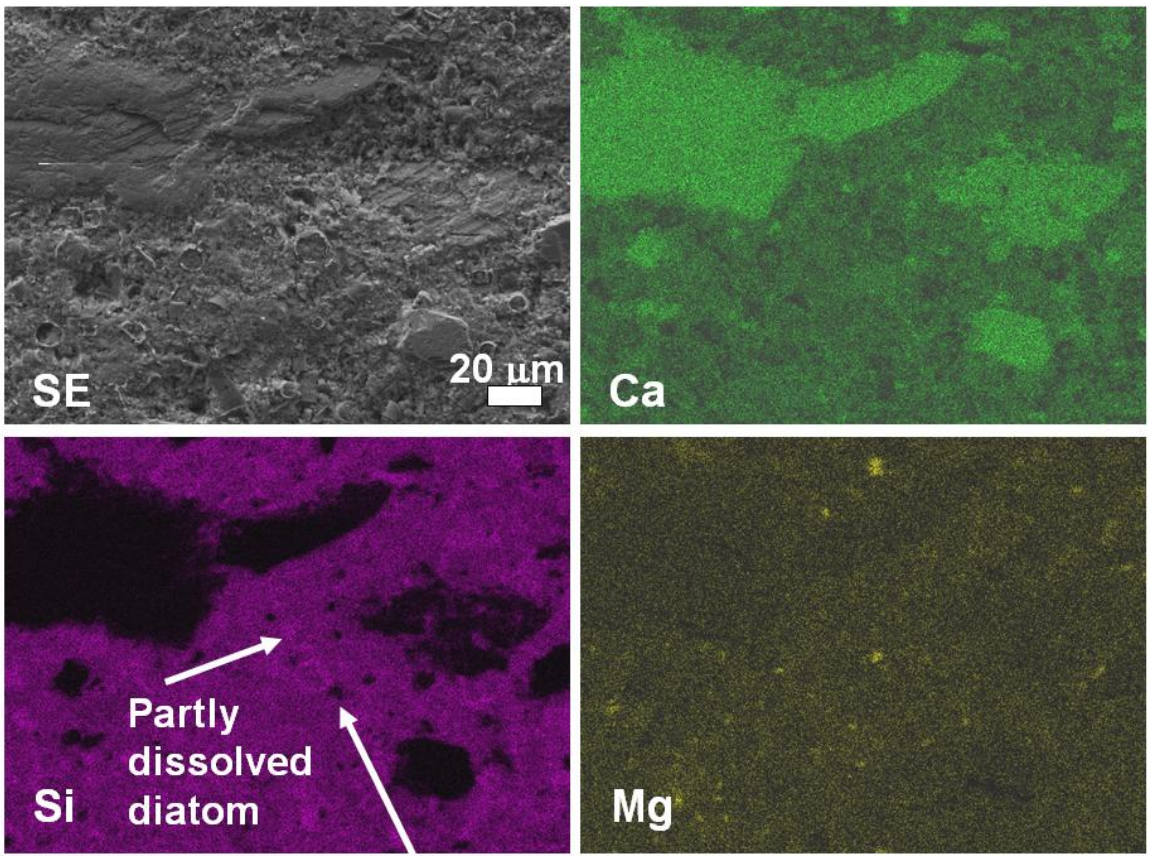

Figure 21: EDS of high DE 28 d Humidity Cured Sample
The EDS of the high DE formula after 28 d in the humidity chamber shows overlapping dispersion of Si and Ca to form C-S-H. The bright green Ca spots are from limestone particles and the bright purple spots in the Si region are from partial undissolved diatoms. The Mg in the concrete results from the dolomite in the limestone aggregate used.

The concern with the high DE formula was whether or not it had good distribution of Si after the dissolution of DE to combine with the Ca ions in solution and form C-S-H. The EDS image in Figure 21 shows that the high DE formula has good distribution of Si ions which overlap the distribution of Ca ions. It can therefore be concluded that the high DE formula is able to form a network of C-S-H instead of just pockets of hydraulic phases. The bright green spots in the Ca region result from the limestone aggregate particles. If the Si region is looked at closely small regions of bright purple areas can be

seen. These bright Si regions correspond to parts of less dissolved diatoms as seen in the previous SEM images. The black spots in the Si region correspond to the limestone particles seen in the Ca region. The Mg occurs in the concrete due to the small percentage of dolomite, $CaMg(CO_3)_2$, in the limestone used. The next step is to look at the EDS of a low DE sample to see if the reason it achieves less strength than the high DE formula is due to poor distribution of C-S-H. Figure 22 shows EDS of a low DE sample cured in the humidity chamber for 28 d.

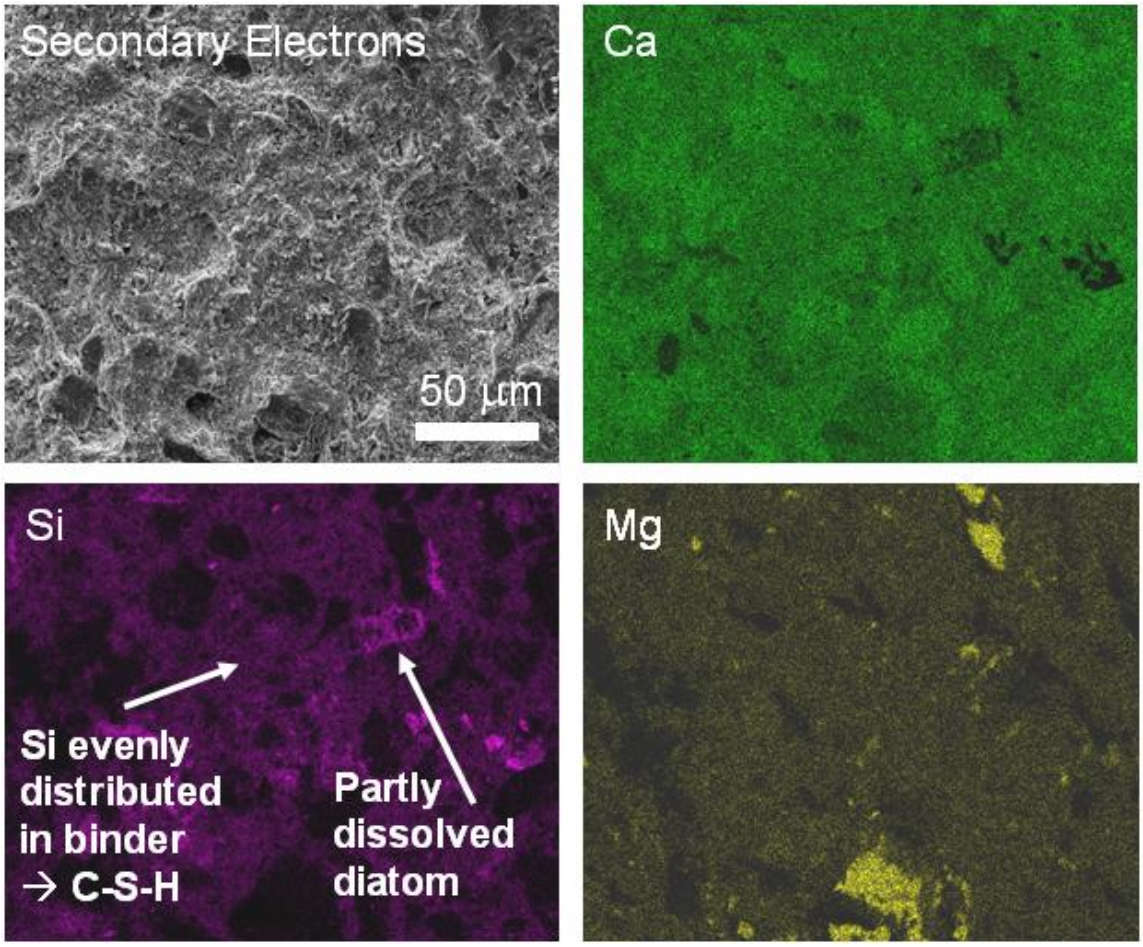

Figure 22: EDS of Low DE 28 d Humidity Cured Sample
The EDS of the low DE formula after 28 d in the humidity chamber shows overlapping dispersion of Si and Ca to form C-S-H.

The EDS of the low DE sample in Figure 22 shows that the low DE formula also has good distribution of overlapping Si and Ca to form a network of C-S-H like the high DE sample in Figure 21. A few undissolved diatoms can be seen in the Si region in Figure 22 as bright purple/pink spots. These undissolved diatoms are not clearly visible in the secondary electron image of Figure 22 and thus must be just barely under the surface. Figures 21 and 22 combine to prove that special distribution of C-S-H is not an issue in either formulae and thus the difference in strength most probably results from their differences in Ca/Si ratio as previously thought.

SEM images were also taken from the NHL-5 and non-hydraulic lime mortar samples to see how their microstructures differed from that of the hydraulic lime, low and high DE formulas. Since the non-hydraulic lime mortar samples harden only by carbonation, the SEM images should show the formation of calcite crystals as the concrete hardens. Figure 23 shows two SEM images at different magnification of the lime mortar 28 d air-cured sample.

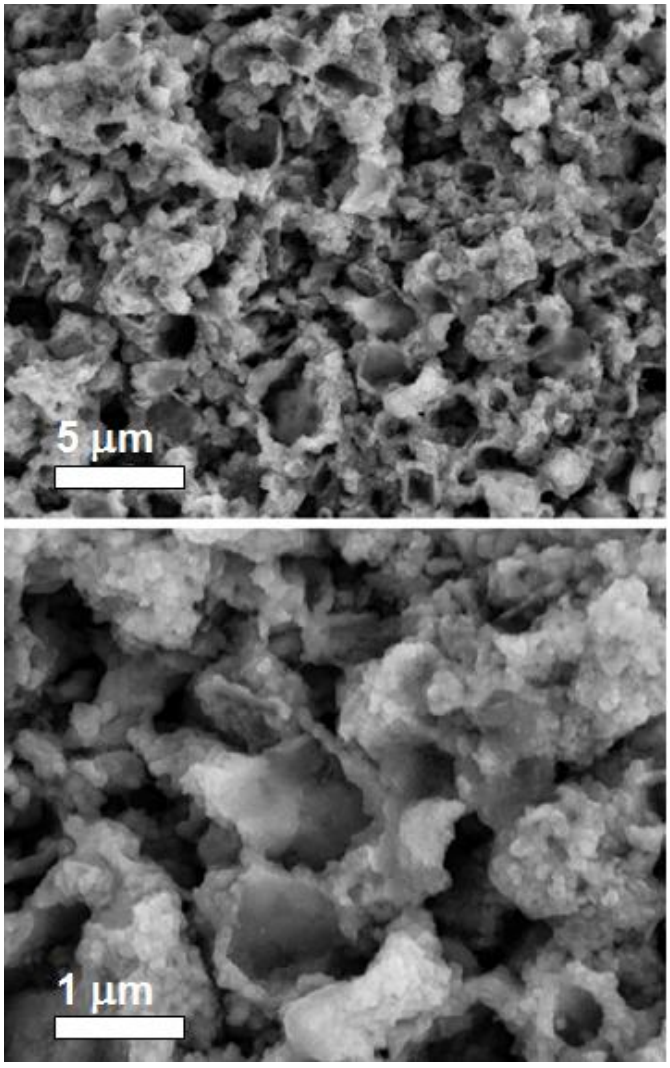

Figure 23: Two SEM Images of Lime Mortar Air Cured 28 d Sample
SEM images of the air cured lime mortar sample after 28 d showing the formation of calcite crystals as the sample absorbs CO_2 and hardens.

Figure 23 shows the formation of calcite crystals in the lime mortar 28 d air-cured sample as it carbonates. The SEM images also show the very porous microstructure of the lime mortar sample. Such open porosity is necessary for carbonation of the center sections of the concrete sample to occur.

The important thing to look at in the NHL-5 SEM images is what the natural hydraulic lime C-S-H looks like and how it differs from the C-S-H that forms in the low

and high DE formulas. Figure 24 shows an SEM image of NHL-5 14 day air cured sample.

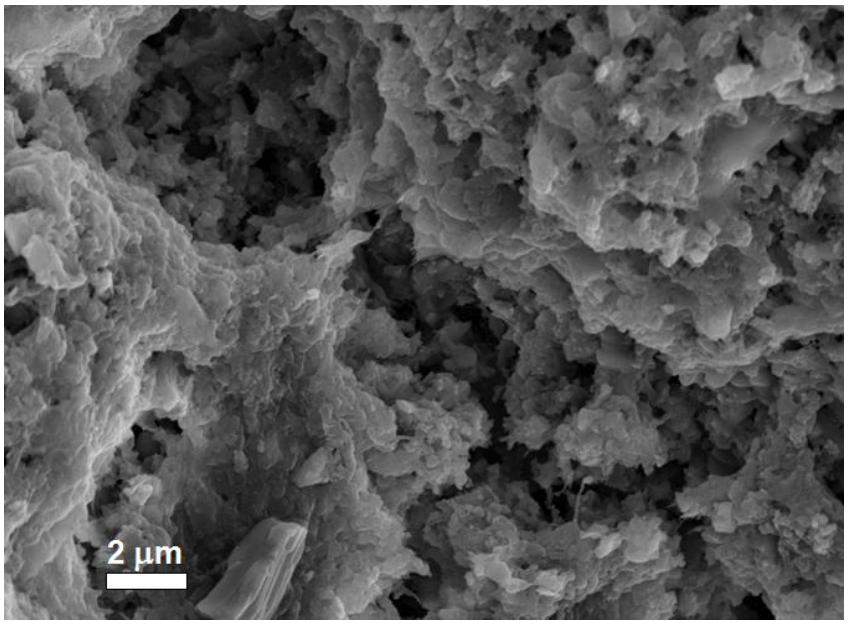

Figure 24: SEM Image of NHL-5 Air Cured 14 d Sample
High magnification SEM image of air cured 14 d NHL-5 sample showing the leafy like hydraulic binding phase.

From the 180 d compressive strength data it was established that the humidity and container-cured NHL-5 samples have less than half of the strength of the low and high DE formulas. According to Figure 24 it appears that NHL-5 is forming a leafy hydraulic binding phase that looks similar to the C-S-H forming in the low and high DE samples. There must therefore be some difference between their hydraulic binding phases. Figure 25 shows SEM images of the low DE and NHL-5 binding phases after 28 d of curing.

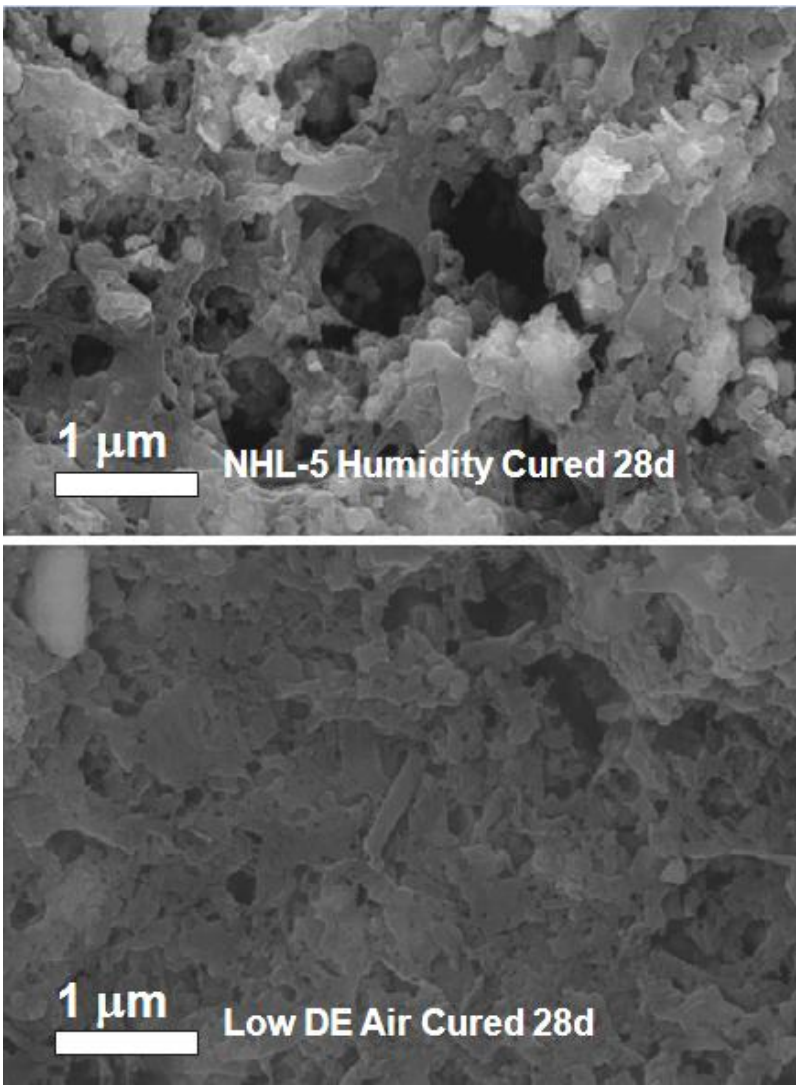

Figure 25: SEM Image of the Binding Phase in NHL-5 Humidity Cured and Low DE Air Cured 28 d Samples
Both the NHL-5 and low DE samples show similar leafy like hydraulic binding phases typically associated with C-S-H.

Figure 25 shows that there are some similarities and differences between the leafy binding structures in the NHL-5 concrete and that which forms in the low DE samples. One difference may be the density of the leafy structure as it appears that the low DE sample has a denser microstructure. Whether or not the possible C-S-H density difference seen in Figure 25 is consistent throughout the samples and the cause of the difference in

strength seen between the NHL-5 and DE formulas is not certain. XRD can be used to determine how the binding phases differ between NHL-5 and the DE formulas if their binding phases have semi-crystalline structure.

2.2.4 XRD Results

The goal of using XRD to analyze the concrete samples is to see what crystalline phases are forming over the 6 month trial. The hope was that semi-crystalline C-S-H phases would show up in on the XRD and show which specific type of C-S-H is forming. Unfortunately the XRD results were not as successful as hoped for a few reasons. One of issues came from having limestone as an aggregate in the formulas. The intensity of the limestone calcite peaks in the XRD diffractograms not only drown out the small C-S-H peaks, but the main calcite peak at around 29º 2θ overlaps with the expected C-S-H peak in the low and high DE formulas. Figure 26 below shows a XRD of the inner section of the humidity cured low DE concrete after 14 and 180 d.

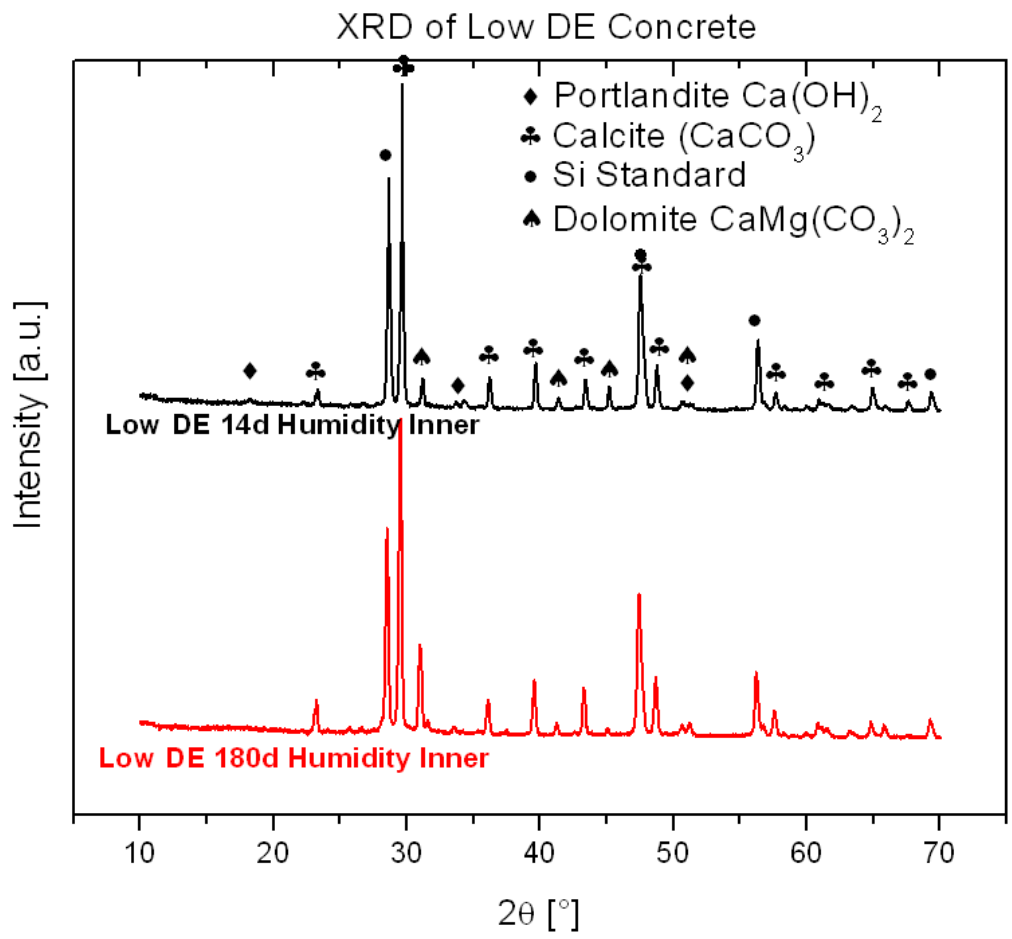

Figure 26: XRD of Inner Section of the Low DE Sample Cured in Humidity Chamber
The XRD diffractogram shows peaks of portlandite, calcite, dolomite, and Si standard but does not show any sign of C-S-H.

The low DE concrete XRD in Figure 26 shows the challenges that the XRD had in helping understand the 6 month trial formulas. The XRD diffractogram shows peaks of portlandite, calcite, dolomite, and Si standard but does not show C-S-H peaks. The dolomite peaks exist because the limestone aggregate has 11 wt.% dolomite. The lack of C-S-H peaks in any of the low or high (not shown) DE XRD at 180 d testing period is concerning since from the SEM imaging it is known that a leafy like hydraulic binding phase is forming during that time frame. This occurs because the C-S-H peaks are

masked by other more crystalline peaks in the XRD. Since the XRD of the concrete formulas is unable to identify hydraulic binding phases, the usefulness of the XRD testing is greatly diminished. The only difference that can be seen, and the only difference that was shown during all of the XRD testing in the 6 month trial, was the existence of portlandite in some samples and not in others. It can be seen in Figure 26 that the 14 d low DE sample has a small portlandite peak around 18º 2θ and the 180 d sample does not. This shows that $Ca(OH)_2$ exists in the 14 d sample but at 180 d it has disappeared. Although it can be seen that the portlandite has disappeared it is impossible to determine where it has gone using the concrete XRD data. It is known that the portlandite either turned into C-S-H or calcite but the detection limit of the XRD prevent it from determining which it is. The issue as mentioned is due to the limestone aggregate. The strong limestone peak at 29º 2θ in Figure 26 not only caused issues with the C-S-H peaks by drowning them out and over lapping with the expected C-S-H peak at 29º, it also caused issues with the carbonation hardening process. Since limestone calcite and calcite which has formed due to the carbonation of portlandite show up as the same peaks in XRD, it is impossible to determine if carbonation had occurred over the 180 d of testing since the limestone aggregate peaks are always there. The only way to see C-S-H and calcite hardening phases in the 6 month trial formulas by X-ray diffraction is to use cement pastes with no limestone aggregate. The cement paste tests which were set up with the same formulas from the 6 month trial but with no aggregate are discussed in Chapter 3.

The issues raised by Figure 26 extend into the XRD of all four 6 month trial formulas. Figure 27 shows XRD of the inner section of the air-cured four formulas after 28 d.

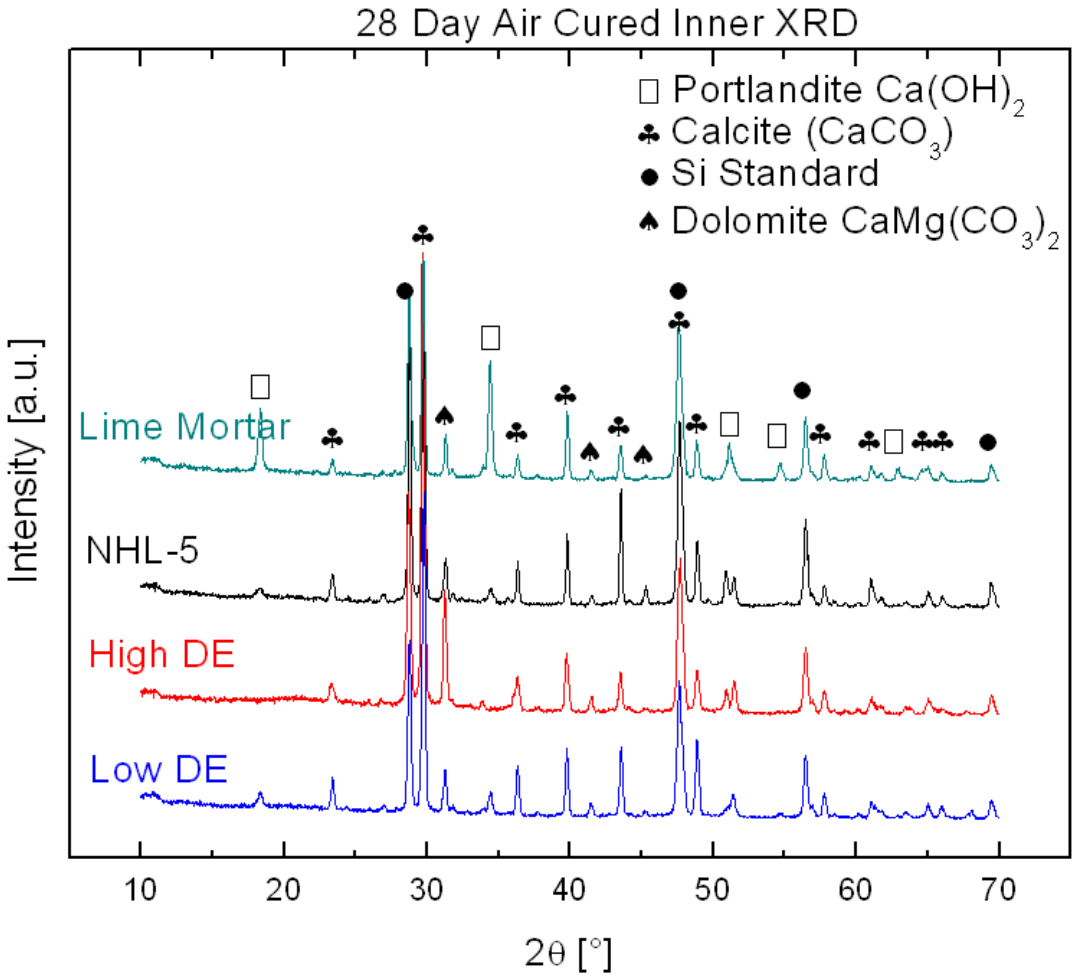

Figure 27: Inner Section of Air Cured 28 d XRD of All Four 6 Month Trial Formulas The XRD diffractogram shows that the only difference that can be distinguished between the four concrete samples is the existence of portlandite.

Figure 27 again shows that the only beneficial information that was gained from the XRD tests during the 6 month trial was the existence of portlandite. The figure shows that the low DE, NHL-5, and lime mortar formulas all have portlandite peaks while the

high DE formula does not. The lime mortar sample shows the strongest portlandite peaks at 28 d. The high DE formula appears to have a slight hump at 20º 2θ which corresponds to the amorphous silica hump from the excess DE in the formula. This excess DE was seen throughout the SEM images discussed earlier. The low DE formula does not appear to have an amorphous hump from DE as it has much less undissolved diatoms.

One of the main goals of the XRD was to be able to distinguish between the hydraulic phases in the natural hydraulic lime samples and the hydraulic phases in the artificially hydraulic low and high DE samples. Unfortunately just like in the DE formulas, the XRD is unable to identify C-S-H in the NHL-5 samples most likely due to the same limestone interference issues. The hope is that the cement paste experiments in Chapter 3 will help to distinguish between the binding phases in the 6 month trial formulas.

2.2.5 TGA Results

The goal of the TGA tests during the 6 month trial was to be able to observe how much portlandite and C-S-H existed in the concretes over time. It was expected that over time the weight loss due to portlandite between 400-600ºC would decrease as the portlandite turned into C-S-H or calcite. If the portlandite turned into C-S-H, then the weight loss from 50-400ºC in the TGA was expected to increase. Unfortunately, just as with the XRD, the TGA concrete results had many limitations. The first limitation came from the same problem as in the XRD, the interference of the limestone aggregate with the calcite that formed due to carbonation. The weight loss from the limestone aggregate

and carbonated binding phase occurs over the same temperature range in the TGA and therefore it is impossible to distinguish between them. Another issue had to do with the temperature limitations of the TGA instrument. Weight loss from calcite occurs from 600-900ºC, the TGA used however could only go up to 800ºC. This means that the TGA data does not show a full decarbonation of calcite and thus it is impossible to accurately determine how the amount of calcite changed over time, even if there was not a limestone aggregate interference issue.

The second issue that occurred in the TGA data had to do with the interference between unbound water and C-S-H. In the TGA, the weight loss from unbound water in the concrete is lost between 50-200ºC. Unfortunately, the weight loss from C-S-H gel also occurs in that region making it impossible to distinguish between the two. This is a huge limitation for the TGA data since the amount of C-S-H weight loss that occurs over time can no longer be measured.

The final issue that occurred was unexpected and not well understood. The final issue had to do with the moisture in the concrete samples during TGA testing and its effect on the weight loss curves and their accuracy between 400-600ºC. Figure 28 shows the TGA of the low DE samples after 90 d. There are inner section and outer section TGA graphs for each curing environment.

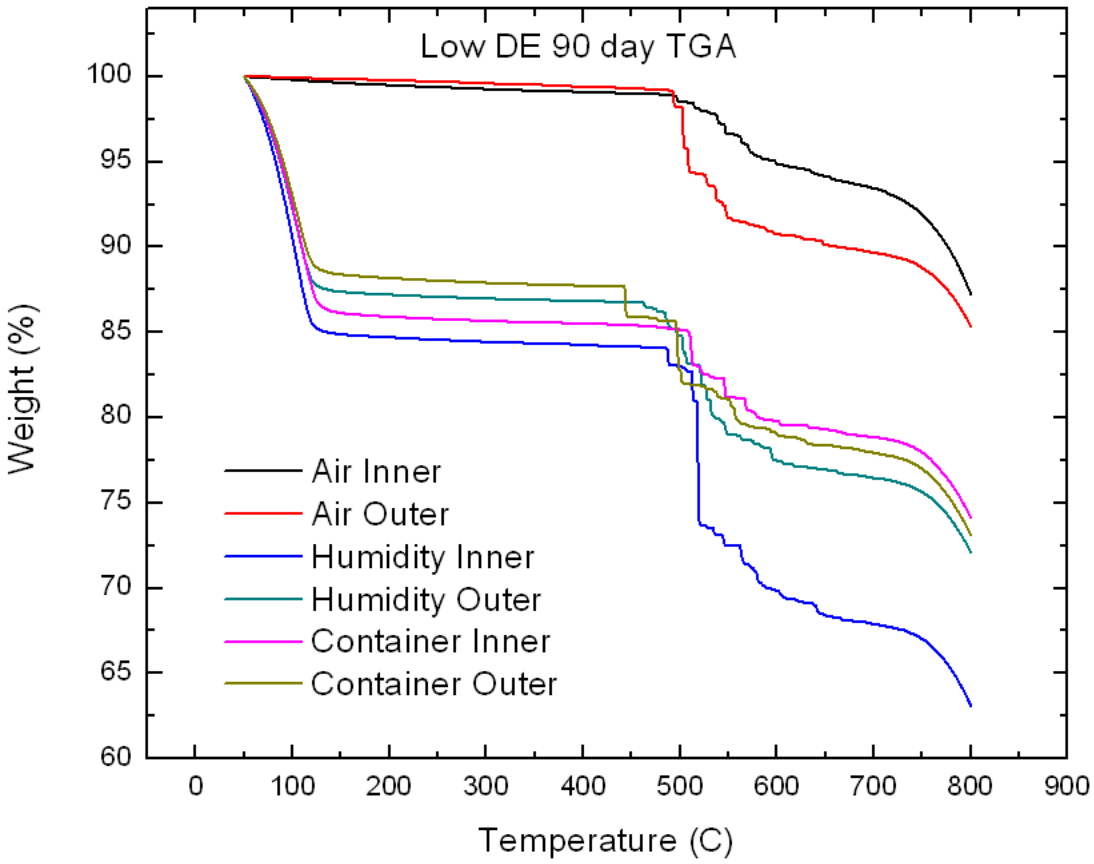

Figure 28: Low DE 90 d TGA
90 d TGA of the low DE formula showing the weight loss issue between 400-600ºC seen throughout the TGA testing in the 6 month trial

Figure 28 demonstrates the unexpected weight loss issue between 400-600ºC seen in all of the four 6-months trial formulas. Between 400-600ºC the weight loss in the TGA is due to the dehydroxylation of portlandite $Ca(OH)_2$. For some reason the TGA in this region shows a very unsmooth step like weight loss that at first was not very well understood. The issue was consistent through the 6 month trial and over time it was observed that small particles of sample appeared to be exploding out of the TGA testing cup during the tests. That observation led to the hypothesis that the problem with the TGA between 400-600ºC was occurring due to the buildup of dehydroxylation weight

loss. It appears that as the bound water from $Ca(OH)_s$ was removed it would build up in the powder and then burst causing a drastic weight loss and sometimes causing particles to explode out of the TGA testing cup. The build up and bursting of bound water continues on and off throughout the 400-600ºC range and causes the TGA data to look as it does in Figure 28. It addition to causing the data to look bad between 400-600ºC this issue more importantly makes the TGA inaccurate.

Figure 28 shows the low DE TGA after 90 d. It is expected that as carbonation occurs in the air cured samples the outer sections should show less weight loss due to portlandite than the inner sections which have not been carbonated yet and thus have much more unreacted portlandite. The opposite is shown in Figure 28 as the outer section of the low DE air cured sample shows a larger amount of portlandite weight loss between 400-600ºC than the inner air cured sections.

As mentioned, over time the amount of portlandite in the low and high DE samples is expected to drop as the $Ca(OH)_2$ is either carbonated or used to form C-S-H. Figure 29 shows how the issue of bound water build up and explosion between 400-600ºC affects the accuracy of the low and high DE TGA data over time.

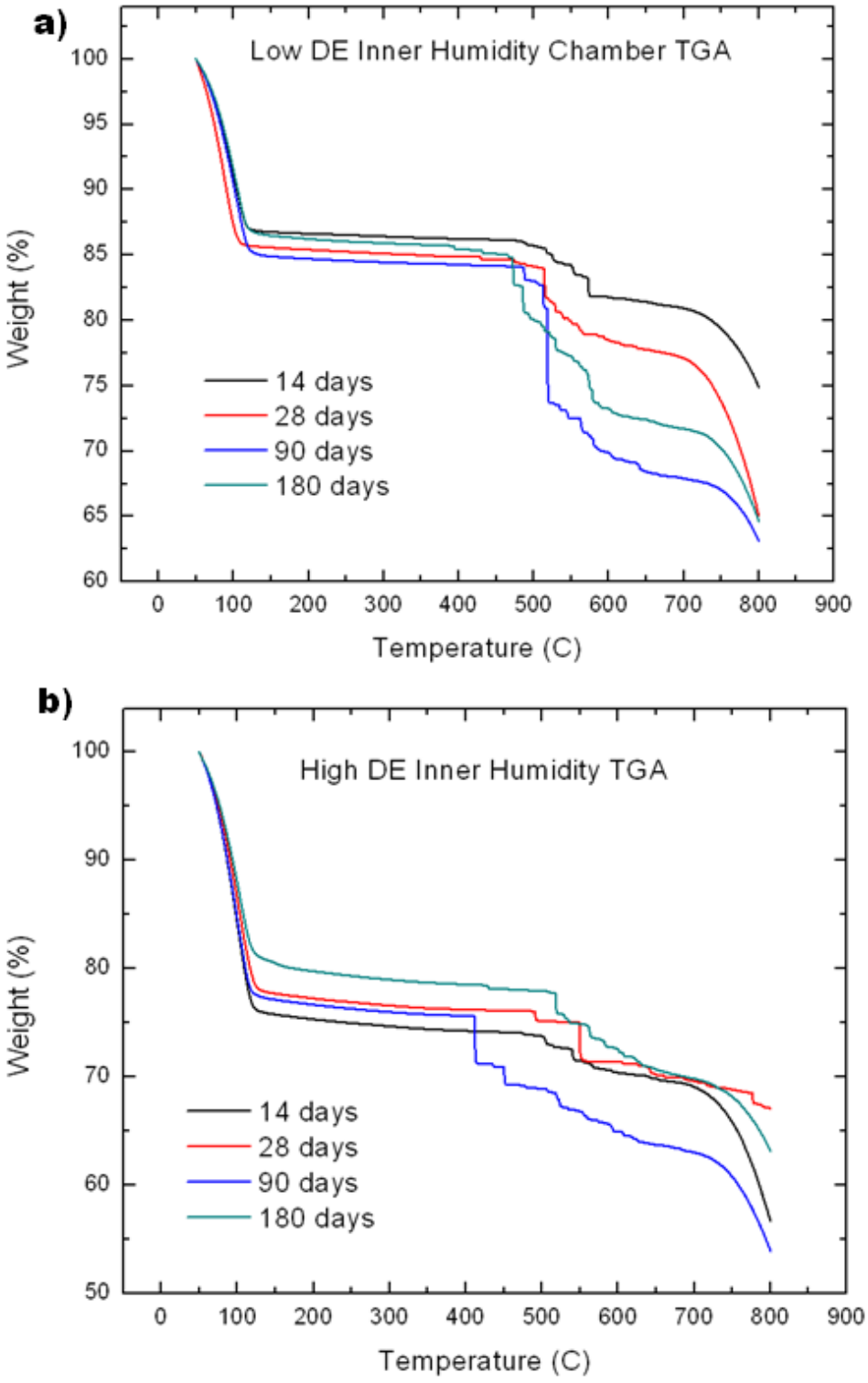

Figure 29: Low and High DE Humidity Cured Inner Section TGA
TGA of the humidity cured inner sections of the, a) low and, b) high DE formulas after 180 d curing, showing the affect of the weight loss issue between 400-600ºC.

If accurate, the TGA of the low and high DE samples cured in the humidity chamber should show a decrease in weight loss between 400-600ºC over time as the $Ca(OH)_2$ carbonates to form calcite or combines with Si ions to form C-S-H. Both Figure 29a and Figure 29b show a different trend over the 180 d tests as a result of the dehydroxylation of bound water in $Ca(OH)_2$ issue. Both Figures 29a and 29b show that the 90 d sample has the largest weight loss between 400-600ºC, while the 14 d samples have the lowest weight loss. This is opposite of what the TGA should look like over the 180 d in the 400-600ºC region.

To deal with the problems faced in the TGA tests a set of experiments was set up using the same cement pastes designed to help with the XRD issues previously discussed. By using cement paste samples with the TGA tests the issue of limestone interference between 600-800ºC is avoided. To deal with the problem of unbound water interfering with C-S-H weight loss below 200ºC the cement paste samples were freeze dried using a lypholizer to sublime the unbound water from the cement samples. The freeze dried samples should also eliminate the dehydroxylation of $Ca(OH)_2$ issue observed throughout the TGA 6 month trial. The cement paste experiments are discussed in detail in Ch. 3.

2.2.6 Phenolphthalein

The purpose of the phenolphthalein tests was to get a general idea of the rate of carbonation in the samples over the 180 d tests. Phenolphthalein, when sprayed on the fresh cut concrete sample surface, will indicate which areas have unreacted $Ca(OH)_2$ by turning a dark pink color. The pink areas correspond to high pH (above 9.5) sections

which have not carbonated. The areas of the samples which do not turn pink have carbonated as the phenolphthalein does not change color in sections with pH below 9.5. Figure 30 shows the phenolphthalein test results from all four of the 6 month trial formulas after air curing for 180 d.

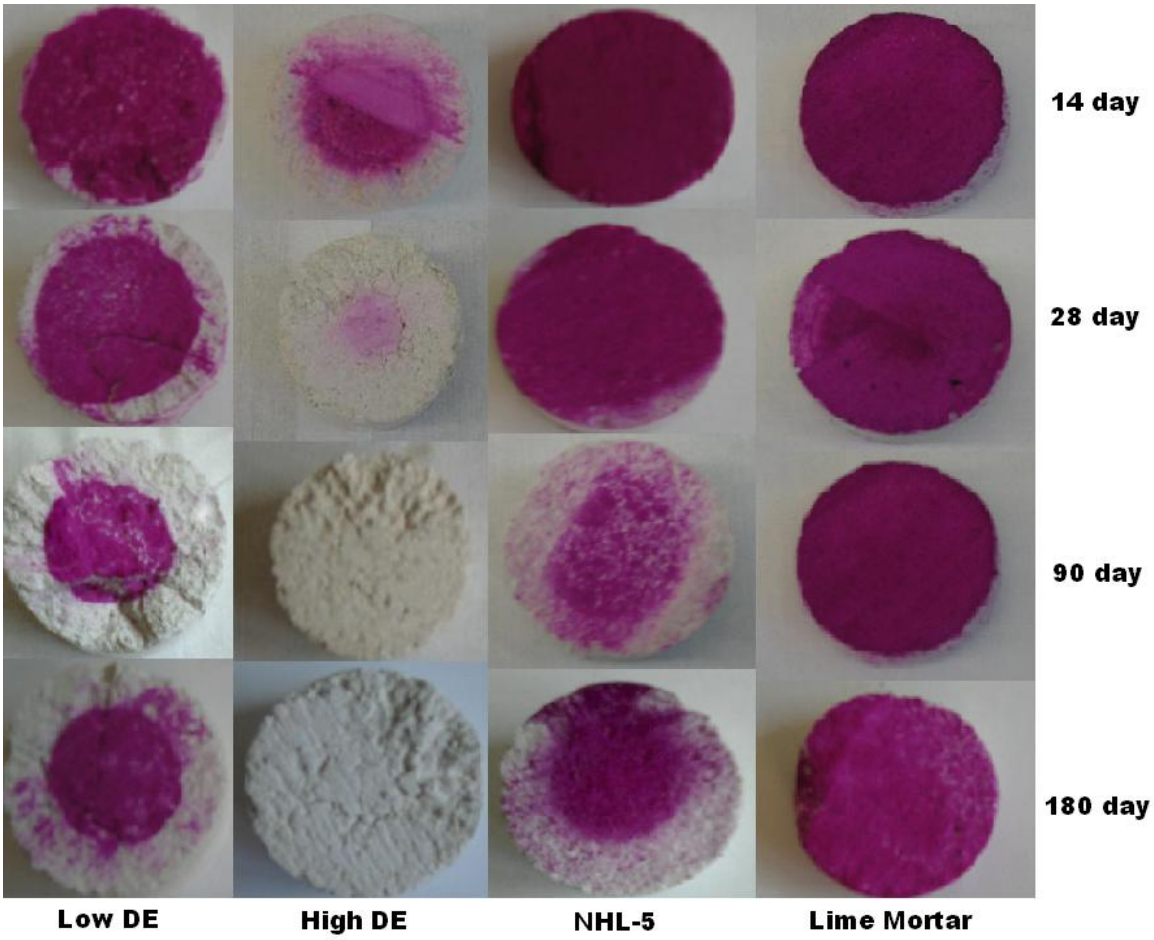

Figure 30: Phenolphthalein Tests On All Four 6 Month Trial Formulas Over 180 d
The images show the level of carbonation that has occurred (white areas) in the formulas as they air cure for 180 d.

Although the phenolphthalein test results in Figure 30 can not be used to calculate the exact amount of carbonation that has occurred in the samples, it does give a general understanding of the rate of carbonation in each formula. Figure 30 shows interesting results for a few reasons. Figure 30 shows that the high DE sample was the only sample to fully carbonate during the 180 d of testing. Between the 14 and 90 d test, the high DE samples cured in air became fully carbonated and no longer showed a pink uncarbonated area. The low DE and NHL-5 samples both show a much slower carbonation rate as they are approximately half carbonated after 180 d. The lime mortar showed an unexpected result as it showed no phenolphthalein carbonation ring over the 180 d tests despite the fact that partial carbonation has occurred as shown by the 3 MPa strength after 180 d. This was unexpected because the lime mortar is the only formula which hardens solely through the carbonation process.

The explanation for why the high DE formula has the highest level of carbonation and why the lime mortar sample shows no carbonation in Figure 30 has to do with the amount of portlandite in each sample. Since the high DE formula has such a large amount of DE in the formula, it is expected to have the least amount of free portlandite available for carbonation as all of the $Ca(OH)_2$ is used to dissolve the DE and form C-S-H. Therefore, the high DE formula shows fast carbonation as there is less free portlandite that must be carbonated before the pH drops below 9.5.

The lime mortar, on the other hand, has the largest amount of free portlandite of all of the formulas as it has no DE to form C-S-H and therefore all of its portlandite is available for carbonation. Due to the observed compressive strength of 3 MPa in the air cured lime mortar, it is obvious that the lime mortar has carbonated. The fact that

incomplete carbonation is seen in phenolphthalein test must solely have to do with the pH level of the sample surface. The lime mortar has so much free portlandite that even though carbonation has occurred, it is not enough to cause the pH to drop below 9.5. This result further supports the claim that the lime mortar will continue to gain strength past 180 D as the phenolphthalein tests show it has a large amount of portlandite that can carbonate and harden.

2.3 Conclusion

The goal of the 6 month trial was to understand the long term strength development and properties of hydraulic lime mortars with DE as the source of silica and limestone as the aggregate. The four formulas in the 6 month trial were set up to investigate how carbonation, formation of C-S-H, Ca/Si ratio, and the use of natural vs. artificial lime mortars affect the properties of a fine-limestone-aggregate concrete. Although some challenges were faced the 6 month trial produced great insight into the materials and hardening processes going on.

The compressive strength results showed that the high DE formula with a low Ca/Si ratio had the highest strength after 180 d at around 7 MPa. The low DE formula had the second highest strength at 5 MPa and the air cured lime mortar had the third highest strength. The issue of strength retention in the high DE formula was discovered and a possible explanation was presented. The explanation had to do with the excess undissolved diatoms in the high DE formula becoming basically defects once the sample was left to dry in air.

This explanation was supported by the SEM images taken of all four samples over the 180 d testing period. Under SEM the high DE formula had visible undissolved diatoms throughout the sample, as opposed to the low DE formula in which it was much more difficult to spot undissolved diatoms. The SEM images were also able to identify the leafy microstructure of the C-S-H in the low and high DE formulas as well as the calcite crystals forming in the lime mortar samples. The hydraulic binding phase of the NHL-5 product was observed under SEM and compared with the C-S-H from the DE formulas.

It was hoped that XRD and TGA would provide further insight and understanding but their contribution was limited due to interference issues. In the XRD results the large calcite peaks from the limestone aggregate drowned out the smaller binding phase peaks that were expected and actually overlapped with the expected C-S-H peak at 29º 2θ. Because of this interference issue the only real information that was gained from the XRD results was the existence, or lack of, portlandite in each sample over time.

The limestone aggregate also contributed to the issues with the TGA results as its weight loss occurred in the same temperature range as the newly carbonated calcite. The TGA also had issues with unbound and bound water affecting the results. The weight loss due to unbound water overlapped with the expected weight loss from C-S-H gel, making the weight loss due to C-S-H gel indistinguishable. In addition the loss of bound water from $Ca(OH)_2$ occurred in such a way that the moisture or water would build up and then burst in spurts causing discontinuous weight loss drops and at times even causing small pieces to explode out of the TGA sample cup.

It was determined that the issues with both the XRD and TGA results could be avoided by creating a side set of experiments using cement paste. These cement paste formulas would have the same formulas as in the 6 month trial only with no limestone to cause interference. In addition these cement pastes would be freeze dried using a lypholizer to remove any unbound water in the samples and eliminating the unbound water TGA issue. The results from the cement paste experiments can be seen in Ch. 3.

The final conclusion of this chapter deals with the current cost of the alkali activated cements with DE as the source of silica developed in the 6 month trial. Currently OPC costs approximately $102 per ton in the U.S.[56] The average cost for the lime and DE, the two materials used to make the DE based cement, is as follows: lime $84 per ton,[57] DE $220 per ton.[35] The price of the DE is simply an average cost reported by the U.S. Geological Survey and is not actually the cost of the Perma-Guard DE. By using weight percents of the dry cement materials only, ignoring the limestone aggregate and the price of water, the approximate price of the low and high DE formulas from the 6 month trial can be determined. The low DE formula has an approximate price of $139 per ton, while the high DE formula has an approximate price of $193 per ton. The difference in their costs results from the fact that the high DE formula has much more DE at $220 per ton. As mentioned, this assumption for the DE price of $220 per ton is on the high end and thus there is much room for improvement in the cost of the DE based cements. Two simple ways to lower the cost of the DE based cement would be to change the type of DE used or to increase the Ca/Si ratio and use less DE in the formula. Even with the high priced DE the low DE and high DE formulas are not drastically more expensive than OPC.

CHAPTER 3. CEMENT PASTE EXPERIMENTS

3.1 Introduction

The goal of the cement paste experiments was to help further understand the chemistries of the binding phases of the four formulas in the 6 month trial in Chapter 2. The need for the cement paste experiments arose from the challenges faced during the XRD and TGA tests in Chapter 2. To be able to conduct XRD and TGA tests with no interference issues the same four formulas from the 6 month trial were made, only this time with no limestone aggregate. Table 9 shows the formulas for the cement paste experiments.

Table 9: Cement Paste Formulas

Formula	Water (ml)	Water weight %	Ca/Si ratio	DE (g)	CaO (g)	NHL-5 (g)
Low DE	601.56	30.60	1.75	100.55	146.30	-
High DE	1012	27.7	0.281	481.5	120.4	-
Lime Mortar	818.13	29.50	-	-	335.70	-
NHL-5	535	16.14	1.77	-	-	395

In addition to having no aggregate, the cement paste formulas differed from the 6 month trial in how they were cured and prepared for testing. Each cement paste formula was cured in the 100 % relative humidity chamber only. This was done because the goal of the cement paste experiments was to understand and identify the hydraulic binding

phases in the formulas and how they differ. By curing in the humidity chamber there is unlimited water for the formulas to form hydraulic binding phases with. The samples were left in the humidity chamber for 180 d and tested at 14, 28, 90, and 180 d.

At each testing date 20-40 g of each formula was taken and placed in plastic test tubes. These test tubes were then placed in an open top, liquid nitrogen dewar and frozen in liquid nitrogen for 10-15 minutes. Once frozen, the samples were placed in a lypholizer (FTS Systems Flexi Dry, Stone Ridge, NY) for a minimum of 24 h to freeze dry them. The lypholizer works by putting the samples at cold temperature (-80ºC) and low pressure (-300 millitorr) to sublimate the unbound water in the cement from liquid to vapor, leaving the samples totally dry. Once the lypholizer process is complete the cement paste samples were ground to a powder using a mortar and pestle and placed in air tight containers. This process was done quickly to prevent the absorption of moisture or CO_2 from the air. The process was repeated at 14, 28, 90 and 180 d. XRD and TGA were then carried out on the freeze-dried samples (Section 1.5).

3.2 Results and Discussion

3.2.1 XRD Results

Figure 31 shows XRD of the low DE formula over the 180 d testing period.

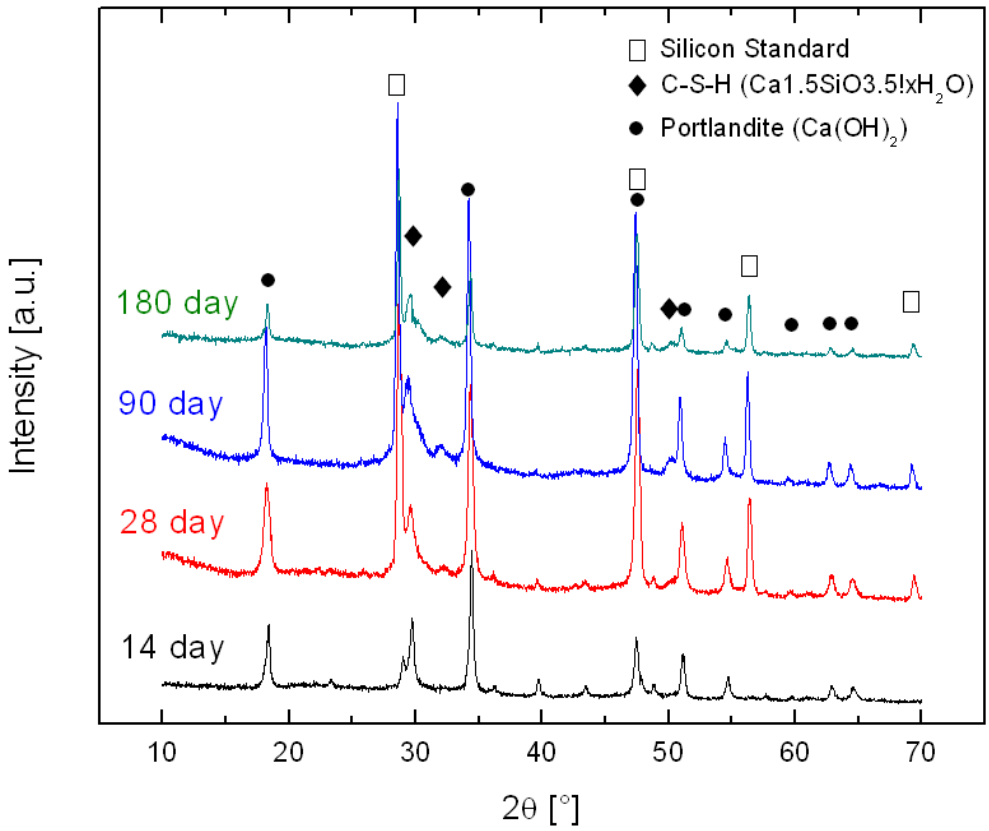

Figure 31: XRD of the Low DE Cement Paste Formula Over 180 d
The XRD shows the existence of C-S-H and portlandite throughout the 180 d testing period.

Figure 31 supports the observation that the limestone aggregate in the 6 month trial was not only drowning out the hydraulic C-S-H peaks, it was also overlapping with the strong C-S-H peak at 29º 2θ. The low DE cement paste XRD in Figure 31 shows $Ca_{1.5}$ $SiO_{3.5}$·xH_2O C-S-H peaks throughout the 180 d. It also shows portlandite peaks but no calcite peaks. From the low DE XRD it can be concluded that strength providing binding phase in the low DE samples comes from C-S-H and not from carbonation as there are no evidence of calcite peaks. It also can be concluded that one specific type of C-S-H is forming ($Ca_{1.5}$ $SiO_{3.5}$·xH_2O) and that the low DE formula has unreacted $Ca(OH)_2$ even after 180 d. The existence of this unreacted $Ca(OH)_2$ is important for

strength development as without excess $Ca(OH)_2$ no more C-S-H can form. Because of the existence of $Ca(OH)_2$ it is expected that the low DE formula will continue to gain strength and form C-S-H past 180 d. The high DE formula XRD can be seen in Figure 32.

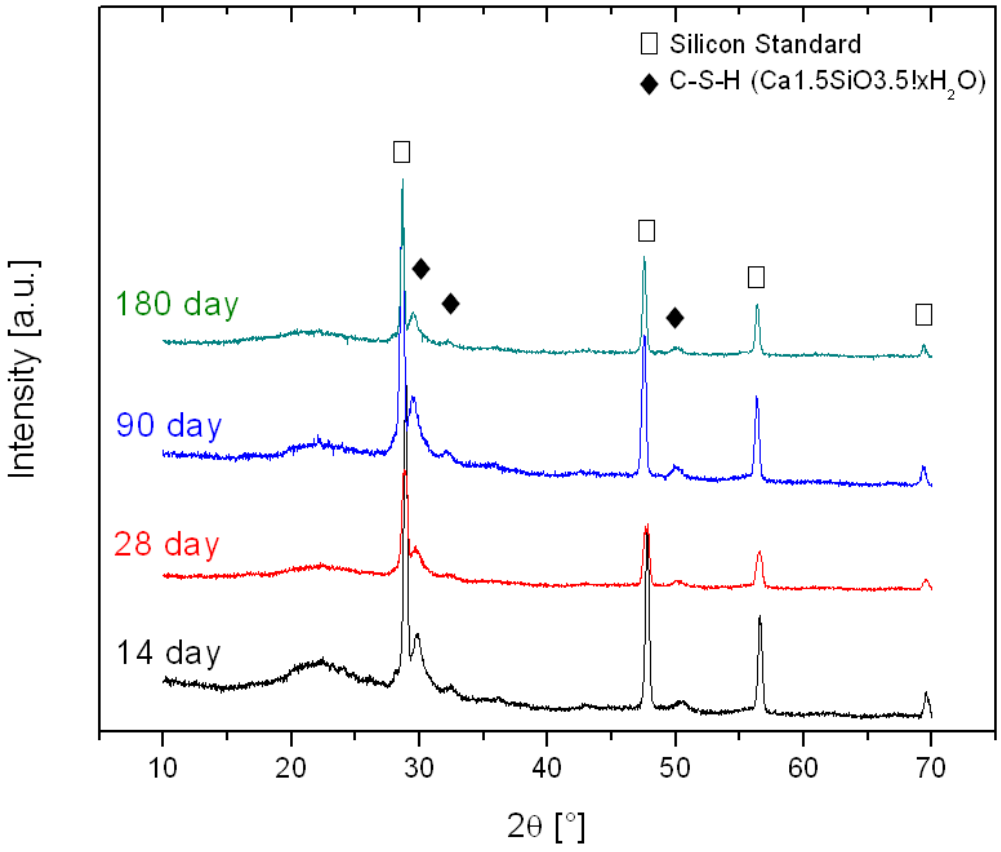

Figure 32: XRD of the High DE Cement Paste Formula Over 180 d
The XRD shows the existence of C-S-H and an amorphous hump around 22º, but no portlandite throughout the 180 d testing period.

Figure 32 shows that there are some differences between the high and low DE cement paste XRDs. The high DE XRD shows an amorphous hump at around 22º 2θ but no portlandite peak as seen in the low DE XRD. The amorphous hump results from the amorphous silica of the diatoms, which were visible in the 6 month trial SEM imaging. It

is these excess diatoms which cause the decrease in compressive strength in the high DE concrete upon drying.

The lack of portlandite peaks in the high DE XRD shows another difference from the low DE formula. Since there is no excess $Ca(OH)_2$ in the high DE cement paste it can be concluded that all of the calcium has been used to form C-S-H. This is another result of having such a high DE content and explains why the high DE formula did not have a large strength gain between 28 and 180 d in the 6 month trial compression tests. Once all of the $Ca(OH)_2$ is used, the cement loses its' ability to dissolve diatoms and form C-S-H, thus it loses its' ability to increase in strength over time. As seen in the 6 month trial compression tests, the high DE formula peaks in strength around 28 d and then gains very little strength from that point on (see Fig. 10).

One thing that the low and high DE formulas have in common according to their cement paste XRD is the binding phase holding them together. Figure 32 shows that the high DE formula forms the same specific type of C-S-H as the low DE formula. The figure also shows that just like the low DE, the high DE formula does not form calcite. This result is contradictory to the phenolphthalein tests in the 6 month trial which showed that both the low and high DE formulas carbonated over time. The high DE formula actually showed full carbonation between 28 and 90 d. The contradictory results occur due to differences in curing environment. The phenolphthalein images shown in Figure 30 are of air cured samples which had dried out over the 180 d. Once dry these samples can no longer form C-S-H and thus carbonation can occur on the portlandite that exists in the samples. The cement pastes, on the other hand, were cured in the humidity chamber giving the samples unlimited access to water. With this unlimited water the low and high

DE cement pastes form C-S-H but do not carbonate. This conclusion supports the observed compressive strength data in the 6 month trial showing the humidity- and container-cured low and high DE formulas having the highest strengths as a result of them having the highest amount of C-S-H.

One of the goals of the cement paste XRD testing was to be able to distinguish between the hydraulic binding phase forming in the DE formulas vs. that which forms in the natural hydraulic lime formula. Figure 33 shows the NHL-5 cement paste XRD.

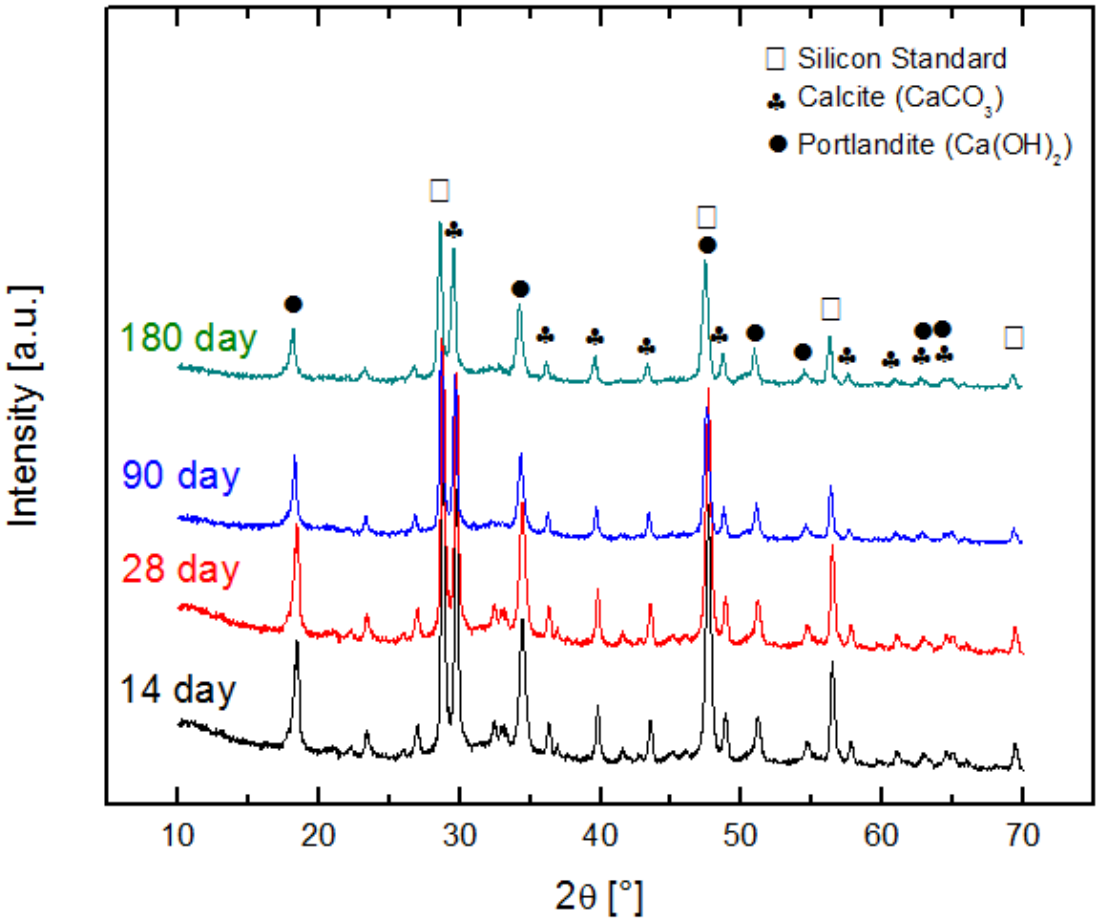

Figure 33: XRD of the NHL-5 Cement Paste Formula Over 180 d
The XRD shows portlandite and calcite peaks. The calcite peaks most likely result from the 22 wt.% unburned $CaCO_3$ in the NHL-5 product and not from carbonation of portlandite.

The NHL-5 cement paste had peaks of portlandite and calcite, but no clear C-S-H peaks (Fig. 33). The calcite peaks most likely result from the 22 wt.% unburned $CaCO_3$ in the NHL-5 product and not from the carbonation of portlandite to form calcite. There are two unidentified peaks at approximately 24º and 27º 2θ which could correspond to the hydraulic binding phase observed under SEM for the NHL-5 in the 6 month trial. Unfortunately the Jade software used to analyze the XRD could not clearly match these peaks. One of the reasons that the Jade may not have been able to identify any C-S-H is due to the same problem of calcite interference that occurred in the concrete XRD. The 22 wt% unburned $CaCO_3$ in NHL-5 may again be overlapping with a C-S-H peak at around 29º, preventing proper identification of the type of C-S-H in NHL-5. If the two unidentified peaks between 20º-30º are assumed to be from C-S-H then the C-S-H in NHL-5 is not the same as the one which forms in the low and high DE formulas since the DE formula XRDs do not show C-S-H peaks in that region. This conclusion would support the microstructural differences observed in the SEM images of the hydraulic phases between the low DE and NHL-5 concrete samples in Figure 25 in the 6 month trial.

The cement paste XRD of the lime mortar can be seen in Figure 34.

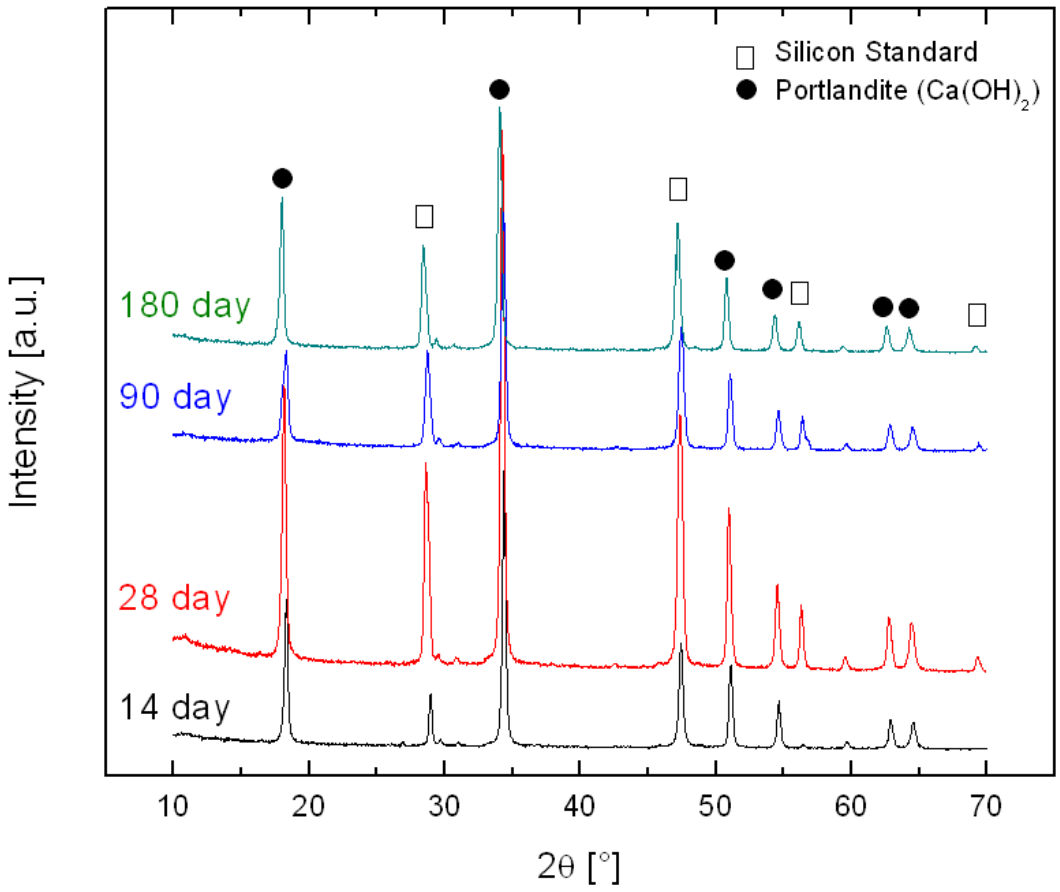

Figure 34: XRD of the Lime Mortar Cement Paste Formula Over 180 d
The XRD shows only portlandite peaks.

The lime mortar cement paste XRD in Figure 34 shows only portlandite peaks and no calcite. This result confirms what is already known about lime mortars and their inability to carbonate in excessively moist environments. The excess water prevents carbonation and explains why the lime mortar samples cured in the humidity chamber in the 6 month trial never hardened.

3.2.2 TGA Results

It was hoped that by doing TGA on the cement paste samples many of the issues that the concrete TGA had in the 6 month trial would be avoided. Since the cement paste samples are freeze dried prior to testing the problem of weight loss from unbound water overlapping with weight loss from C-S-H gel below 200ºC should be avoided. Since there is no limestone in the cement pastes the problem of weight loss from limestone aggregate overlapping with weight loss from carbonation from 600-800ºC should also be avoided. The final hope was that the cement pastes would not face the same issues of bound water loss between 400-600ºC that the 6 month trial TGA faced.

Fortunately the freeze dried cement paste TGA eliminated these issues. Figure 35 shows the low DE cement paste TGA over the 180 d period.

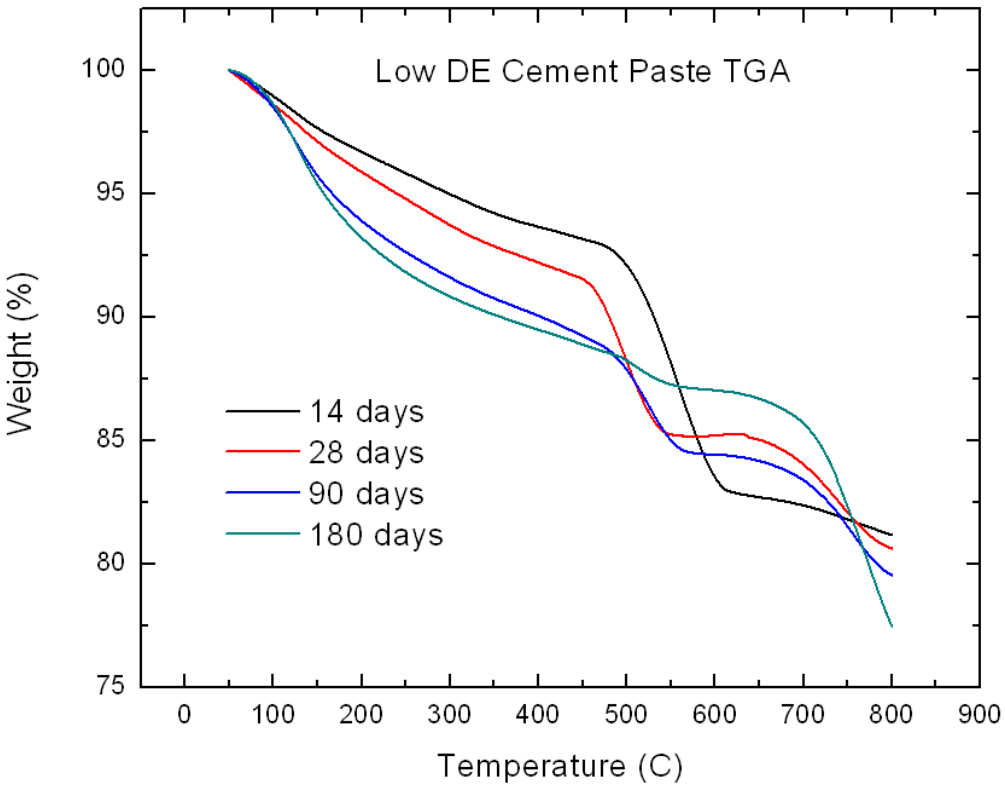

Figure 35: Cement Paste TGA of the Low DE Formula Over 180 d
Over time the weight loss due to portlandite decreases as the weight loss due to C-S-H and carbonation increase.

The low DE cement paste TGA in Figure 35 shows that the cement paste experiments were successful in eliminating the bound water build up and release issue between 400-600ºC as the curves are smooth and consistent in this region. The figure also shows that over time the amount of portlandite weight loss between 400-600ºC decreases. This decrease in $Ca(OH)_2$ corresponds with increases in weight loss due to C-S-H below 400ºC and increases in weight loss due to calcite carbonation from 600-800ºC. Over time the amount of portlandite in the low DE formula decreases as it either turns into C-S-H or absorbs CO_2 to form calcite. However, the TGA can not determine how much portlandite turns into which binding phase specifically because the TGA does not reach a high

enough temperature to show full decarbonation. It is likely that the location of the portlandite determines what binding phase it becomes. If it is near a diatom the $Ca(OH)_2$ will dissolve the diatom and form C-S-H. If the portlandite is near the sample's surface where the concrete has dried out, or in a location where there are no diatoms then the portlandite will carbonate if it has access to CO_2. From the TGA data it can be concluded that the initial amount of portlandite weight loss in the cement paste is the amount of potential strength gain that the sample has over time. As long as the sample has portlandite it has the ability to form C-S-H or calcite at some point. This is a key concept to consider when looking at the high DE cement paste TGA in Figure 36.

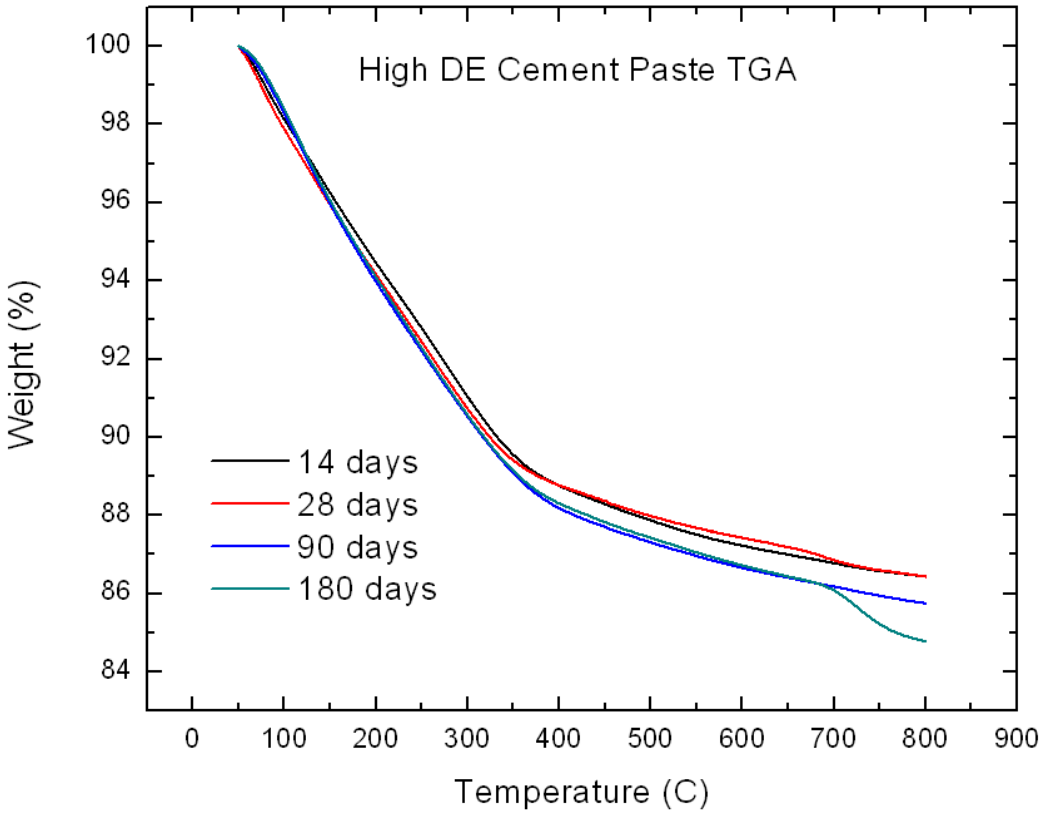

Figure 36: Cement Paste TGA of the High DE Formula Over 180 d
The high DE formula has very little portlandite weight loss and therefore shows very little increase in C-S-H weight loss in the TGA over time.

The high DE TGA in Figure 36 differs completely from the low DE TGA in Figure 35. The former has very little weight loss due to portlandite between 400-600ºC. This data agrees with the cement paste high DE XRD previously discussed in which the high DE XRD had no portlandite peaks. The TGA also agrees with the 6 month trial compressive strength data in which the high DE formula has the highest strength of all of the four samples, but then shows very little strength gain after 28 d. This lack of strength gain can thus be directly linked to the lack of portlandite.

The TGA of the lime mortar cement paste in Figure 37 shows very different weight loss due to portlandite compared to the high DE TGA.

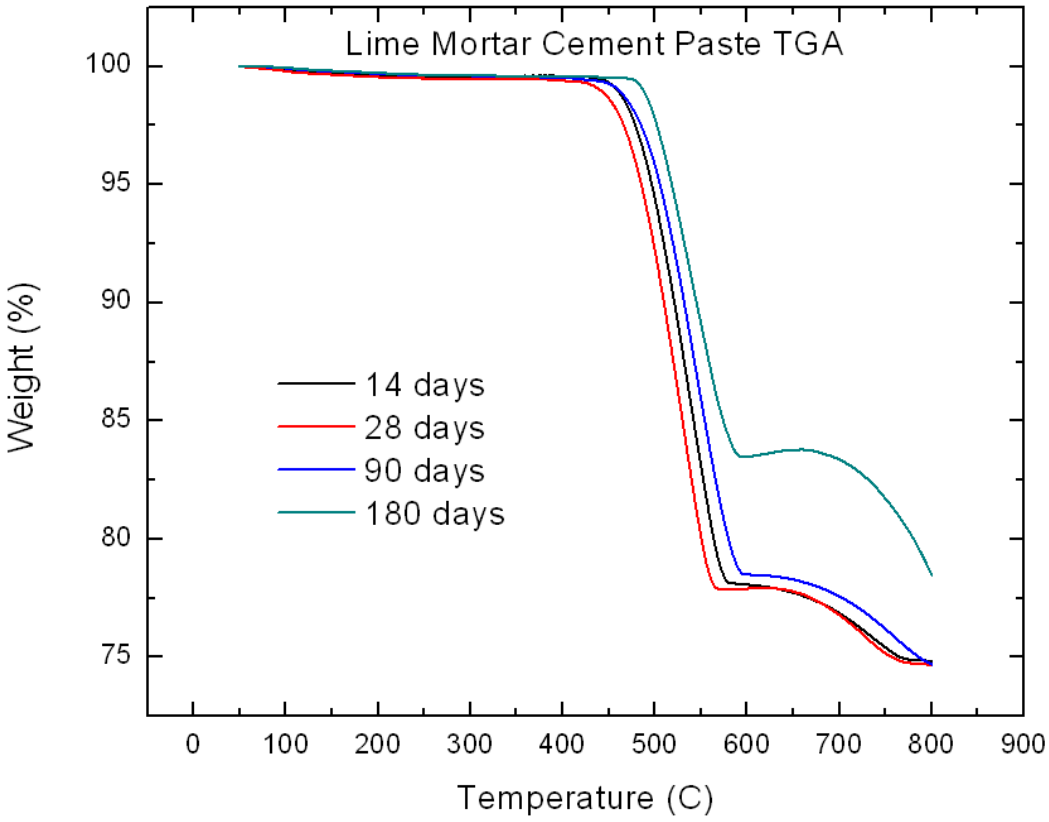

Figure 37: Cement Paste TGA of the Lime Mortar Formula Over 180 d
The lime mortar shows large weight loss between 400-600ºC in the TGA corresponding to portlandite. Over time this portlandite decreases as it carbonates.

Compared to the high DE cement paste TGA, the lime mortar TGA in Figure 37 has almost the opposite curve, with large weight loss due portlandite, but none due to C-S-H. The lime mortar cement paste TGA in Figure 37 shows slight decreases in the weight loss due to portlandite between 400-600ºC over time. As the weight loss due to portlandite decreases the weight loss due to calcite in the 600-800ºC should increase. This is not the case in Figure 37 because the TGA used in these experiments had a maximum temperature of 800 ºC. Had the experiment been conducted up to 1000 ºC where full decarbonation is expected then such a correlation between decrease in portlandite and increase in calcite should have been visible. The lime mortar TGA confirms the idea that the lime mortar samples in the 6 month trial would have continued to harden over time and gain strength past the 180 d mark. Figure 37 shows how much excess portlandite remains in the lime mortar after 180 d. All of this portlandite is free to carbonate over months and years, ultimately increasing the strength of the samples possibly past the strength of the high DE formula.

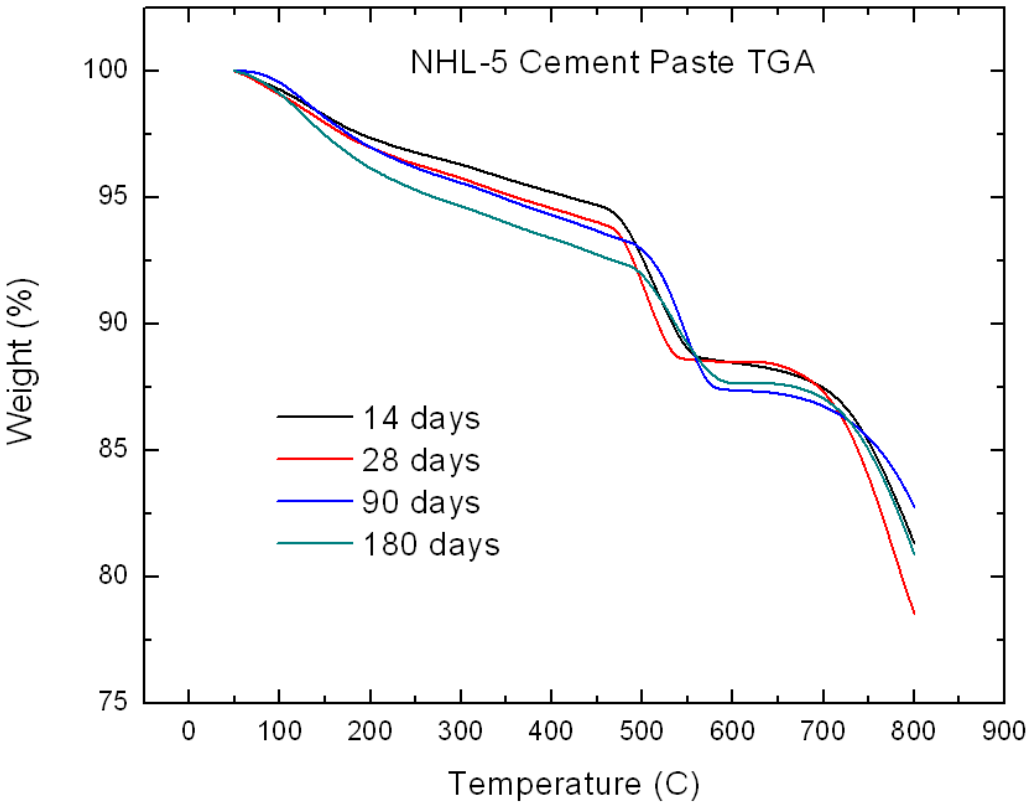

Figure 38: Cement Paste TGA of the NHL-5 Formula Over 180 d
The NHL-5 TGA shows slight decreases in portlandite between 400-600ºC and slight increases in C-S-H below 400ºC.

The final TGA samples to be looked at are the NHL-5 cement paste samples in Figure 38. The NHL-5 cement paste TGA in Figure 38 did not have as clear a correlation in change in weight loss over time as the other three cement paste formulas. If looked at closely Figure 38 shows a slight decrease in weight loss due to portlandite between 400-600ºC and a slight increase in weight loss due to C-S-H below 400ºC over time. This correlates well with the compression strength data from the 6 month trial which showed that the NHL-5 concrete samples increased in strength by a small amount over time and had some of the lowest strength values of all four formulas after 180 d. It is easiest to see

these changes when the TGA data is shown as actual weight percent loss values. Table 10 shows the weight loss values for all four cement past formulas over the 180 days.

Table 10: Weight Loss % From All Four Cement Paste Formulas Over 180 d

		Low DE		
Temp Range (ºC)	**0-200**	**200-400**	**400-600**	**600-800**
14 days	3.31	3.03	10.15	2.33
28 days	4.11	3.67	6.99	4.59
90 days	6.09	3.85	5.61	4.89
180 days	5.84	3.63	4.11	5.88
		High DE		
Temp Range (ºC)	**0-200**	**200-400**	**400-600**	**600-800**
14 days	5.54	5.70	1.54	0.78
28 days	5.84	5.39	1.34	0.99
90 days	6.02	5.79	1.53	0.91
180 days	5.90	5.79	1.58	1.94
		NHL-5		
Temp Range (ºC)	**0-200**	**200-400**	**400-600**	**600-800**
14 days	2.64	2.15	6.73	7.13
28 days	3.02	2.41	6.06	9.94
90 days	3.02	2.68	6.92	4.62
180 days	3.84	2.77	5.71	6.77
		Lime Mortar		
Temp Range (ºC)	**0-200**	**200-400**	**400-600**	**600-800**
14 days	0.35	0.06	21.52	3.23
28 days	0.46	0.15	21.49	3.21
90 days	0.31	0.18	21.02	3.80
180 days	0.27	0.15	16.10	5.01

Table 10 shows TGA data supporting the conclusions that were drawn for each formula in the cement paste experiments. It is also be beneficial to see how the TGA for the four formulas differed from each other over time as shown in Figure 39.

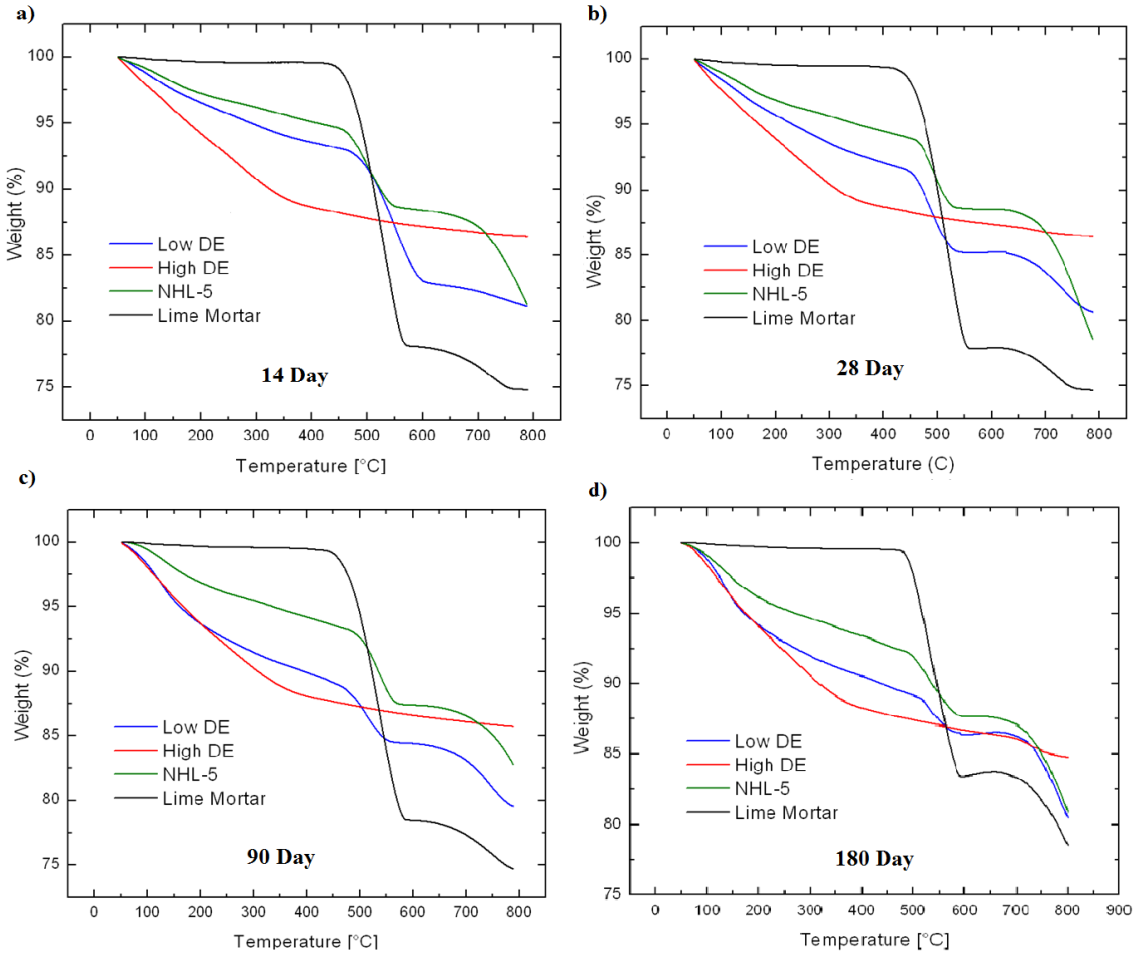

Figure 39: Cement Paste TGA of All Four Formulas Over 180 d
Cement paste TGA of all four formulas after a) 14, b) 28,
c) 90, and d) 180 d.

Figure 39 shows the differences between the TGA of the four cement paste formulas over the 180 d. At 14 d, (Figure 39a) the high DE formula has the largest amount of weight loss due to C-S-H below 400ºC, and the low DE formula has the second largest weight loss. This correlates well with the observed compressive strength data for these formulas in the 6 month trial showing the high DE with the highest strength at 14 d, followed by the low DE formula. If the low DE TGA curve is observed over the 180 d it can be seen that its' weight loss below 200ºC gradually nears and then becomes

equal with that of the high DE formula at the 180 d mark. This shows that after 180 d the high DE and low DE formulas have the same weight loss due to C-S-H gel below 200ºC. The observed differences in compressive strengths at 180 d may therefore have to do with the weight loss differences between the two samples in the 200-400ºC region which corresponds to weight loss due to more ordered C-S-H. After 180 d the low DE has not caught up with the high DE formula in this TGA temperature region.

3.3 Conclusion

The cement paste experiments on freeze-dried samples eliminated the XRD and TGA interference issues that occurred in the 6 months trial. As a result the XRD and TGA data from the cement paste experiments provided great characterization of the formulas in the 6 month trial. The cement paste XRD was able to identify the specific type of C-S-H that formed in both the low and high DE formulas. It was not however, able to identify the specific type of C-S-H in the NHL-5 formula unfortunately due to the existence of 22 wt.% unburned $CaCO_3$ which caused the same interference issues as in the 6 month trial.

By freeze drying the cement paste samples prior to TGA testing the issues of unbound water interfering with C-S-H weight loss and the issue of bound water from $Ca(OH)_2$ building up between 400-600ºC were eliminated. The TGA results showed a great correlation with the compressive strength data in the 6 month trial. The TGA showed that the amount of $Ca(OH)_2$ is the key to strength development over time as it converts to C-S-H or calcite. The high DE formula was the only cement paste that did not

show a decrease in the amount of portlandite over time. This correlates to the high DE formulas lack of strength development past 28 d in the 6 month trial. After 180 d the lime mortar TGA sample, on the other hand, had a large amount of portlandite, confirming the XRD, phenolphthalein tests, and showing that the lime mortar has the ability to continue to gain strength past 180 d

.

CHAPTER 4. CELITE DE EXPERIMENTS

4.1 Introduction

Since there are thousands of types of DE around the world the purpose of the Celite DE experiments was to explore how changing the type DE used will affect the properties and strength of the low and high DE formulae. If these samples were ever used in countries around the world they would have to be able to deal with varying types of DE. Also if the low or high DE formulae were ever turned into a product then using the cheapest DE possible would be ideal, and thus investigation how the formula properties change by varying the type of DE is important.

The low and high DE formulas from the 6 month trial and cement paste experiments were used in this set of experiments with only the type of DE changing. Both concrete samples and cement paste samples were created with the concrete samples being used for compressive strength testing, and the cement paste samples being used for XRD

and TGA testing. Figure 40 shows SEM images of how the Celite DEs differ from the Perma-Guard DE. Table 11 shows the slight differences in wt.% composition and BET surface areas between the three types of DE

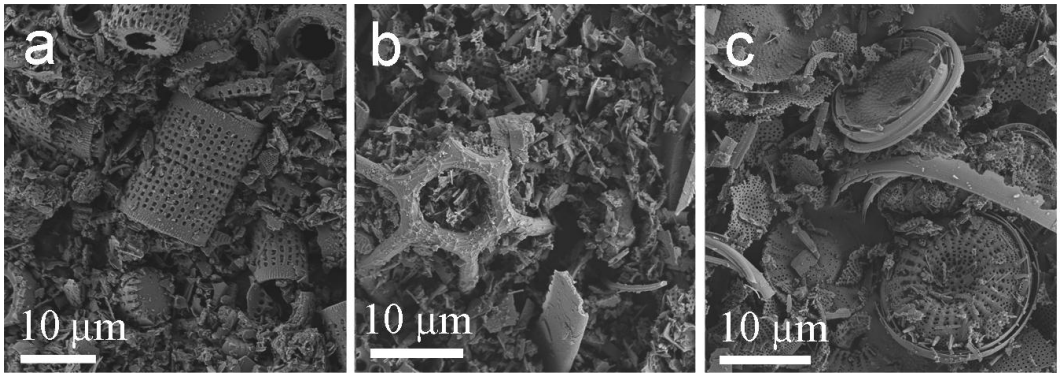

Figure 40: SEM Images of As Received DE a) Perma-Guard b) Celite 266 c) Celite 400

Table 11: As Received DE Composition in wt. % and Surface Area

Permaguard Fresh Water DE	**Celite 266** Plankton Marine DE	**Celite 400** Plankton Fresh Water DE
89 wt% SiO_2 4 wt% Al_2O_3 1.7 wt% Fe_2O_3 1.4 wt% CaO 1.2 wt% Na_2O 0.6 wt% MgO 0.5 wt% K_2O Crystalline silica < 0.5 wt%	89 wt% SiO_2 3 wt% Al_2O_3 1.4 wt% Na_2O 1.4 wt% K_2O 1 wt% Fe_2O_3 0.7 wt% MgO 0.4 wt% CaO 0.2 wt% TiO_2	92.5 wt% SiO_2 3.2 wt% Al_2O_3 1.7 wt% Fe_2O_3 0.8 wt% CaO 0.6 wt% Na_2O 0.6 wt% K_2O 0.4 wt% MgO 0.2 wt% TiO2 0.1 wt% P_2O_5
BET Surface Area: 28.1 m^2/g	BET Surface Area: 30.0 m^2/g	BET Surface Area: 36.7 m^2/g

The Celite 266 DE (Fig. 40b) has a starfish-like shape, while the Celite 400 DE has a plate-like shape (Fig. 40c). Both shapes differ from the barrel shaped Perma-Guard

DE (Fig. 40a). Table 11 shows how these observed shape differences affect the surface area of the DE. The correlation between DE surface area and cement and concrete properties is something that will be kept track of throughout this chapter. Table 11 also shows that all three types of DE have about the same wt.% amorphous SiO_2. Figure 41 shows XRD of the three as received DE.

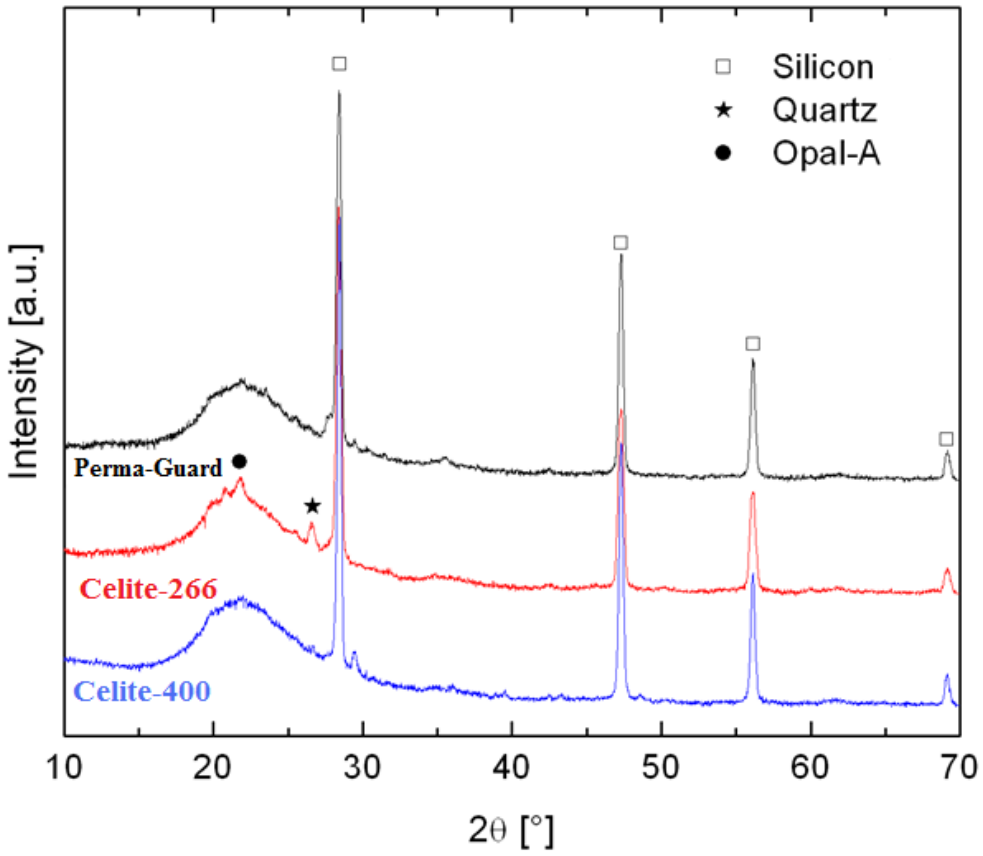

Figure 41: XRD of As Received Perma-Guard, Celite 266, and Celite 400
All three types of DE show a hump due to amorphous SiO_2 around 22° 2θ.

Figure 41 shows the large silica amorphous hump that exists with each DE XRD. The only difference between the three types of DE is the existence of minor quartz and Opal-A peaks in the Celite 266 DE.

Concrete samples were created with the three types of DE based on the low and high DE formulas in the 6 month trial. The samples were then cured in the 100% relative humidity chamber and then compression tested at 14 and 28 d. Cement pastes were also created of each type of DE using the low DE cement paste formula. These cement pastes were then placed in the humidity chamber and allowed to cure for 180 d. At 14, 28, 90, and 180 d the cement paste samples were freeze dried using a lypholizer and tested using XRD and TGA.

4.2 Results and Discussion

4.2.1 Compression Testing

Figure 42 shows the compressive strength of the three DE samples created using the high DE (low Ca/Si ratio) formula.

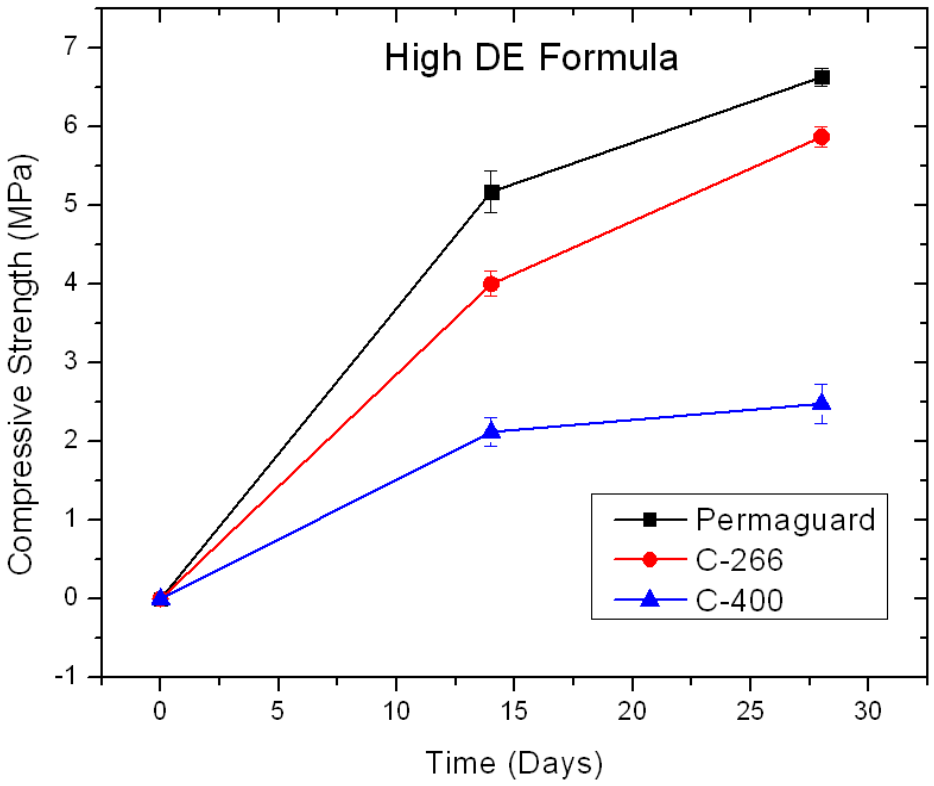

Figure 42: Compressive Strength Using High DE Formula
The Perma-Guard DE has the highest strength followed by Celite 266, and then Celite 400.

Figure 42 shows that the Perma-Guard DE has the highest strength of the three types of DE when they are used in the high DE formula. It should be noted that the Celite 400 was difficult to use in the high DE formula due to its high surface area and low density. Extra water was needed to make the Celite 400 concrete workable and may have had an impact on the results. From Figure 42 it appears there may be a correlation between compressive strength and surface area as the lower the surface area the higher the compressive strength. This correlation is somewhat counterintuitive however as it makes sense that the higher the surface area the more exposed silica that can dissolve and quickly form C-S-H. Figure 43 shows the compressive strength of the three types of DE used in the low DE (high Ca/Si ratio) formula.

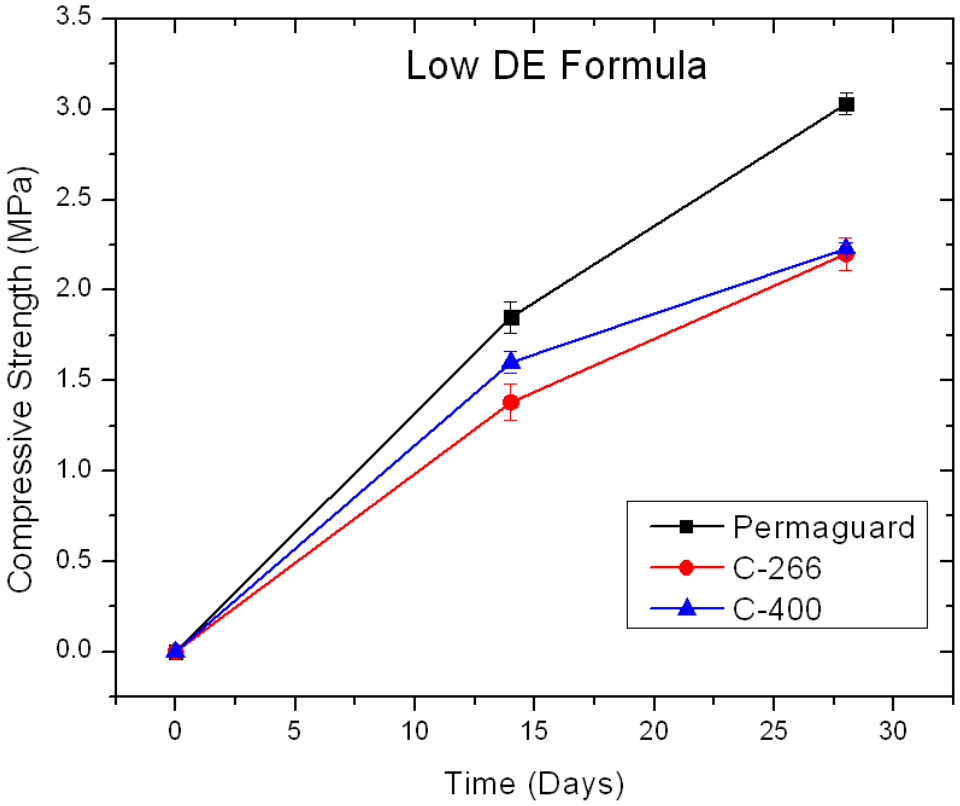

Figure 43: Compressive Strength Using Low DE Formula
The Perma-Guard DE has the highest strength of the three types of DE, although the curves are much closer than in the high DE Formula samples in Figure 42.

Figure 43 shows a similar trend between types of DE and compressive strength as the high DE formula based samples in Figure 42. Perma-Guard DE again has the highest strength, although in this case the difference is less. In the low DE based formula samples the Celite 400 has slightly better strength than the Celite 266 samples, contrary to the high DE formula samples previously reported. The relationship between surface area and compressive strength is also not as clear in Figure 43 as it was in Figure 42. The fact that only minor differences were seen between the three types of DE using the low DE formula most likely has to do with the low strength of the low DE formula below 28 d.

Had the experiments been continued past 28 d it is likely they would have separated themselves more clearly as they gained strength. Thus, it is still possible that there is a relationship between lower DE surface area and higher compressive strength.

4.2.2 XRD Results

The goal of conducting XRD on the three DE cement pastes was to identify what type of C-S-H forms in each sample and how they differ. From the cement paste experiments in Chapter 3 it is known that the Perma-Guard DE forms the C-S-H $Ca_{1.5}SiO_{3.5}{\cdot}xH_2O$. Figure 44 shows the XRD of the Celite 266 and Celite 400 DE cement paste over 180 d.

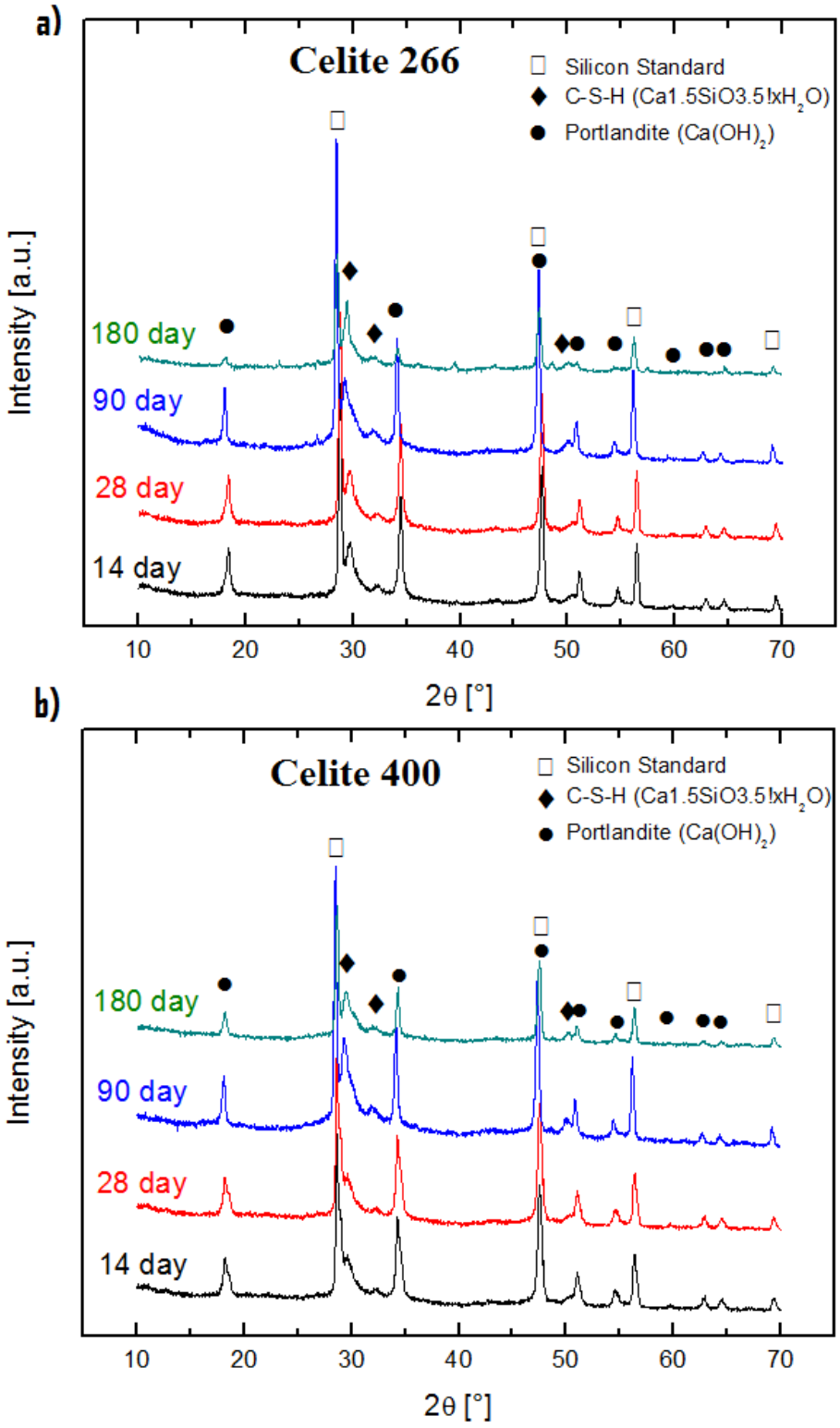

Figure 44: XRD of a) Celite 266 and b) Celite 400 Over 180 d

The XRD shows portlandite, silicon standard, and Ca1.5SiO3.5·xH2O C-S-H peaks in both the Celite 266 and Celite 400 cement paste over 180 d.

Figure 44 shows very similar XRD diffractograms between the Celite 266 and Celite 400 DE cement paste with both having portlandite and C-S-H peaks. Figure 44 shows that both the Celite 266 and Celite 400 DE form the same type of C-S-H as the Perma-Guard DE. This is an interesting result as it may turn out that the $Ca_{1.5}SiO_{3.5}\cdot xH_2O$ type of C-S-H is the C-S-H that will always form in artificially hydraulic lime mortars with DE as the source of silica. To further confirm this, future work is needed using other types of DE. Since it is known that the three types of DE form the same C-S-H then it may be the amount of C-S-H that causes the samples to have differing compressive strengths.

4.2.3 TGA Results

Figure 45 shows the cement paste TGA of the Celite 266 and Celite 400 DE over 180 d.

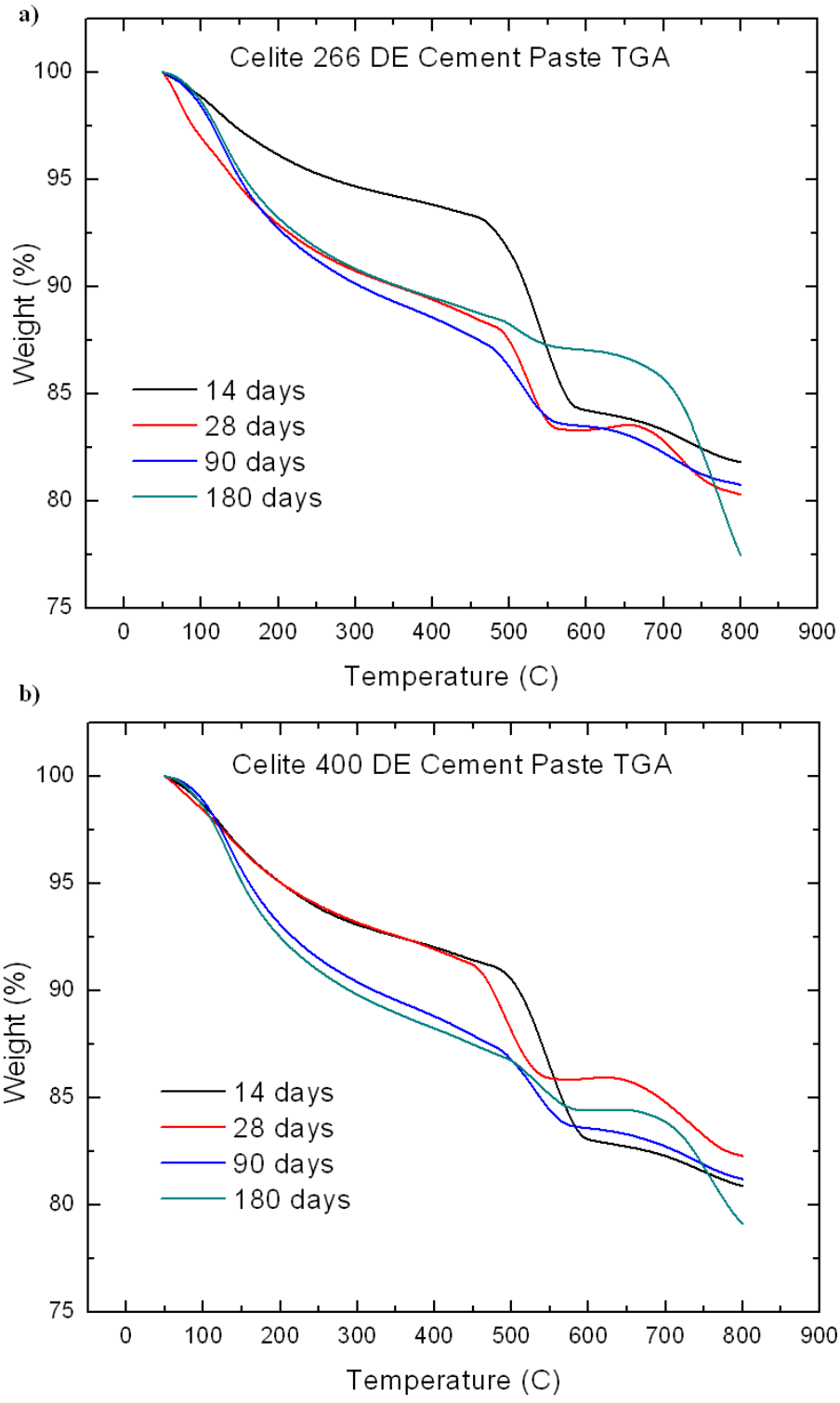

Figure 45: Cement Paste TGA of, a) Celite 266 and, b) Celite 400 over 180 d
The TGA shows a decrease in weight loss from portlandite and increases in weight loss due to C-S-H and carbonation over the 180 d for both types of DE.

Figure 45 shows that the Celite 266 and Celite 400 DE both have similar TGA curves over 180 d to that of the Perma-Guard DE (Fig. 35). Both TGA graphs show a decrease in weight loss due to portlandite between 400-600ºC over the 180 d. This decreasing weight loss due to portlandite is turned into increased weight loss due to C-S-H below 400ºC and weight loss due to carbonation from 600-800ºC. This data shows that like in the Perma-Guard DE samples, the Celite DE samples are forming C-S-H over the 180 d which should result in increased strengths. The specific TGA weight loss percentages for the Celite DEs over the 180 d can be found in Table 12.

Table 12: Celite DE Cement Paste TGA Weight Loss %
The TGA weight loss data shows a decrease in weight loss from portlandite and increases in weight loss due to C-S-H and carbonation over the 180 d.

		Celite-266		
Temp Range (ºC)	**0-200**	**200-400**	**400-600**	**600-800**
14days	3.85	2.32	9.59	2.42
28 days	7.10	3.50	6.09	3.01
90 days	7.28	4.15	5.07	2.73
180 days	6.78	3.72	2.45	9.57
		Celite-400		
Temp Range (ºC)	**0-200**	**200-400**	**400-600**	**600-800**
14days	3.85	2.32	9.59	2.17
28 days	7.10	3.50	6.09	3.61
90 days	7.28	4.15	5.07	2.37
180 days	7.51	4.25	3.83	5.27

Figure 46 shows cement paste TGA of the three types of DE compared to each other over the 180 d.

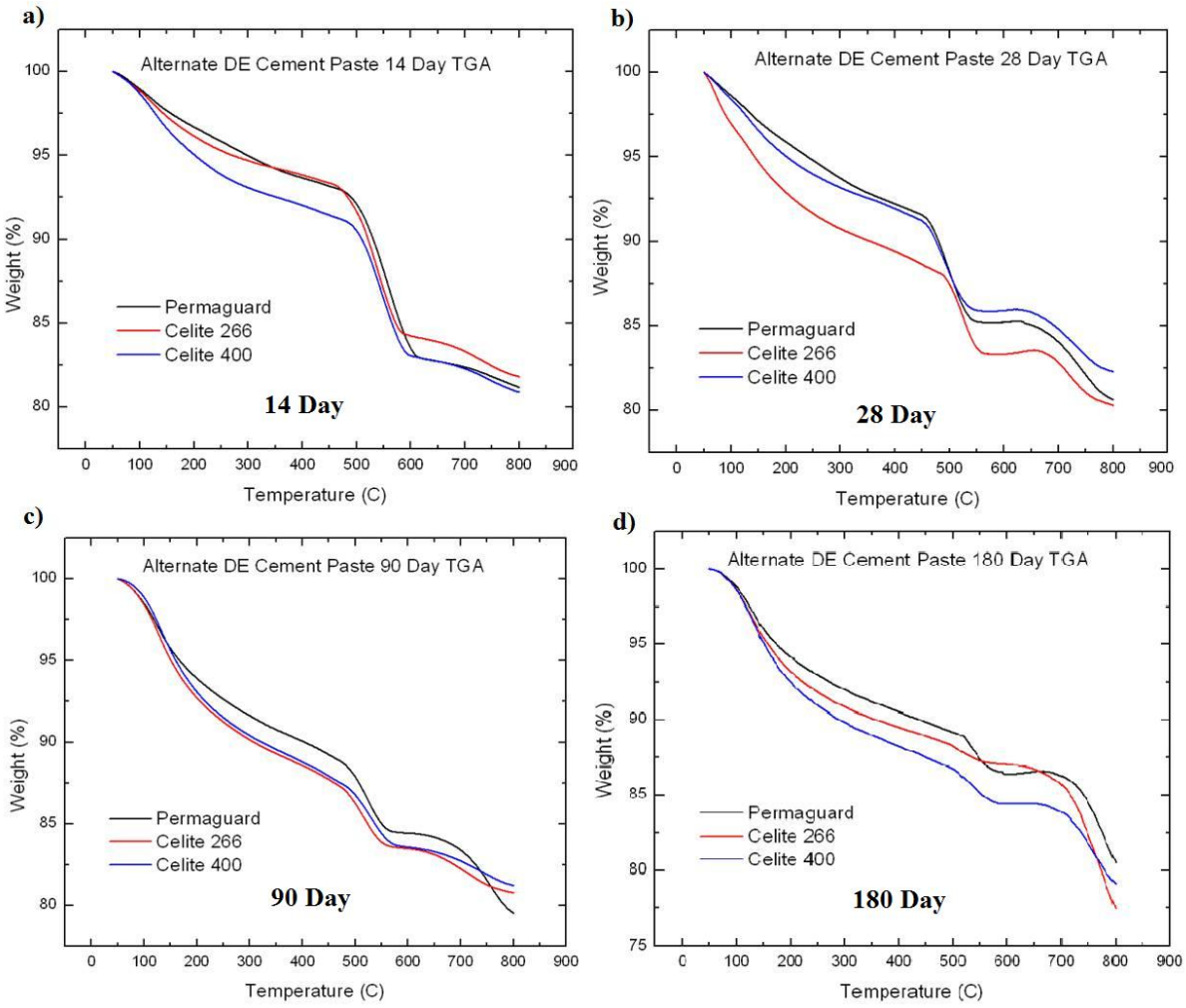

Figure 46: Celite 266, Celite 400, and Perma-Guard DE TGA Over 180 d
Over 180 d the TGA for the three types of DE remain very similar with decreasing weight loss due to portlandite and increasing weight loss due to C-S-H.

Figure 46 shows that the three types of DE have very similar cement paste TGA over the 180 d, which explains why their compressive strengths are comparable in the low DE formula (Fig. 10)

4.3 Conclusion

The Celite DE experiments were successful in determining what differences if any, result from using a different DE in the low and high DE formulae. The compression testing showed that the Perma-Guard DE has the highest strength and that there may be a correlation between lower surface area and higher strengths. This correlation is counterintuitive however as the higher the surface area the easier it should be to dissolve the diatoms and form C-S-H. This observed relationship may be explained in a few ways. The shape of the DE may play a role in the strength development as it is known that the barrel shaped Perma-Guard DE is used as a pesticide because of its robust qualities and shape. If the shape of partially dissolved diatoms plays a role in the compressive strength in the high DE formula then the differences in strength values may result from the shape and not the surface area of the diatoms. This idea needs to be further tested in the future work section however, to prove its validity.

CHAPTER 5. CA/SI RATIO TEST

5.1 Introduction

The final experiment that was conducted during this research had the aim to investigate one of the first issues encountered, the poor strength retention in the Perma-

Guard high DE formula from the 6 month trial. One of the results of the 6 month trial was that the high DE formula had a compressive strength retention problem, while the low DE formula did not. It was hypothesized, and supported by SEM imaging that the reason the high DE formula had a strength retention issue was because of the excess undissolved diatoms that existed throughout the samples (Section 2.2.3). Once the concrete sample was left to dry in air these excess diatoms became micron size pores/defects throughout the sample, decreasing its' strength. The low DE concrete had little to no excess diatoms and therefore did not have strength retention issues (Fig. 12).

The Ca/Si ratio test was developed to vary the Ca/Si ratio in the Perma-Guard DE concrete by adjusting the amount of DE in the formula. The formulas had Ca/Si ratios varying from 0.25 (approximately that of the original high DE formula) to 2.25. The amount of aggregate added to each formula was kept constant and each formula had almost exactly the same amount of water. The water varied slightly because those formulas with high contents of DE required more water, and the formula with little DE needed less water. The Ca/Si ratio formulas can be seen in Table 13.

Table 13: Ca/Si Ratio Test Formulas

Ca/Si ratio	Water (ml)	Water weight %	DE (g)	CaO (g)	Limestone Aggregate (g)	Cement/Agg Volume Ratio
0.25	750	18.52	245.90	54.10	3000	1:2.04
0.28	750	18.52	240.00	60.00	3000	1:2.07
0.65	700	17.50	189.90	110.10	3000	1:2.37
1.05	700	17.50	155.44	144.56	3000	1:2.63
1.45	700	17.50	131.00	169.00	3000	1:2.86
1.75	700	17.50	117.20	182.80	3000	1:3.00
1.85	700	17.50	113.20	186.80	3000	1:3.04
2.25	674	16.96	100.00	200.00	3000	1:3.20

As Table 13 shows that the Ca/Si ratio formulas all had a cement to aggregate volume ratio between 2 and 3.2. All of the formulas had the same cement-to-aggregate mass ratio, but not the same cement to aggregate volume ratio due to the differences in density between the CaO, DE, and the limestone aggregate.

Once the concrete samples were made of each formula they were placed to cure in a 100% relative humidity chamber. After 14 and 28 d, samples were removed and compression tested. At 14 and 28 d samples were also removed from each formula and placed in ambient air to dry for 7 d. Thus at 21 and 35 d samples that were left to dry for 7 d were also compression tested. These samples are the ones that served to investigate how the strength was retained in each formula as the samples dried.

5.2 Results and Discussion

Figure 47 shows the compressive strength results from the Ca/Si ratio test.

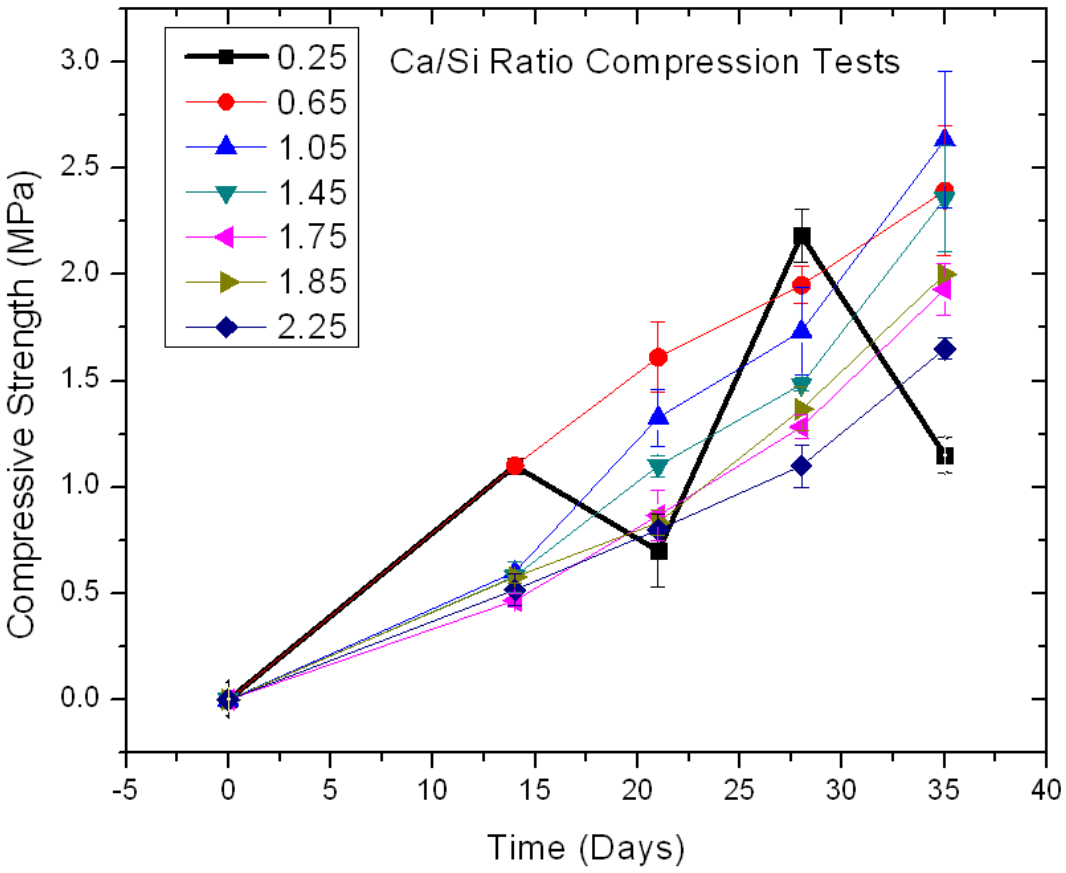

Figure 47: Ca/Si Ratio Compression Testing Results
The results show that only the Ca/Si ratio 0.25, seen as the bold black line, had issues with strength retention at the 21 and 35 d tests.

Figure 47 clearly shows that only the Ca/Si ratio of 0.25, seen as the bold black line, had issues with strength retention. At the 21 and 35 d tests after the samples were left to dry for 7 d in air the 0.25 Ca/Si ratio line showed large strength drops. This data confirms the strength retention issues seen in the high DE 6 month trial formula which had a Ca/Si ratio of 0.28. It is interesting that only the Ca/Si of 0.25 had a strength retention issue, with even the next lowest Ca/Si ratio of 0.65 having no issue. Figure 47 also shows a correlation between Ca/Si ratio and strength. As the Ca/Si ratio increases the compressive strength decreases.

5.3 Conclusion

Clearly only the 0.25 Ca/Si ratio formula had strength retention problems. Increasing the ratio to 0.65 solves the problem. To better understand this it would be best to do future experiments by varying the Ca/Si between 0.25-0.65 and seeing if there is an exact point at which the switch occurs. It would also be beneficial to do SEM on these concrete samples to see if the switching point also correlates to it being difficult to see undissolved diatoms throughout the sample.

Although it is not fully known why the strength retention results occurred as they did, the Ca/Si ratio test provided a lot of information that can be used to optimize the Perma-Guard DE based concrete. It is now known that using a Ca/Si of 0.65 and above will give a concrete product with no strength retention issue. It is also known that as the Ca/Si ratio is increased, the early strength development decreases. This occurs because as the Ca/Si increases there is less DE that can be dissolved to form C-S-H. From the previous chapter it is known that as the Ca/Si ratio increases however, so does the amount of portlandite which can be used for long term strength development as it turns into C-S-H or calcite.

The final optimization information that the test provided has to do with why the 0.25 Ca/Si ratio compressive strength values were so low compared to the 14 and 28 d strength values of the original high DE formula in the 6 month trial. The humidity cured high DE formula in the 6 month trial had strength 5 MPa after 14 d and 6.6 MPa after 28 d, all while having a cement to aggregate volume ratio of 1:1. The 0.25 Ca/Si ratio formula had strength of 1 MPa after 14 d and 2 MPa after 28 d, while having a cement to

aggregate volume ratio of 1:2. The varying strength between the two experiments occurred because of the difference in cement to aggregate volume ratios. There was twice as much aggregate in the 0.25 Ca/Si ratio formulas as the original high DE formula in the 6 month trial. Since there was less cement in the Ca/Si ratio formula there was less cementitious binding phase available to hold all of the excess aggregate together. This information helps to optimize the DE formulas as the effect of cement to aggregate ratio and the importance of having a higher amount of cement for good early strength is now known

CHAPTER 6. SUMMARY AND CONCLUSIONS

6.1 Summary and Conclusions

The goal of this research was to understand the role of DE as a source of silica in the formation of alkali-activated fine-aggregate concrete with lime as the alkali and limestone as the aggregate. Experiments were developed to investigate the strength and characterize the binding phases of these hydraulic lime mortars. In the 6 month trial four formulas were developed to investigate how hydraulic lime mortar, using DE as the source of silica differs in strength and properties from naturally hydraulic lime mortar and non-hydraulic lime mortar. Formulas with low and high DE contents were created and compared with the naturally hydraulic and non-hydraulic lime mortar controls. The

strength and binding phase properties of the four formulas were investigated over a 180 d testing period.

The results from the 6 month trial showed that the high DE formula had the best compressive strength of the four formulas, and the low DE formula had the second best strength. A major issue was discovered with the high DE formula however, as it was observed that its' humidity and container cured concrete samples lost 50% of their strength when left to dry for 7 d in air. The low DE formula did not have this issue and thus it was hypothesized and supported by SEM images that the strength retention issue in the high DE formula resulted from the existence of undissolved diatoms throughout the sample. Once dry, these undissolved diatoms become micron size pores and holes throughout the sample, decreasing the sample's strength.

In addition to compressive strength tests and SEM imaging, the 6 month trial used XRD, TGA, and phenolphthalein tests to help characterize the competing hydraulic and carbonation binding phases that form during hardening. The phenolphthalein tests were successful in visually showing the rate of carbonation in each of the four formulas. Unfortunately, the XRD and TGA experiments in the 6 month trial were not nearly as successful. The limestone aggregate and moisture in the formulae provided interference issues that prevented the XRD and TGA from properly characterizing what binding phases formed in the formulae.

To deal with the characterization issues faced during the 6 month trial another set of experiments were created using cement pastes of the same four formulas. These cement pastes contained no limestone aggregate and were freeze dried to eliminate all of the interference issues of the previous experiments. The cement paste XRD was able to

successfully identify the specific type of C-S-H forming in the low and high DE formulas, Ca1.5SiO3.5·xH2O. The cement paste TGA showed how strength is developed in the samples over 180 d. The TGA showed decrease in weight loss due to portlandite over time as the weight loss due to C-S-H and calcite increased. This result also showed that the amount of portlandite in the sample represents potential increase in the samples' strength as the portlandite turns into either C-S-H or carbonates to form calcite. The TGA data showed that the non-hydraulic lime mortar had the largest amount of portlandite after 180 d and thus had the highest potential to continue to gain strength over months and possibly years.

To investigate whether the type of DE used affected the properties and strength of the alkali activated fine aggregate concrete, experiments were set up using Celite 266 and Celite 400 DE to replace the original Perma-Guard DE. The cement paste XRD part of the experiments showed that the same specific type of C-S-H forms with all three types of DE, Ca1.5SiO3.5·xH2O. This data supports the conclusion that this specific type of C-S-H is what will form in this system, no matter what type of DE is used. The compressive strength results showed that the Perma-Guard DE had the highest strength using the high DE and low DE formulas, followed by Celite 266 and then Celite 400. When compared to the surface area this result showed a correlation between lower surface area and higher compressive strength. This relationship is counterintuitive as the higher the surface area of the DE, the more exposed silica can be dissolved in an alkali environment to form C-S-H and increase the strength of the sample. The observed odd relationship may be explained in a few ways. The shape and robustness of the DE may play a role in the strength development as it is known that the barrel shaped Perma-Guard DE is used as a

pesticide because of its robust qualities and shape. If the shape of the partially dissolved diatoms plays a role in compressive strength in the high DE formula than the differences in strength values may result from the shape and not the surface area of the diatoms. This idea needs to be further tested in the future to prove its validity.

If it is found that the structure of the partially dissolved diatoms does affect compressive strength than it may go a long way to explaining why the Perma-Guard high DE concrete samples in the 6 month trial had good strength when wet, and half the strength when dry as discussed with the strength retention issue. Partially dissolved diatoms form just surface C-S-H gel as seen under SEM. Upon drying it is possible that this surface C-S-H gel deteriorates and goes away as the C-S-H may not be stable enough or developed enough to retain its form when dry. When wet, this surface C-S-H gel provides strength by binding to fully developed and more ordered C-S-H, as well as to other surface C-S-H gel. When dry however, the partially undissolved diatoms lose their surface binding phase and become micron size pores that hurt the strength of the concrete. Although this is a viable explanation, it is something that needs to be looked at in future work.

To further investigate the high DE strength retention issue a Ca/Si ratio experiment was created. By varying the Ca/Si ratio in a set of formulas from 0.25-2.25 while keeping all other variables relatively constant the influence of the amount of DE on concrete strength retention was investigated. The results of the experiment showed that between a Ca/Si ratio of 0.25 and 0.65 the DE concrete changes from having strength retention issues to none at all. For optimization of the formula it is known that to avoid strength issues a Ca/Si ratio around 0.65 or higher is necessary. Since the C-S-H that is

forming in the DE based cements is $Ca_{1.5}SiO_{3.5}\cdot xH_2O$, the Ca/Si ratio from this phase is 1.5/3.5, or 0.43. The Ca/Si value of 0.43 lies between 0.25 and 0.65 and thus may be the Ca/Si ratio where the samples go from having a strength retention issue to none at all.

The Ca/Si ratio results also showed that there is a direct correlation between early strength and Ca/Si ratio as the higher the Ca/Si ratio the lower the early strength. This is explained by the fact that at higher Ca/Si ratios there is less DE to dissolve and form C-S-H and provide strength. Higher Ca/Si ratio formulas are not all bad however as they have a better ability to gain strength in the long term. From the cement paste experiments it is known that as the Ca/Si ratio increases, so does the amount of portlandite which can be used for long term strength development as it turns into C-S-H or calcite over time.

The final optimization information that was provided by the Ca/Si ratio experiment has to do with the amount of cement and aggregate used in the formulas. The 0.25 Ca/Si ratio formula repeated the high DE formula from the 6 month trial, only this time with twice as much aggregate. The effect of doubling the amount of aggregate decreased the strength of the concrete. At 28 d for example the strength dropped from 6.6 MPa to 2 MPa by doubling the amount of aggregate. This occurs because with a lower cement to aggregate volume ratio there is less cement to hold the large amount of aggregate together. This information is important for formula optimization as it shows that the alkali activated fine aggregate concretes with DE as the source of silica need a cement to aggregate volume ratio of around 1:1 for good early strength properties.

Since one of the goals of this research was to create an alternative cement to possibly replace OPC it is important to keep in mind the cost of the developed DE based cements. As mentioned in Section 2.3 the low DE formula has an approximate price of

$139 per ton, and the high DE formula has an approximate price of $193 per ton.[37,58] OPC currently costs around $102 per ton in the U.S.[56] The problem is that in addition to being more expensive, the low and high DE formulas are not nearly as strong as OPC. After 180 d the humidity cured high DE concrete had a maximum strength of approximately 7 MPa, while the low DE concrete had strength of approximately 5 MPa. These values are far inferior to the strength values of OPC which on average range from 20-40 MPa after 28 d.[59] Another issue results from the fact that the highest strength low and high DE samples were ones that were cured in the humidity chamber or in their container. Both DE formulas have air curing problems that will be a large stepping stone to overcome for the formulas to ever be used in real life applications. Since the strength of the DE based concretes is not close to that of OPC, it appears that they will be limited to use in developing countries. For simple one story structures in developing countries 7 MPa should be more than enough strength, as long as the strength retention and air curing issues are solved. It may also be possible to produce a DE based concrete with higher strength by combing the results from the various experiments in this research to create an optimized formula. This initial optimized formula would have a Ca/Si ratio around 0.65, a cement to aggregate volume ratio around 1:1, use Perma-Guard DE, and be cured in the humidity chamber or in the container cured environment. Further optimization steps included changing the type of DE and aggregate, both of which could increase the strengths of the formulae.

The area in which the DE based alkali activated cements are better than their OPC counterparts is in their environmental impact. For every 1 ton of OPC roughly 0.8 tons of CO_2 are released into the environment.[9] If it is assumed that CaO, the material that causes

almost all of the CO_2 released during the production of OPC, makes up about 64 wt.% of OPC then the percent reduction in the amount of CO_2 released by using the low and high DE formulas can be calculated.[58] The high DE formula would reduce the amount of CaO used by roughly 31%, and the low DE by roughly 10%. This reduction is with neither the low nor high DE formulas being optimized for CO_2 reduction and so just like with the cost estimates, there is room for improvement going forward.

All in all the 4 experiments were successful in understanding the role of DE as a source of silica in alkali-activated fine-aggregate concrete with lime as the alkali. Due to price and strength issues the DE based cements are not a viable replacement for OPC at this point, but remain a possibility to someday be used as simple building materials in developing countries.

6.2 Future Work

One of the first things that could be done in future work is to scale up the project to larger tests and larger concrete pours. Currently samples were produced at the small size of 2”x4” cylinders. By scaling up to larger cylinders such as 4”x8” it will be interesting to see if the properties and strength of the four formulas used in the original 6 month trial change. Scaling up the project will also go a long way to determining the DE based cement’s viability as a real product for developing countries.

Another future work topic is to use the results from the various experiments to create an optimized formula. The optimized formula at this point would have a Ca/Si ratio around 0.65, a cement to aggregate volume ratio around 1:1, use Perma-Guard DE,

and be cured in the humidity chamber or in the container cured environment. It would then be interesting to take this optimized formula through the gauntlet of tests and scale it up as well.

Past the initial optimized formula there remain many more options for improving the formula. It is unclear where between a Ca/Si ratio of 0.25 and 0.65 the DE concrete changes from having a strength retention issue to no issue at all. For optimization purposes it would important to determine if there is an exact ratio where the properties change and why.

There is also room for optimization in terms of the DE used. Various other types of DE should be tested to further investigate the data showing a relationship between lower DE surface area and increased strength. The correlation between strength and price of DE should also be looked at since DE has a broad range of prices. Investigating the use of inexpensive DE as a source of silica is important for lowering the price of the DE based cements.

The future work should include work to reduce the cost and environmental impact of the cements as well. By using a low Ca/Si ratio formula with a high amount of DE and a lower amount of CaO the CO_2 impact of the cement will be reduced. This type of formula will not however reduce cost since at $220 per ton, DE is more expensive than lime at $84 per ton. Thus it becomes increasingly important to find a DE which has similar or better properties than Perma-Guard DE, and which is cheaper than $220 per ton so that a cost effective environmentally friendly alkali activated fine aggregate concrete with DE as the source of silica can be developed.

Finally, to greatly reduce the environmental impact of the DE based cements other alkalis besides lime should be considered. Since the production of lime is by far the major source of the CO_2 released by OPC and the DE based formulas discussed, the best way to improve the environmental friendliness of alkali activated cement is to use an alkali that is less harmful to the environment than lime, such as Na_2CO_3.

LIST OF REFERENCES

1. J. Davidovits, and M. Morris. The Pyramids: An Enigma Solved, 1 ed. Dorset Press: New York, 1988.

2. J. Davidovits. In X-Rays Analysis and X-Rays Diffraction of Casing Stones from the Pyramids of Egypt, and the Limestone of the Associated Quarries, edited by David, R.A, Science in Egyptology Symposia. (1986) 511.

3. J. Davidovits. Geopolymers and Geopolymeric Materals. Journal of Thermal Analysis. 35 (1989) 429-441.

4. P. Duxson et al. Geopolymer Technology: the current state of the art. Journal of Materials Science. 42 (2007) 2917-2933.

5. M. W. Barsoum and A. Ganguly. Microstructural Evidence of Reconstituted Limestone Blocks in the Great Pyramids of Egypt. J. Am. Ceram. Soc., 89 [12] (2006) 3788–3796.

6. R.M.H. Lawrence. The use of TG to measure different concentrations of lime in non hydraulic lime mortars. Journal of Thermal Analysis and Calorimetry, v 85, n 2, August, (2006) 377-382.

7. W. H. Gourdin and W. D. Kingery. The Beginnings of Pyrotechnology: Neolithic and Egyptian Lime Plaster. Journal of Field Archaeology. 2 (1975) 133-150.

8. Carlos Rodriguez-Navarro et al. Calcium Hydroxide Crystal Evolution upon Aging of Lime Putty. J. Am. Ceram. Soc., 81 [11] (1998) 3032–34.

9. Olga Cazalla et al. Aging of Lime Putty: Effects on Traditional Lime Mortar Carbonation. J. Am. Ceram. Soc., 83 [5] (2000) 1070–76.

10. S. Pav´ıa E. Treacy. A comparative study of the durability and behaviour of fat lime and feebly-hydraulic lime mortars. Materials and Structures. 39 (2006) 391–398.

11. J. Lanas, J.I. Alvarez. Masonry repair lime-based mortars: factors affecting the mechanical behavior. Cement and Concrete Research 33 (2003) 1867–1876.

12. R.M.H. Lawrence et al. Determination of carbonation profiles in non-hydraulic lime mortars using thermogravimetric analysis. Thermochimica Acta. 444 (2006) 179-189.

13. J. Lanas et al. Mechanical properties of masonry repair dolomitic lime-based mortars. Cement and Concrete Research. 36 (2006) 951–960.

14. Moropoulou et al. Strength development and lime reaction in mortars for repairing historic masonries. Cement & Concrete Composites 27 (2005) 289–294.

15. Z. Zhou et al. Strength Characteristics of hydraulic lime mortared brickwork. Construction Materials. 161 (2008) Issue CM4.

16. M. Stefanidou, I. Papayianni. The role of aggregates on the structure and properties of lime mortars. Cement & Concrete Composites. 27 (2005) 914–919.

17. J. Lanas et al. Mechanical properties of natural hydraulic lime-based mortars. Cement and Concrete Research. 34 (2004) 2191–2201.

18. A. El-Turki et al. The influence of relative humidity on structural and chemical changes during carbonation of hydraulic lime. Cement and Concrete Research. 37 (2007) 1233–1240.

19. D.A. Silva et al. Comparative investigation of mortars from Roman Colosseum and cistern. Thermochimica Acta. 438 (2005) 35–40.

20. A. Moropoulou et al. Composite materials in ancient structures. Cement & Concrete Composites. 27 (2005) 295–300.

21. John W. Phair. Green chemistry for sustainable cement production and use. Royal Society of Chemistry. Green Chem. 8 (2006) 763–780.

22. Della M. Roy. Alkali-Activated cements Opportunities and challenges. Cement and Concrete Research. 29 (1999) 249–254.

23. Franco Massazza. Pozzolanic Cements. Cement & Concrete Composites. 15 (1993) 185-214.

24. Weimin Jiang PHD Thesis: Alkali Activated Cementious Materials: Mechanisms, Microstructure, and Properties. Penn State University 1997.

25. V.D. Glukovski. Alkali-Earth Binders and Concretes Produced with Them, Visheka Shkola, Kiev, USSR (1979).

26. Hua Xu et al. Characterization of Aged Slag Concretes. ACI Materials Journal. March-April (2008).

27. Caijun Shi, A. Fern´andez-Jim´enez. Reduction of disinfection by-products precursors by nanofiltration process. Journal of Hazardous Materials. B137 (2006) 1656–1663.

28. C. Shi, X. Shen, X. Wu, M. Tang. Immobilization of radioactive wastes with Portland and alkali-slag cement pastes, Il Cemento. 91 (1994) 97–108.

29. Peter Duxson, John L. Provis. The role of inorganic polymer technology in the development of ‘green concrete’. Cement and Concrete Research. 37 (2007) 1590–1597.

30. M. M. Miller. USGS 2005 Mineral Yearbook**,** 44.1 (2006).

31. Energy Information Association. Emissions of Greenhouse Gases in the United States, DOE/EIA-0573(2002), Washington, DC, 2003.

32. Ellis Gartner. Industrially interesting approaches to "low-CO_2" cements. Cement and Concrete Research. 34 (2004) 1489–1498.

33. Thomas P. Dolley. Diatomite. U.S. Geological Survey Minerals Yearbook—2000.

34. A. Chaisena, K. Rangsriwatananon. Synthesis of sodium zeolites from natural and modified diatomite. Materials Letters. 59 (2005) 1474– 1479.

35. U.S. Geological Survey. Diatomite. (2008) <http://minerals.usgs.gov/minerals/pubs/commodity/diatomite/mcs-2008-diato.pdf>.

36. Abdelfattah Zalatl, Simone Servant Vildary. Journal of Paleolimnology. 34 (2005) 159–174.

37. Roger J. Flower. Diatoms in ancient building materials: application of diatom analysis to Egyptian mud bricks. Nova Hedwigia, Beiheft, 130 (2006) 245-264.

38. Iler, R. K. The Chemistry of Silica. John Wiley & Sons: New York, 1979.

39. C. Rees et al. In Situ ATR-FTIR Study of the Early Stages of Fly Ash Geopolymer Gel Formation. Langmuir 23 (17) (2007) 9076.

40. J.J.Chen et al. Solubility and structure of calcium silicate hydrate. Cement and Concrete Research. 34 (2004) 1499–1519.

41. E. Bonaccorsi et al. The crystal structure of jennite, Ca9Si6O18(OH)6 8H2O. Cement and Concrete Research. 34 (2004) 1481–1488.

42. Krassimir Garbev et al. Cell Dimensions and Composition of Nanocrystalline Calcium Silicate Hydrate Solid Solutions. Part 1: Synchrotron-Based X-Ray Diffraction. J. Am. Ceram. Soc. 91 [9] (2008) 3005–3014.

43. H.F.W. Taylor. Nanostructure of C-S-H: Current Status. Advn Cem Bas Mat. 1 (1993) 38-46.

44. Stepowska et al. Hydration Products in Two Aged Cement Pastes. J. Therm. Analysis and Cal. 82 (2005) 731-739.

45. I.G. Richardson. The nature of C-S-H in hardened cements. Cement and Concrete Research. 29 (1999) 1131–1147.

46. L. Gatty et al. A transmission electron microscopy study of interfaces and matrix homogeneity in ultra-high-performance cement-based materials. Journal of Materials Science. 36 (2001) 4013–4026.

47. K. Pimraksa, P. Chindaprasirt. Lightweight bricks made of diatomaceous earth, lime and gypsum.Cermaics International.(2008), doi:10.1016/j.ceramint. 2008.01.013.

48. D.R. Moorehead, Cementation by the Carbonation of Hydrated Lime. Cement and Concrete Research. 16 (1986) 700-708.

49. Perma-Guard. Information Center. (2009) <http://perma-guard.com/DE_ Information_ Center.html>.

50. Mississippi Lime. MicroCal Calcium Oxide. (2009) <http://www.mississippilime. com/products/quicklime/microcalocalciumoxide>.

51. PA Lime Works. Natural Hydraulic Limes. (2009) <http://www.palimeworks.com /lwus/default.asp?page=limemortar.html>.

52. St . Astier Natural Hydraulic Limes and Lime Products. Mineralogy and Chemistry of Raw Materials and Products. (2009) <http://www.stastier.com/.>.

53. D. O. McPolin et al. New Test Method to Obtain pH Profiles due to Carbonation of Concretes Containing Supplementary Cementitious Materials. Journal of Materials in Civil Engineering © ASCE. November (2007) 937.

54. Krassimir Garbev et al. Cell Dimensions and Composition of Nanocrystalline Calcium Silicate Hydrate Solid Solutions. Part 2: X Ray and Thermogravimetry Study. J. Am. Ceram. Soc., 91 [9] 3015–3023 (2008).

55. Lucia Alarcon-Ruiz et al. The use of thermal analysis in assessing the effect of temperature on a cement paste. Cement and Concrete Research 35 (2005) 609-613.

56. U.S. Geological Survey. Cement (2007) <http://minerals.usgs.gov/minerals/pubs/commodity/cement/mcs-2008-cemen.pdf>.

57. U.S. Geological Survey. Lime (2008) <http://minerals.usgs.gov/minerals/pubs/commodity/lime/mcs-2008-lime.pdf>.

58. Rob Scot McLeod. Ordinary Portland Cement. Building for a Future. Autumn (2005). <http://www.buildingforafuture.co.uk/autumn05/ordinary_portland_cement.pdf>.

59. M. Baris Ozer, Hulusi Ozkul. The influence of initial water curing on the strength development of ordinary portland and pozzolanic cement concretes. Cement and Concrete Research. 34 (2004) 13-18.